PARAMETRIC STUDY ON THE BEHAVIOR OF COUPLED SHEAR WALLS WITH HIGH-PERFORMANCE FIBER-REINFORCED CONCRETE COUPLING BEAMS: INFLUENCE OF KEY DESIGN PARAMETERS

By

Mostafa Hassan Fathi Abdelhafeez

A Thesis Submitted to the
Faculty of Engineering at Cairo University
in Partial Fulfillment of the
Requirements for the Degree of

MASTER OF SCIENCE

in

Structural Engineering

FACULTY OF ENGINEERING, CAIRO UNIVERSITY
GIZA, EGYPT
2020

ACKNOWLEDGEMENT

This thesis represents a comprehensive study on the **behavior of coupled walls with high-performance fiber-reinforced concrete coupling beams**, a portion of which was presented as a paper titled "**Behavior of Coupled Walls with High-Performance Fiber Reinforced Concrete Coupling Beams**" at the **SEMC 2022** held in **Cape Town, South Africa**. The conference paper serves as a condensed version of the broader research contained in this thesis. I would like to express my gratitude to the conference organizers and peer reviewers for their invaluable feedback and contributions during the preparation of the paper.

I would also like to extend my deepest thanks to my advisor, **Dr. Hamed Salem**, for his unwavering support, guidance, and encouragement throughout the development of this research. Additionally, I am grateful for the insights and collaboration from my colleagues at the **Department of Structural Engineering, Cairo University, Egypt**.

TABLE OF CONTENTS

LIST OF TABLES

LIST OF FIGURES

Nomenclature

HPFRC	High-performance fiber-reinforced concrete
ECP	Egyptian code of practice
ELS	Extreme Loading for structures
AEM	Applied Element Method
ACI	American concrete institute
fc'	Cylinder compressive strength of concrete
fy	The yield strength of diagonal reinforcement.
FRCCs	Fiber reinforced cement composites
FRC	Fiber reinforced concrete
HPFRCCs	High-performance fiber reinforced cement composites
MPa	Megapascal
s	Second
Vf	Fiber volume fraction.
ksi	Kilo pound per square inch
in	Inch
KN	Kilonewton
f_t	Splitting tensile stress
FEM	Finite element method
DEM	Discrete element method
RBSM	Rigid Body and Spring Model
EDEM	Extended discrete element method
τ	Shear strength under coupled normal and shear stresses
τ_o	Shear strength under pure shear
μ	Coefficient of friction = tan (ϕ)
ϕ	Angle of internal friction
σ	Normal compressive stresses
Es	Steel young's modulus
εc	Compressive strain.
ε_o	Compressive strain corresponding to f'c
DL	Dead load
LL	Live load
SL	Seismic Load
S	The soil amplification factor
S_a	The acceleration of the equivalent SDOF system
$S_d(T)$	Design response spectrum for elastic analysis at period T
T_1	The fundamental period of the building

T_B	The first characteristic period of the design response spectrum
T_C	The middle characteristic period of the design response spectrum

ABSTRACT

Coupling beams significantly influence the performance of coupled shear wall systems under lateral forces. To ensure adequate behavior under lateral load-induced deformations and stresses, coupling beams are typically reinforced with complex reinforcement configurations, such as diagonal bars and confinement reinforcement. However, these reinforcement schemes can complicate construction. In slender coupling beams with an aspect ratio of approximately 3.0, the shallow angle of the diagonal reinforcement (less than 20 degrees) relative to the beam's longitudinal axis raises questions about the effectiveness of this reinforcement. This study investigates the impact of utilizing tensile strain-hardening high-performance fiber-reinforced concrete (HPFRC) in coupling beams. A nonlinear static analysis using the Applied Element Method was conducted to assess the behavior of coupling beams with HPFRC. The analysis was validated using previously tested specimens. A parametric study was performed, considering factors such as the material type (HPFRC vs. regular concrete), the longitudinal reinforcement ratio in coupling beams, the incorporation of HPFRC within the coupled walls, the presence of diagonal reinforcement with or without confining stirrups, the coupling beam's aspect ratio, and the fiber ratio. The results indicated that the use of HPFRC enhances the beam's capacity and provides superior energy dissipation compared to traditional reinforced concrete.

CHAPTER 1: INTRODUCTION

High rise buildings exposed to lateral forces as inertia forces resulted from ground shaking must have systems to resist shear forces and bending moments acting on the building. Shear walls have been the most common system used to construct high rise buildings in addition to frames systems. However, frames systems have less efficiency for buildings that are taller than 10-storeys. Therefore, the determination of the required system to resist such loads depends on the number of storeys.

Shear walls have been used to develop the lateral stiffness efficiency under earthquake loading. The individual walls can be more efficient if they are connected by a coupling beam as shown in Figure (1-1). The coupled shear walls produce larger lateral stiffness and strength. Therefore, to dissipate the required energy, coupling beams must be rigid and ductile.

Under lateral load, shear is resisted by the wall units while overturning moment is resisted by individual flexure in the wall units, M1 and M2, and the couple from axial forces developed in the wall units. However, coupling beams are hard to construct due to the necessity of diagonal reinforcement as shown in Figure (1-2). Therefore, a substitutional method to construct these coupling beams without using diagonal reinforcement is needed.

Previous studies focused on investigating high-performance fiber-reinforced concrete (HPFRC). This material shows a compression behavior and cracking under uniaxial tension similar to confined concrete. [1].

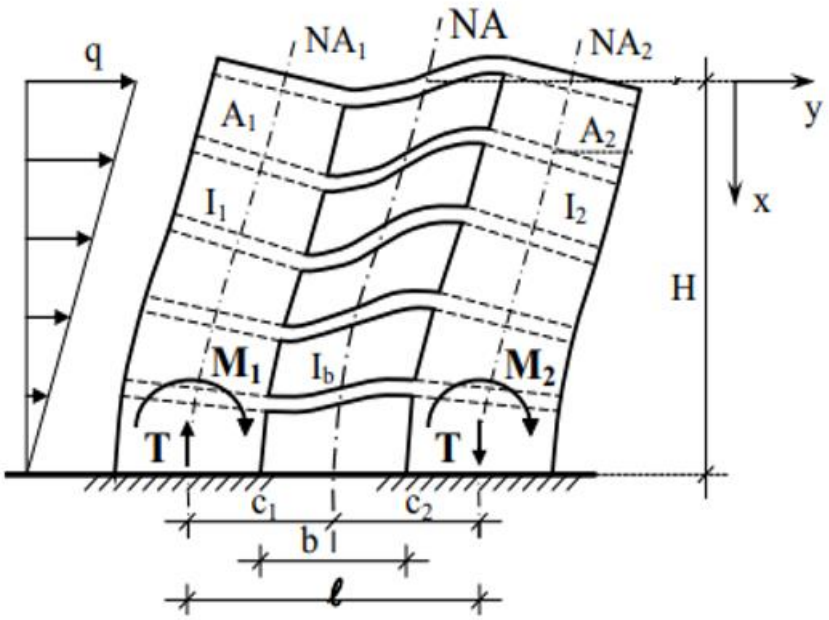

Figure (1-1): Coupled shear walls [2]

Figure (1-2): Diagonal reinforcement in coupling beams [3]

1.1. Thesis Objective

The goal of this study is to assess the effect of using of HPFRC to construct coupling beams in a multi-storey reinforced concrete structure under gravity and seismic load, designed according to the Egyptian code of practice (ECP 203-2018) [4]. To accomplish the research objective, coupled shear wall models, which is considered as a part of a residential building, were created.

For this purpose, a twelve-storey reinforced concrete multi-storey frame was modeled one with regular concrete and the other with HPFRC. The software used for the analysis is 'Extreme Loading for structures' (ELS) which uses the 'Applied Element Method' (AEM). The AEM is based on discrete crack approach which is capable of tracking the actual behavior of structure up to total collapse. The results were based on nonlinear dynamic analysis scheme.

1.2.Thesis Outline

This thesis contains six chapters in addition to this chapter. Each chapter discusses a certain issue as follows:

Chapter 2: Literature review

This chapter presents the conclusions of previous work related to the behavior of coupling beams under seismic load and the use of HPFRC to construct coupling beams.

Chapter 3: Analytical method

This chapter discusses the analytical method used (AEM) and the software used in the analysis (ELS).

Chapter 4: Case study

This chapter describes chosen structure used in this study, its concrete dimensions, reinforcement detailing for different cases, and different loading values. Moreover, it presents the material properties used in this study.

Chapter 5: Analysis results

This chapter presents the results obtained from analysis for each case.

Chapter 6: Discussion of the analytical results

This chapter discusses the obtained results and compare between the results of different cases.

Chapter 7: Conclusions and recommendations

This chapter contains the conclusions and recommendations for future research.

CHAPTER 2: LITERATURE REVIEW

2.1.Introduction

In this chapter, a summary of past studies carried out on the behavior of conventionally and diagonally reinforced concrete coupling beams will be discussed. It will also give brief background information on fiber reinforced concrete and previous studies on fiber reinforced coupling beams. Finally, it will give an introduction of the 2011 ACI Building Code seismic provisions [5] for coupling beams.

2.2.Overview of Previous Studies on Coupling Beams

2.2.1 Background

Structural wall systems have been used to resist seismic loading acted on high rise buildings, coupling beams also have been used to connect the walls to provide more stiffness for the system. Coupling beam can sustain the cyclic load on the inelastic stage so it needs to provide sufficient ductility capacity, energy dissipation capability and low degradation of strength and stiffness.

Previous studies have shown that coupling beams are different from the conventional beams in moment resisting frames as coupling beams are able to be exposed to a higher shear stress reaches $6\sqrt{f_c'}$ (psi) or higher and the span-to-depth ratio $^{Ln}/_{h}$ is less than three, in addition coupling beams are encountered to large inelastic end rotation demands and yield excursions [6]. To guarantee high levels of toughness and ductility, the following parameters must be taken into consideration in their design [6] [7].

a. **Aspect Ratio ($^{Ln}/_{h}$):** Coupling beams with aspect ratio equals to or less than two are more common. The behavior of this coupling beam differs from the conventional beam as the arch action contributes more to shear strength than flexural strength especially when the ratio $^{Ln}/_{h}$ decreases.

b. **Shear Stress**: The type of failure of each coupling beam depends on the value of shear stresses. If the value of shear stresses is less than $3\sqrt{f_c'}\ (psi)$, the flexural failure will occur and the coupling beam needn't diagonal reinforcement, only longitudinal and transverse reinforcement is required [6]. When the value of shear stresses is between $3\sqrt{f_c'}$ and $6\sqrt{f_c'}\ (psi)$, flexural-shear failure occurs. Finally, when the value of shear stresses exceeds $6\sqrt{f_c'}\ (psi)$, sliding-shear failure dominate, at this case, the diagonal reinforcement is required.

c. **Reinforcement Details:** Under load reversals, the configuration of the reinforcement controls the behavior of the coupling beams.

d. **Anchorage of Beam Flexural Reinforcement:** The ends of the coupling beams are exposed to inelastic deformations due to load reversals, so the anchorage of reinforcement of coupling beams in the walls affects the response under loading [8][9].

2.2.2 Types of Failure Modes

Applying reversed load on a system of coupled shear walls causes flexural or shear failure depending on the aspect ratio of coupling beams. Flexural failure causes coupling beams to bend in a double curvature pattern but shear failure develops tension forces on top and bottom along beam length. However, deep coupling beam might fail in a diagonal tension mode, this mode cause coupling beams to be separated into two triangle parts, moreover, shear sliding failure mode might be existed in which flexural and shear cracks propagate across beam length at its end [10].

2.2.3 Overview of Proposed Reinforcement Schemes

Prior to 1964 Alaska earthquake, conventional reinforcement used to construct coupling beams. This reinforcement consists of longitudinal flexural bars, transverse reinforcement and horizontal distributed bars. According to Paulay [11] who first tested using of conventional reinforcement to construct coupling beams, with low aspect ratio of 1.02 to 1.29, the conventional reinforcement is not capable of sustaining seismic load. As Shear failure is dominant for these specimens also failure mechanisms such as diagonal tension and sliding shear occurred and there is loss in stiffness after few cycles on inelastic range.

However, coupling beams failed due to insufficient shear capacity as shear is resisted by aggregate interlocking, dowel action and transverse reinforcement so several studies have made to understand the behavior of conventional reinforcement and to find the appropriate reinforcement scheme to construct coupling beams.

Paulay and Binney [12] suggested to construct coupling beams using diagonal reinforcement to improve their behavior by providing shear and moment capacities using diagonal reinforcement as follows assuming that reinforcement reaches yield stress Figure (2-1). Using diagonal reinforcement improved the properties for this element to sustain seismic loading

$$\mathbf{T_u = C_u = A_s f_y} \quad \text{Eq. (2-1)}$$

$$M_u = A_s f_y \cos\alpha\,(h - 2d) \quad \text{Eq. } (2-3) \qquad V_u = 2T_u \sin\alpha = 2A_s f_y \sin\alpha \quad \text{Eq. } (2-2)$$

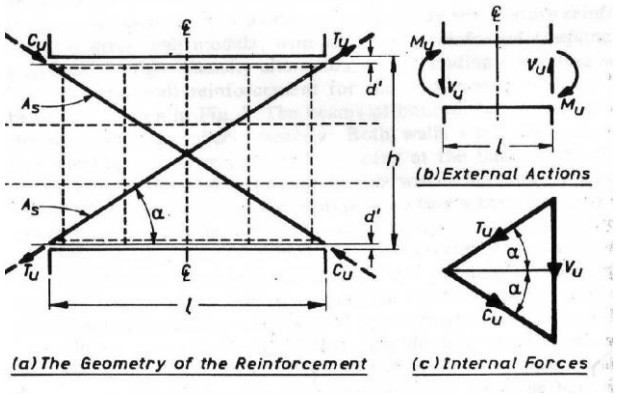

Figure (2-1): Forces in a diagonally reinforced couling beam [13]

Where;
C_u is the compression force in diagonal reinforcement.
T_u is the tension force in diagonal reinforcement.
A_s is the diagonal reinforcement area.
F_y is the yield strength of diagonal reinforcement.
α is the angle of diagonal reinforcement with beam longitudinal axis.
h is the beam depth.
V_u is the shear force exists when the reinforcement yields.
M_u is the moment capacity developed when the reinforcement yields.

Paulay and binney [12] tested three diagonally reinforced coupling beams with aspect ratios of 1.0 to 1.3 to verify the ability of full-length diagonal reinforcement to prevent the sliding shear failure. The slender coupling has a shallow angle of the diagonal inclined bars.

Test results showed that using diagonal reinforcement increases ductility and energy dissipation to short spans coupling beams and the failure occur due to buckling of diagonal reinforcement so it was recommended to use closed stirrups along diagonal bars to confine the concrete inside the steel cage, thus provide more stability. Moreover, Paulay and Santhakumar [13] tested one-quarter scale model of coupled shear wall with coupling beam aspect ratio equals to 1.25. Test results showed that Paulay and binney [12] specimens' reach considerable ductile behavior and failure of this specimens occurred due to buckling of compression reinforcement.

Barney et al. [14] carried out a series of tests at the Portland Cement Association; specimens have aspect ratios equals to 2.5 or 5.0. Different reinforcement configurations were used. Test results showed that diagonally reinforced coupling beams dissipate energy more than conventionally reinforced coupling beams at aspect ratio of 2.5 but it was recommended that no need to use diagonal reinforcement to construct coupling beams with aspect ratio equals to 5.0 as it acted like conventionally reinforced coupling beams.

An experimental investigation was created to reach an approach to prevent elements from splitting shear. Therefore, Tegos and Penelis [15] tested twenty-four column and coupling beams with aspect ratios vary between 2.0 and 5.0 under cyclic or monotonic loading and applied axial load. Eighteen specimens have the rhombic layout, three specimens have longitudinal and transverse reinforcement and their specimens have diagonal reinforcements Figure (2-2). Test results showed that rhombic layout behave slightly like diagonal configuration.

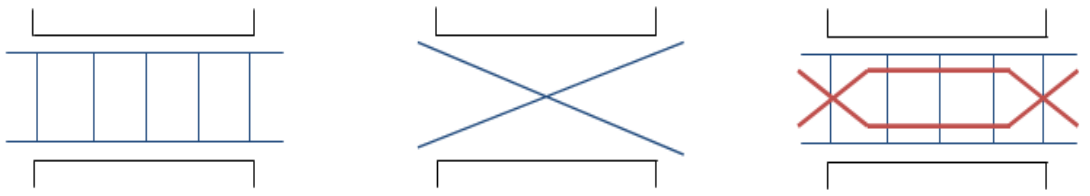

Figure (2-2): Different reinforcement layout [16]

Another testing program was created by Galano and Vignoli [17] to test the behavior of coupling beams under cyclic and monotonic loading. Fifteen short coupling beams with four different reinforcement layouts. The reinforcement layout consisted of a classical scheme, diagonal bars with confining stirrups, diagonal bars without confining stirrups and inclined bars to form a rhombic layout. All specimens have an aspect ratio of 1.5.

Test results showed that beams with diagonal or rhombic reinforcement act better than beams with longitudinal bars. The rhombic arrangement had higher rotational ductility capacity than diagonal reinforcement, but the rhombic layout develops strength 17% less than diagonal reinforcement with the same reinforcement area. The rhombic configuration has great ability to sustain shear load under repeated loading cycles at high rotation ductility. Moreover, it helps to avoid diagonal explosive shear fracture. The energy dissipated by rhombic bars slightly equals to the energy dissipated by diagonal bars. Another observation was noticed that concrete compressive strength highly affects the stability properties of the compressive strut. The specimen provided with ties, but less compressive strength showed stability problems at earlier load levels than specimen without ties and have a higher compressive strength.

Tests on slender coupling beams were also conducted by Gonzalez [18] at University of British Columbia in order to compare the results with formulas given by various codes. A full-scale model with diagonal reinforcement and an aspect ratio of 2.74 was tested under cyclic loading. In order to provide axial restrain to the coupling beam to represent the slab, Dywidag bars were provided. Test results showed higher strength and stiffness than expected using the well-known formulas, also diagonal bars showed higher ductility and energy dissipation.

Eight 1/2- specimens created by Naish et al. [19] to verify the behavior of diagonal reinforcement recommended by ACI 318-05 [20] and straight reinforcement recommended by ACI 318-08 [21]. Moreover, to assess the effect of existence of reinforced slabs. The specimens have various geometry and reinforcement configurations. The aspect ratio was 2.4 or 3.33. Five specimens with an aspect ratio of 2.4 were constructed with 4 in thick slab and two specimens with the same aspect ratio have the same slab thickness and reinforcement but with post-tensioned strands.

Test results showed that beams detailed with straight reinforcement according to ACI 318-08 [21] have strength and ductility slightly better than beams reinforced by diagonal bars. Moreover, existence of RC slabs increases the shear capacity by 15 to 20% and including post-tensioning increases the shear capacity by an additional 10%. The strength increase was due to the increase in beam moment strength. Damage noticed at the beam-wall interface in the form of slip of diagonal reinforcement, also applying axial load using post-tensioning doesn't enhance this behavior. Beams not detailed with full section confinement experience more damage at large rotations.

Another testing program was created by Han et al. [22] to test the behavior of precast coupling beams with bundled diagonal reinforcement Figure (2-3-c). In order to verify the proposed design, four 1/2- scale specimens with aspect ratios between 2 to 3.5 were tested under earthquake type cyclic loading. The use of bundled bars is suggested to check the ability of replacing the recommended diagonal reinforcement Figure (2-3-b) by bundled bars to simplify construction procedure.

Test results showed that precast coupling beams with bundled reinforcement showed an adequate ductility and energy dissipation similar to cast in situ diagonally reinforced coupling beams. Moreover, as a result of bundling the angle between bundled bars and longitudinal axis of the beam increased Figure (2-3-a), thus the moment and shear capacity increased. Bundled bars provide enough space within the beam, Therefore workability increase.

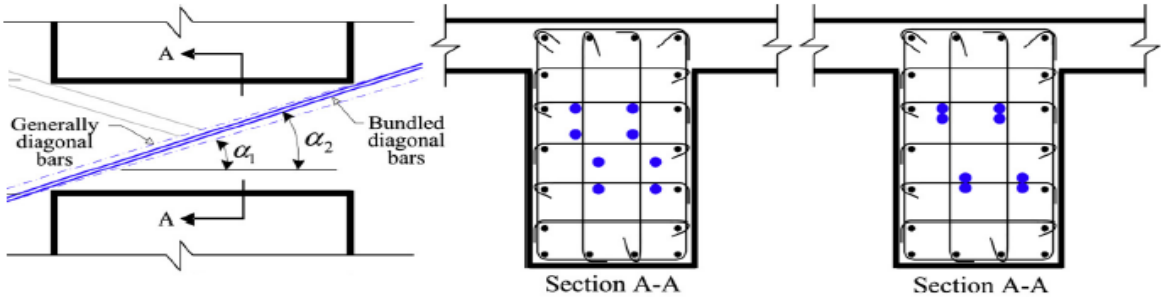

(a) **(b)** **(c)**

Figure (2-3): (a) Increase in the angle of bundled diagonal bars with beam longitudinal axis, (b) Coupling beam reinforcement detail according to ACI 318-11[5], and (c) Bundled diagonal bars coupling beam reinforcement detail. [22]

2.3 Overview of Fiber Reinforced Concrete

The concept of adding fibers to improve material properties is ancient. Egyptian and Babylonian epochs first used straw to reinforce mud bricks ACI 544.1R-96 [23]. In 1874, metallic waste was added to concrete Minelli [24]. Until early 1960s, fibers weren't used in construction. Fibers appeared in the form of fiber reinforced cement composites (FRCCs). The use of fibers as reinforcement in concrete has been growing due to researches made by Romualdi, Mandel and Zollo [25] [26].

FRCCs are composite materials consisted of two components, the matrix and the fibers. The matrix consists of cement paste, aggregates and water. Occasionally, Silica fume and fly ash are added to the matrix. There are a lot of types of fibers such as steel fibers (flat, hooked, twisted and crimped), synthetic fibers, natural fibers and glass fibers. Steel fibers are the most popular in research and industry. The main advantage of FRCCs is the ability of resist significant amount of shear stress after cracking.

FRCCs can be called as fiber reinforced concrete (FRC) when the coarse aggregates are used to form the matrix, only when the fine aggregates are used the composites are called as fiber reinforced cement composites (FRCCs).

The concept of using fibers in concrete is based on the ability of concrete to sustain compression and the ability of fibers to act as reinforcement to provide sufficient post-cracking resistance and to increase both shear and moment capacities. The fibers are randomly distributed within the matrix. When a crack is developed the fibers control the opening, then cracking continues and the maximum load reached by pulling the fibers as the fibers interact with concrete through bond, so they are expected to pull out rather than yield or fracture.

There is a special kind of fiber reinforced cement composites (FRCCs) called high-performance fiber reinforced cement composites (HPFRCCs). Naaman and Reinhardt [27] declared that (HPFRCCs) are similar to FRCCs but with an additional advantage as they can develop a quasi-strain hardening in tension and reach post-cracking

strength higher than the first cracking strength. HPFRCCs create several narrower cracks more than FRCCs and they begin to fail when the fibers start to pull out from the matrix, therefore the failure occurs because of crack localization.

The behavior of HPFRCCs is differ from that of the FRCCs after the linear stage as HPFRCCs have larger toughness due to the strain hardening occurred after first cracking up to a strength higher than the first cracking strength but FRCCs are subjected to a softening response after first cracking although FRCCs and HPFRCCs have the same linear phase as shown in Figure (2-4).

In order to achieve the strain hardening behavior, hooked and twisted steel fibers should be used with a ratio typically less than 2%. Moreover, to achieve this behavior mixture properties and matrix fiber interaction should be considered [28].

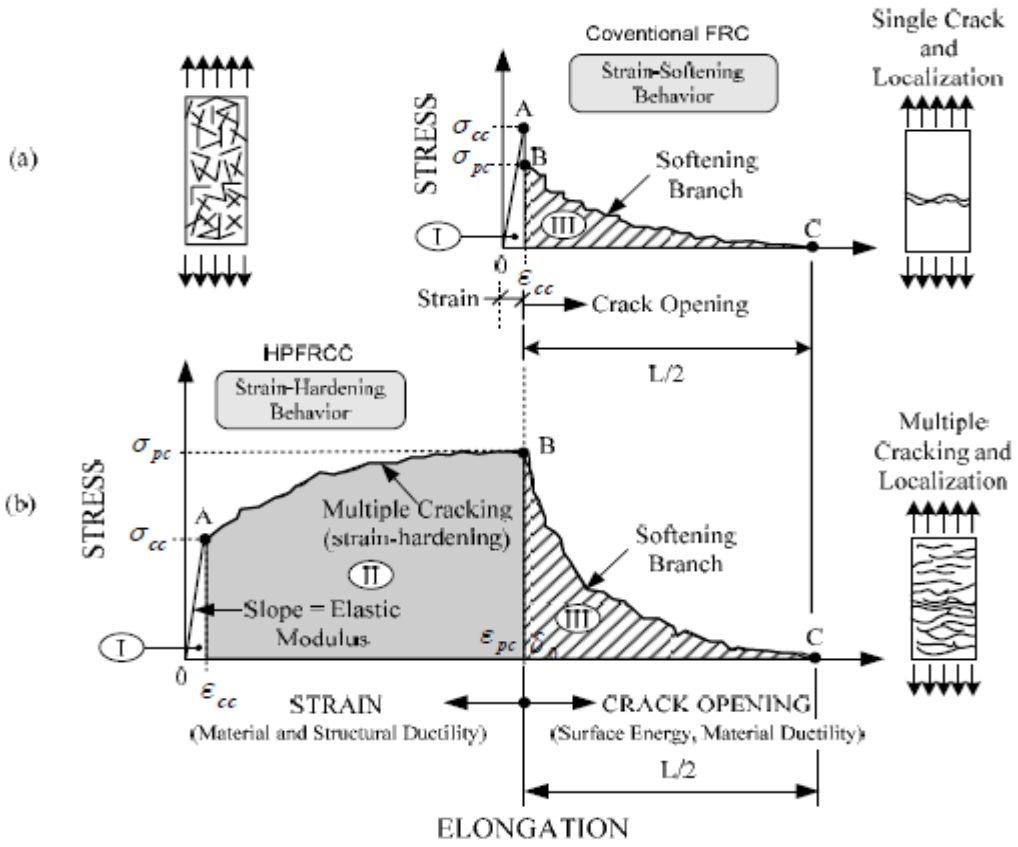

Figure (2-4): Typical tensile stress strain curve of FRC and HPFRCC [29]

For simplicity, HPFRC and FRC are used to describe HPFRCCs and FRCCs, considering using coarse aggregate to form the matrix. HPFRC represent high performance fiber reinforced concrete, and FRC represent fiber reinforced concrete.

2.3.1 Fiber Reinforced Cement Composites Properties

a) Strain Hardening and Strain Softening

Based on stress-strain response in tension, fiber reinforced cement composites can be defined as strain softening or strain hardening. In the strain softening case, the localization of cracks occurs after first crack, after first cracking, localization occurs, and the elongation increases with decreasing of stresses lower than the first cracking stress.

In the strain hardening, after first cracking, stresses increase up to maximum post cracking stress while forming multiple stresses, then stresses decrease similar to strain softening. Figure (2-5-a) shows a typical photograph for a single crack occurred during testing of a strain softening material, Figure (2-5-b) shows multiple cracks formation for a strain hardening material.

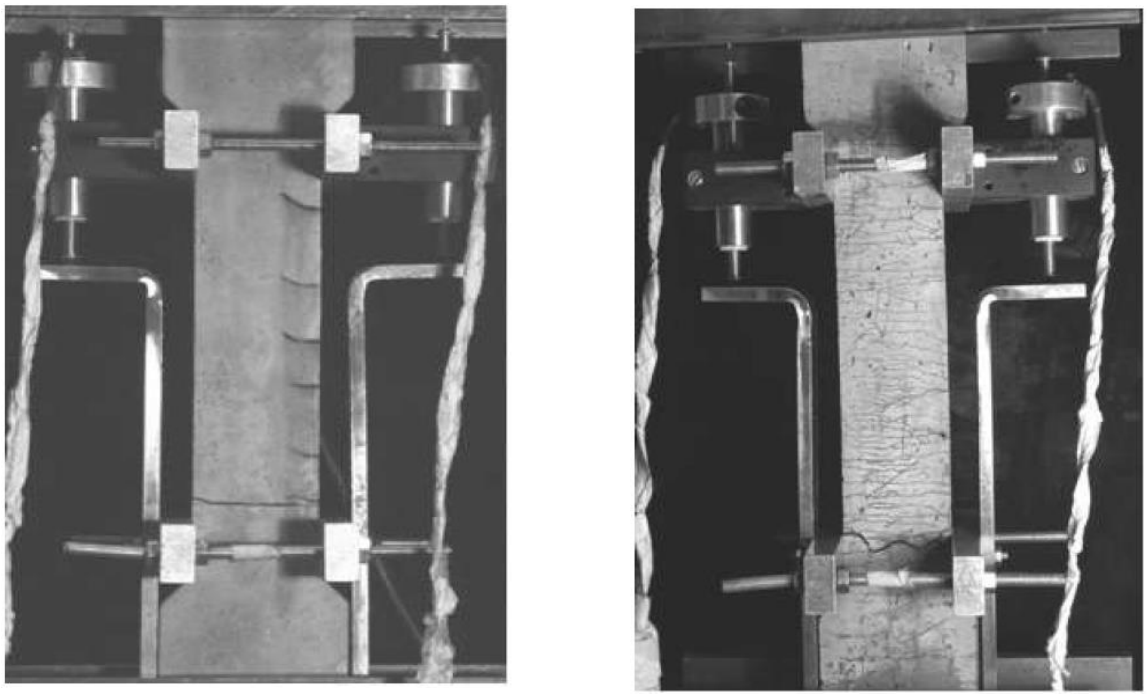

a) Strain-Softening behavior **b) Strain-hardening behavior**

Figure (2-5): Exampling of cracking behavior under tension [30]

b) Mechanical Properties

Adding fibers to FRC doesn't improve their behavior before cracking. Fibers only increase ductility of the matrix because of controlling of crack opening. Adding fibers with low ratio doesn't affect young's modulus, Poisson's ratio, and compressive strength. Fiber's material and shape, fiber aspect ratio, fiber volume fraction, and matrix composition affect mechanical properties of FRC [10].

c) Compressive Strength of FRC

Song and Hwang [31] tested 15 standard cylinders, the cylinders were loaded in a testing machine at a rate of 0.3 MPa/s till failure. The compressive strength of high strength concrete increases with steel fibers addition. At a 1.5% steel fiber fraction, the strength showed its maximum value. However, it showed slight decrease at 2% fraction compared to 1.5% as shown in Figure (2-6).

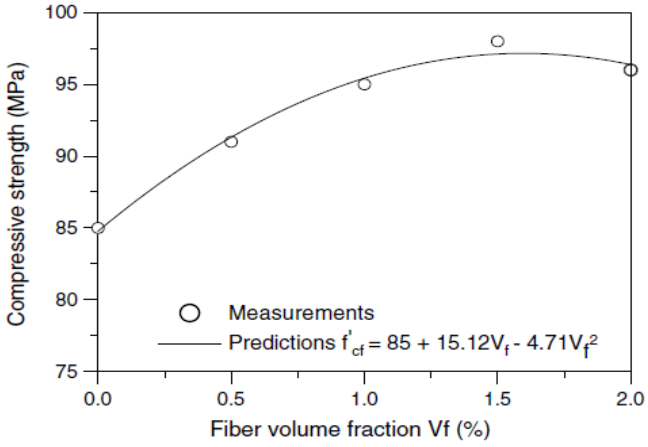

Figure (2-6): Relation between compressive strength and fiber volume fraction [31]

Moreover, existence of fibers enhances concrete ductility and toughness especially in the case of HPFRC as it permits multiple cracks without concrete spalling. Fibers volume fraction, fiber geometry and matrix contents affect ductility of FRC. Increasing fibers volume fraction increases dissipation of energy. Addition of silica fume, for example, increases the bond between fibers and the matrix; therefore this bond increases the ductility as shown in Figure (2-7) [10].

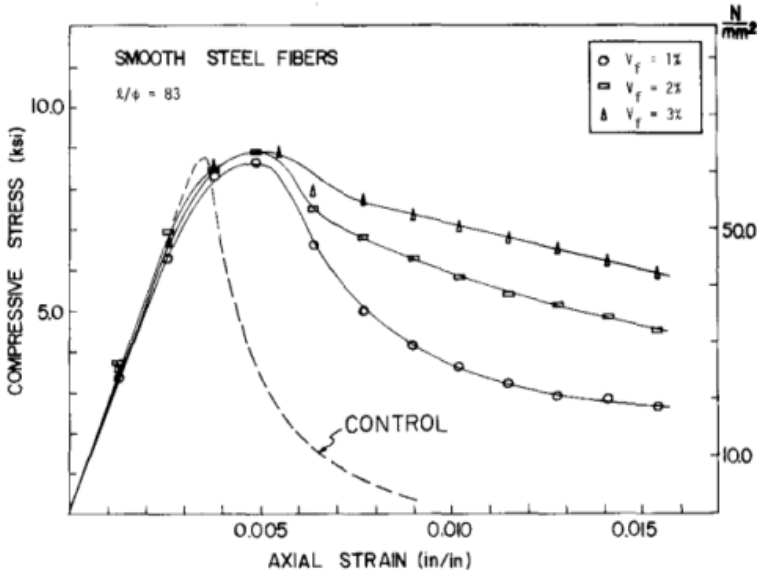

Figure (2-7): Stress-strain behavior of FRC in compression with various fiber contents [32]

d) Flexural Strength of FRC

Using of fibers in structural applications generally with a ratio less than 1.5% doesn't affect first flexural cracking strength; however, flexural post-cracking strength could be enhanced by using of deformed fibers rather than straight fibers due to bond provided by fiber deformation. Flexural toughness increases due to fibers addition, as in compression case. Toughness is measured by calculating area under load deflection curve [10].

Song and Hwang [31] tested fifteen beams under third point loading as recommended by ASTM C1018 for flexural toughness. Using index toughness (I) to compare flexural toughness gained by using fibers with nonfiber-reinforced concrete. The results are shown in Table (2-1).

Table (2-1): Toughness index Vs. fiber volume fraction [31].

Fiber volume fraction (%)	Toughness index		
	I_5	I_{10}	I_{30}
0	1.0	1.0	1.0
0.5	3.0	4.8	8.2
1.0	3.3	6.2	12.4
1.5	4.2	8.3	17.8
2.0	6.5	11.8	20.6

e)Shear Strength of FRC

Increasing shear strength is one of advantages of adding fibers to concrete as fibers randomly distributed within the element, therefore they can bridge and reduce cracks, thus increase contribution of dowel action in shear resistance, so it's important to use fibers to construct members subjected to diagonal cracks due to shear. Several researches showed the effectiveness of adding fibers on increasing shear strength.

Kwak et al. [33] tested twelve reinforced concrete beams specimens. Test parameters included fiber volume fraction (0, 0.5% and 0.75%), span to depth ratio (2, 3 and 4) and two concrete compressive strength (31 and 65 MPa). The results showed that the shear strength increases with increasing of fiber volume fraction, decreasing span to depth ratio as shown in Figure (2-8) and increasing compressive strength. In addition, as the fiber volume fraction increases, the mode of failure changes from shear to flexural.

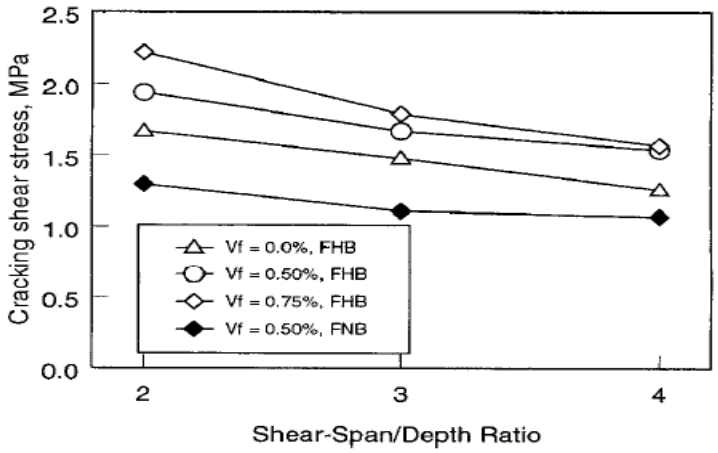

Figure (2-8): Effect of span to depth ratio on cracking shear stress [33]

Araújo et al. [34] studied six beams under shear loading using specific type of fiber. Fiber fractions ratio was 1.0 and 2.0%. The results showed that the great effect of adding fibers to increase strength and reduce crack, also they can reduce stirrups in reinforced concrete elements as shown in Figure (2-9).

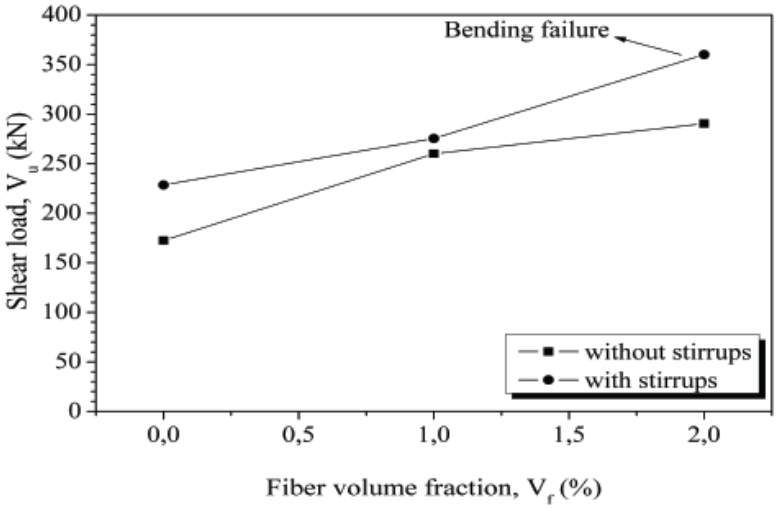

Figure (2-9): Effect of fiber volume fraction and stirrups on maximum shear load [34]

f) Splitting Tensile Strength of FRC

Zhu et al. [35] performed experimental study to determine the effect of using steel fiber on splitting tensile strength using cube and cylindrical specimens. Test results showed that splitting tensile strength increases with fiber volume fraction and aspect ratio as shown in Figure (2-10).

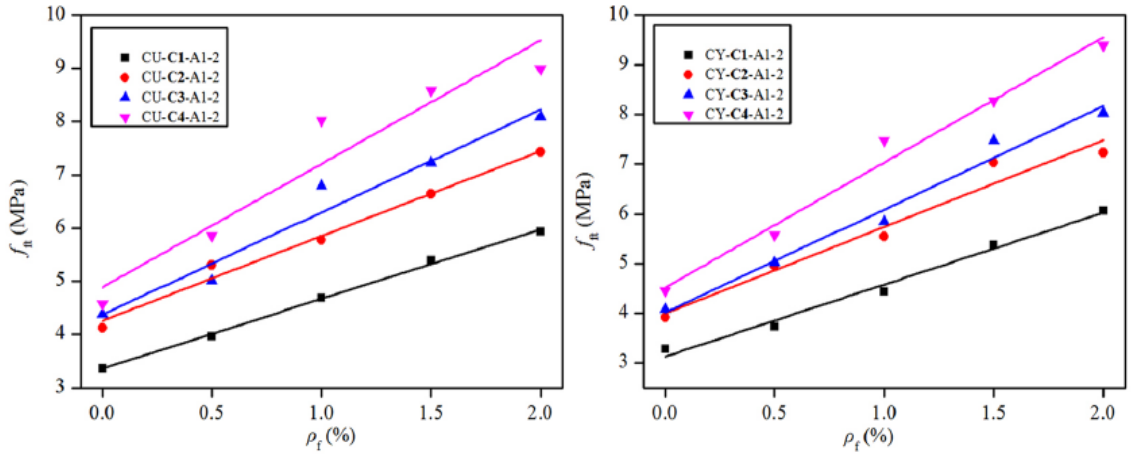

(a) **(b)**

Figure (2-10): Effect of fiber volume fraction on splitting tensile strength for different size of steel fibers (a) cube (b) cylinder [35]

2.4 HPFRC Coupling Beams

Using the advantages of HPFRC, Lequesne et al. [36] tested eight coupling beams specimens with aspect ratios ranging between 1.75 and 3.3 under cyclic load. Due to HPFRC tension and compression ductility, 30% of diagonal reinforcement, relative to ACI Building Code (318-08), was used in beams with 1.75 aspect ratios. Moreover, diagonal reinforcement was eliminated for beams with aspect ratios 2.75 and 3.3 as

shown in Figure (2-11). Results showed that HPFRC provides adequate structural behavior with coupling beams drift lower than drift capacities. Moreover, HPFRC reduces construction time and cost.

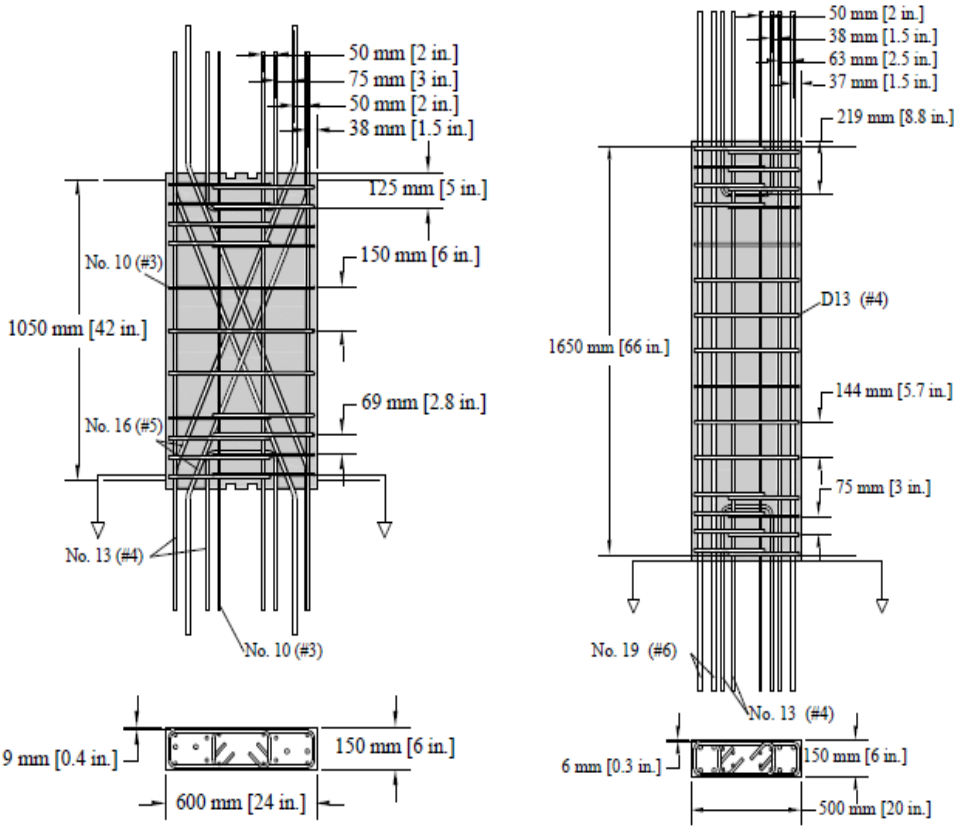

Figure (2-11): Reinforcement details for slender coupling beams [36]

Setkit [10] tested six precast fiber reinforced coupling beams under large displacement reversals in order to reduce or eliminate diagonal bars and confinement reinforcement. The parameters are aspect ratios (2.75 and 3.3), reinforcement configuration and material type (regular concrete and HPFRC). Results indicated excellent damage tolerance, stiffness retention and strength.

Zhao and Yao [37] tested three coupled shear walls specimens with 1:3 reduced scale as shown in the Figure (2-12), under reversed load to verify the effect of using HPFRC in construction of coupling beams. The first specimens were ordinary steel concrete coupled shear wall to be as a control specimen and the remaining specimens were constructed using fiber reinforced concrete. The aspect ratio of coupling beams is 2.0. Results showed that addition of steel fibers to reinforced concrete coupling beams improves stiffness. More cracks are induced to bridge the main crack and provide sufficient energy dissipation.

Cai et al. [38] tested the shear capacity of fiber reinforced concrete. Seventeen specimens consisted of 1/3 scale coupling beam with conventional reinforcement and straight steel fibers as shown in Figure (2-13) were tested under reversed load. The main parameters are the compressive strength of fiber reinforced concrete, aspect ratio and fiber volume fraction. Results showed that steel fibers improve energy dissipation and shear strength of the coupling beams, also when aspect ratio exceeded 2.5 and fiber

volume fraction exceeded 2.5%, brittle shear failure was prevented, and the coupling beam showed excellent seismic behavior.

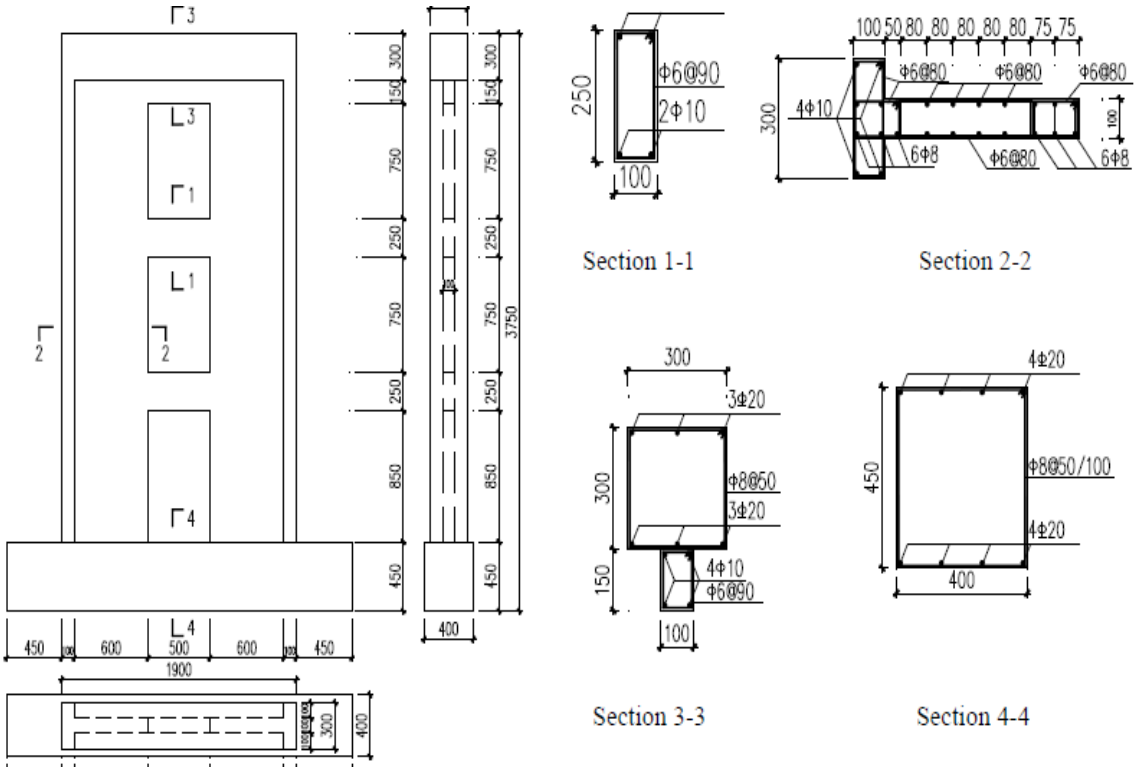

Figure (2-12): Reinforcement details of test specimens [37]

Han et al. [39] studied four coupling beam specimens with aspect ratio 2.0 or 3.5 under reversed load in order to simplify reinforcement details by reducing transverse steel by using of fiber steel and bundled diagonal bars as shown in Figure (2-14). Results indicated that HPFRC coupling beams with bundled diagonal bars and less percentage of transverse reinforcement had excellent seismic behavior if compared with regular concrete coupling beam having code requirements regarding diagonal reinforcement and transverse reinforcement.

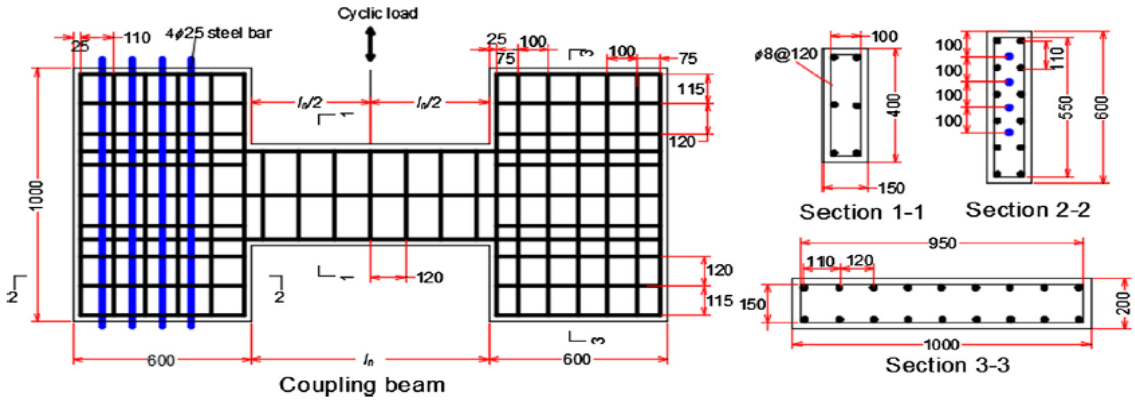

Figure (2-13): Reinforcement details of steel fiber coupling beam [38]

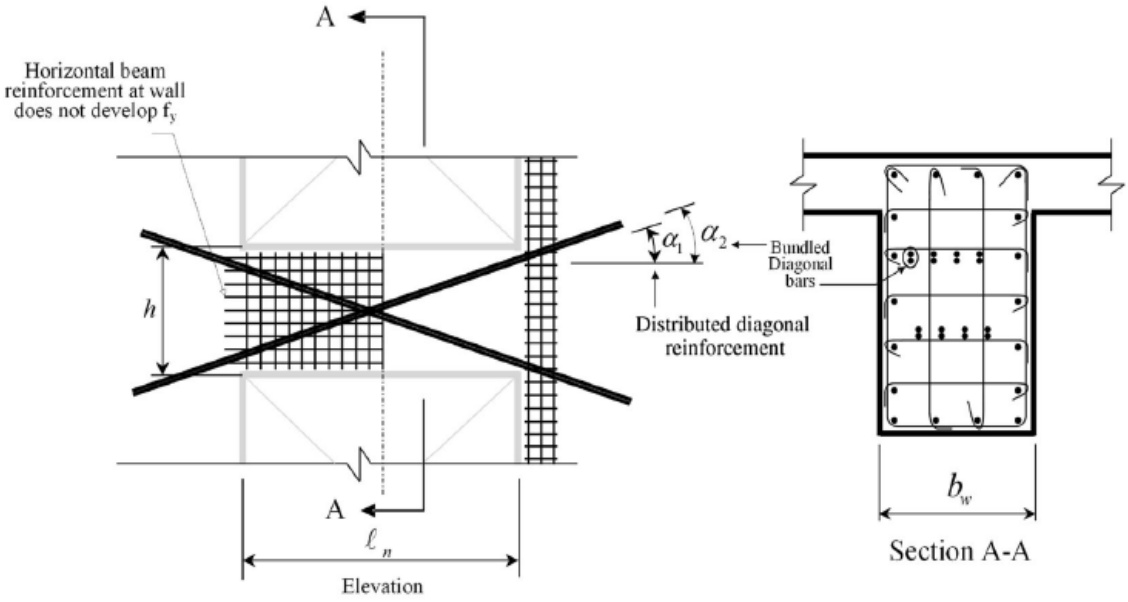

Figure (2-14): Proposed reinforcement configuration using bundled diagonal bars [39]

2.5 ACI building Code Seismic Provisions for RC coupling Beams

Requirements for the design of coupling beams are explained in Chapter 21 (21.9.7) of ACI 318-11 (2011) [5].

According to clear span (L_n) to depth (h) ratios (L_n/h)

- For $(L_n/h) \geq 4$

Coupling beams are designed as flexural members.

- For $2 \leq (L_n/h) < 4$

Coupling beams are reinforced using either conventional or diagonal reinforcement.

- For $(L_n/h) < 2$ and $\mathbf{V_n > 4\sqrt{f_c'}\, A_{cw}}$

Coupling beams are reinforced by two intersecting groups of diagonal bars symmetrical about mid span as shown in Figure (2-15) due to the probability of existence of sliding shear failure, where;

$$\boldsymbol{V_n = 2A_{vd}f_y \sin\alpha < 10\sqrt{f_c'}\, A_{cw}}$$

$\mathbf{V_n}$ is the shear stress subjected to the section.
$\mathbf{f_c'}$ is the concrete compressive strength.
$\mathbf{A_{cw}}$ is the cross-section area of the individual vertical wall considered.
$\boldsymbol{\alpha}$ is the angle between the diagonal bars and the longitudinal axis of coupling beams
A_{vd} is the area of steel reinforcement of one diagonal bars group.

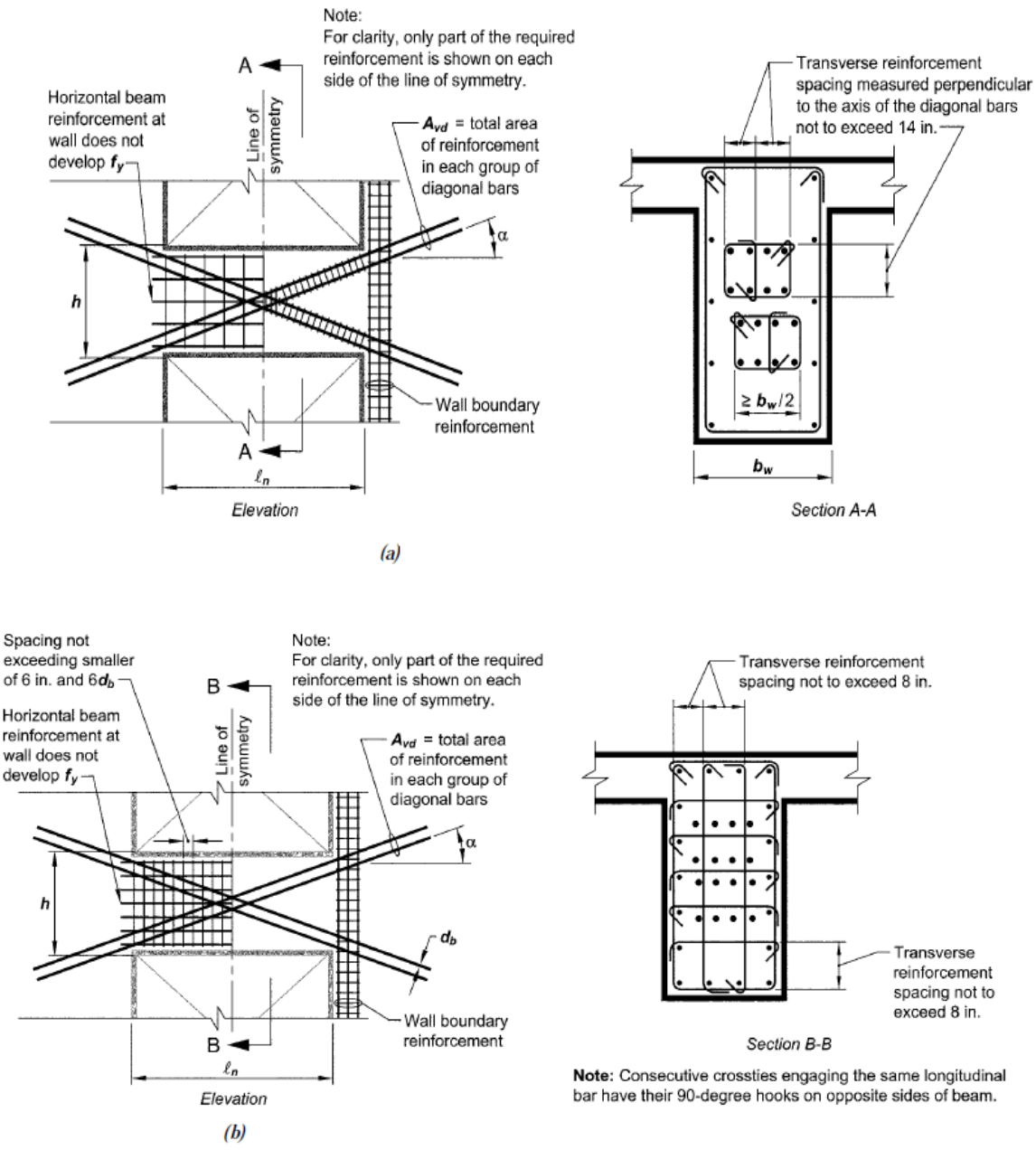

Figure (2-15): Coupling beam reinforcement details (a) Confinement of individual diagonals (b) Full confinement of diagonally coupling beam reinforcement (ACI 318-11) [5]

CHAPTER 3: METHOD OF ANALYSIS

3.1. Introduction

In this chapter, different numerical methods of structural analysis will be discussed then software package used in the analysis of the studied structure (Extreme Loading for Structures (ELS)) and its analytical method adopted by this software (Applied Element Method) will be explained.

3.2. Applied Element Method vs. Finite Element Method

Most of the programs used in seismic analysis are capable of performing nonlinear dynamic analysis. During loading, structures pass through three stages: (1) the small displacement stage where minor change in structure geometry is occurred, (2) the large displacement stage where large deformations lead to failure such as column buckling and (3) the partial or total collapse of the structure in which the structure can't resist the loads thus failure occurs. Therefore, the choice of an accurate structural analysis method to follow the formation of cracks, predict structure inelastic behavior and to determine collapse mechanisms under effect of dynamic loads is essential. The structural analytical methods can be classified into two types:

(1) Continuum material-based methods such as Finite Element Method (FEM). Such methods don't consider materials cracking, so special techniques are essential to take cracks into consideration. One of these techniques is smeared crack technique which modifies stiffness of the cracked structural elements without any existence of discontinuity or separation [41] but this technique cannot model collision of the structure.

(2) Discrete crack methods, in which the direction, propagation and the location of cracks are defined but this technique is only accurate when we can predict the location of cracks prior to analysis and this is unattainable in most structural cases [42][43].

(3) Discrete Element Methods (DEM) such as Rigid Body and Spring Model (RBSM) [44][45]and Extended Discrete Element Method (EDEM) [46].Rigid body and spring model are able to divide structure into small rigid elements connected by springs to model cracks but it cannot simulate structure collapse. The Extended Discrete Element Method (EDEM) can simulate structure collapse but it exhibits large computational errors during small displacement stages results in inaccurate collapse load, also computing geometric changes consumes a lot of time.

Therefore, researchers try to improve previous analysis techniques or to find new techniques. Then the Applied Element Method (AEM) was used to model structure from zero loading till collapse with acceptable accuracy and duration. The AEM is based on discrete crack approach. This method can track the structural behavior through all stages of loading; elastic stage, crack initiation, element separation, partial collapse of structure, and collision with the ground and other structures.

3.3. Applied Element Overview

The AEM is based on dividing the structure virtually into small elements as shown in Figure (3-1-a). Then, each two elements are connected together by one normal and two shear springs at contact points, these contact points are distributed around the element's boundaries. The actual stresses, strains, deformations or failure are represented using these springs as shown in Figure (3-1-b) [47].

In AEM, Elements are 3-D solid elements and not represented by frames or shells as FEM, the representation of elements by 3-D view connected with springs. Moreover, the FEM can't predict automatically locations of cracks due to full compatibility at the nodes . In contrast, AEM can predict crack initiation, crack widening, and full element separation depending on connecting the elements using the entire area surface. Each element has six degrees of freedom, three translations and three rotations. Relative translation and relative rotation between adjacent elements cause strain and stresses in springs at the face of contact as shown in Figure (3-2). Once the springs reach the predefined separation strain, the springs are removed, and the elements behave as rigid bodies. If the elements contacts again, the springs will generate as shown in Figure (3-3)

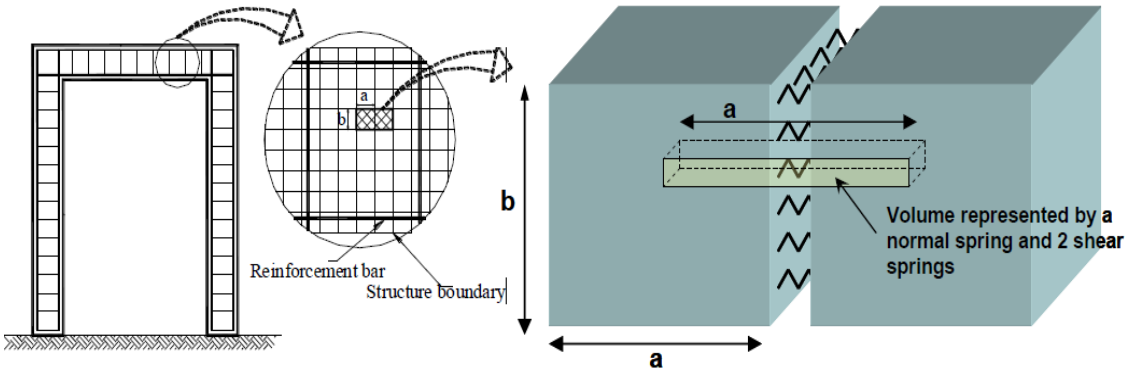

a) Element formation for AEM **b) Spring distribution around elements edges**

Figure (3-1): Structure Modeling using AEM [47]

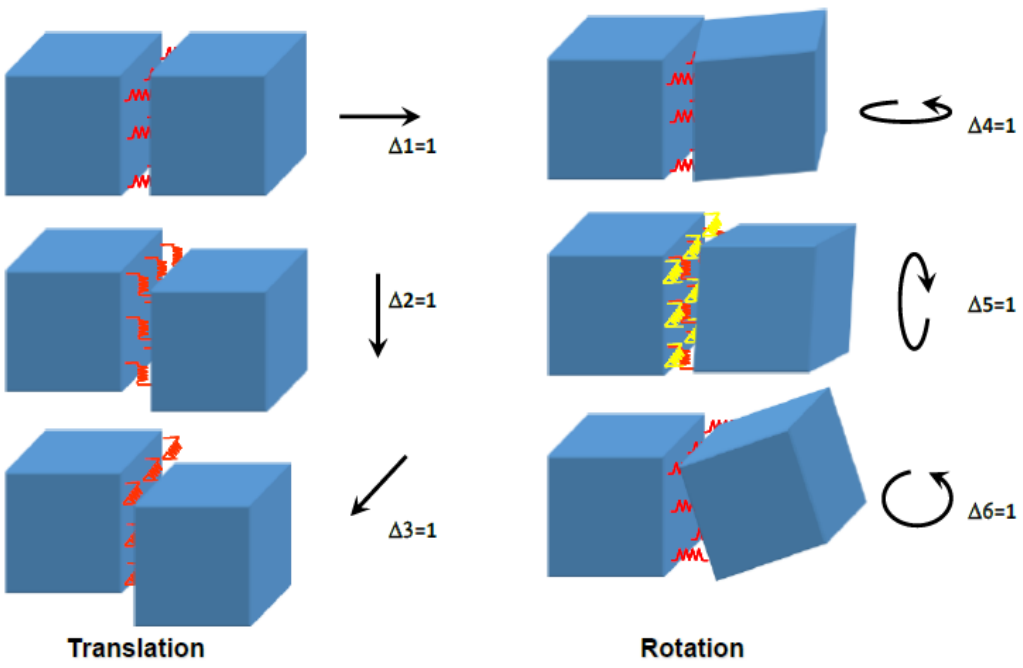

Figure (3-2): Stresses in springs due to relative displacements and rotations [47]

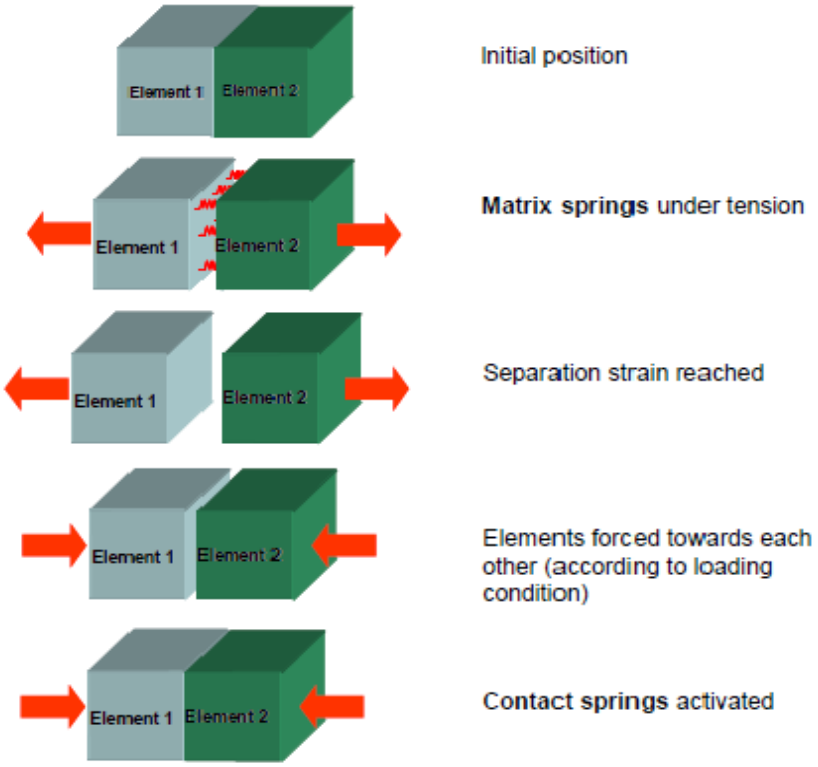

Figure (3-3): Different springs conditions during loading stages [47]

3.4. Extreme Loading for Structures (ELS®) [40]

Extreme Loading for Structures (ELS) is software based on applied element method (AEM). ELS is capable of creating nonlinear, static and dynamic, analysis of structures through elastic and inelastic stages up to structural collapse including automatic detection of cracks' locations, formation of plastic hinges, and buckling of elements.

In order to form the stiffness matrix of any rigid element in the structure. The stiffness of each spring depends on the area it serves. To determine the stiffness matrix corresponding to each degree of freedom, a unit displacement is assumed in the direction studied, then the force at the centroid of each element is calculated. Finally, the formulation of the stiffness matrix for each rigid element in the structure results in constructing the global stiffness matrix of the entire structure.

The reinforced concrete structures are shown in-detail. Each member is modeled as relatively small elements connewhencted together by springs representing the properties of concrete. The reinforcement is modeled as springs which connect concrete elements together [47].

There are several stages in which any two elements may pass through during different loading conditions [47]. First, the elements are in initial stage; the springs between them are not stressed. Second, after load application, the springs are subjected to either tension or compression till they reach the rupture or separation strain then the springs are demolished, and the elements are separated. Finally, in case of elements come in contact again, another group of springs are generated at the surface of contact between elements called contact springs. These springs simulate the state of collision between any two elements.

The AEM was used in this thesis due to its advantages. The AEM avoids the drawbacks of the FEM as it doesn’t predefine locations of cracks. Cracks and elements separations can be modeled by setting the stiffness of springs connecting the elements to zero when a separation strain is reached. Moreover, AEM can model the structural behavior under effect of dynamic loads with accuracy and reasonable time from the elastic stage, the inelastic stage, partial or total collapse, and colliding with other structures. Figure (3-4) shows a comparison between covered domains of AEM and FEM.

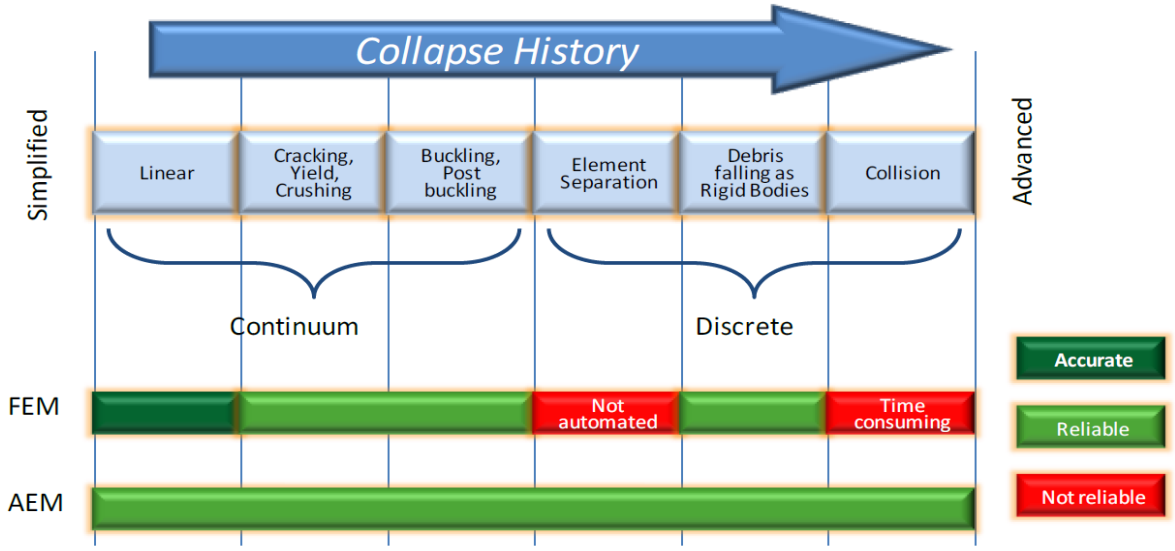

Figure (3-4): Comparison between covered domains by AEM and FEM [47]

3.5 Material Models in ELS

Different types of materials can be represented in ELS as steel, concrete, and user defined materials. The following sections discuss the models used to define these materials and its properties.

3.5.1 Concrete Models

3.5.1.1 Compression and Tension Models

The Maekawa compression model [41], shown in Figure (3-5), is used in ELS to model concrete subjected to compression. The model is presented by several parameters such as the initial Young's modulus, the fracture parameter and the compressive plastic strain. The fracture parameter represents the level of the internal damage of concrete, the plastic strain shows the residual plastic deformations in compression. Strain value at the spring location is used to calculate the tangent modulus. The model can accurately describe the reloading and unloading conditions. When concrete springs are subjected to tension, the spring's stiffness is set to its initial stiffness until it reaches the cracking point. In the next loading step, the residual stresses are redistributed through the application of the redistributed force in the opposite direction.

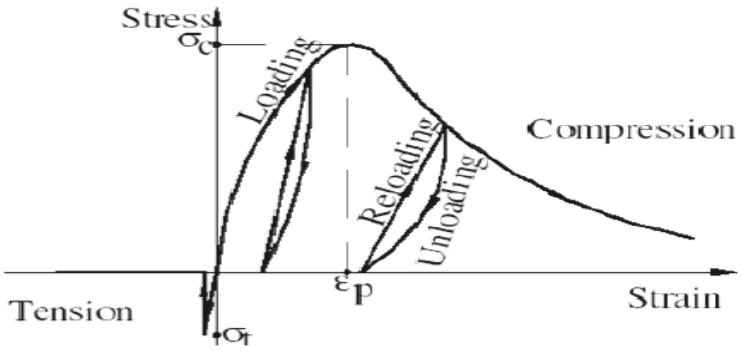

Figure (3-5): Concrete under compression and tension [47]

3.5.1.2 Shear Stresses Model

In the shear model a linear relationship is assumed between the shear stress and the shear strain till concrete cracking. When concrete starts to crack the shear stress immediately drops suddenly as shown on Figure (3-6). For concrete subjected to tension, the normal and shear stresses reach zero. For concrete subjected to compression, the shear stresses reaches a value dependent on the value of the compressive strength as shown in Figure (3-7) The drop in shear stress depends on the aggregate interlock and friction between concrete faces at crack location defined by the residual shear strength factor.

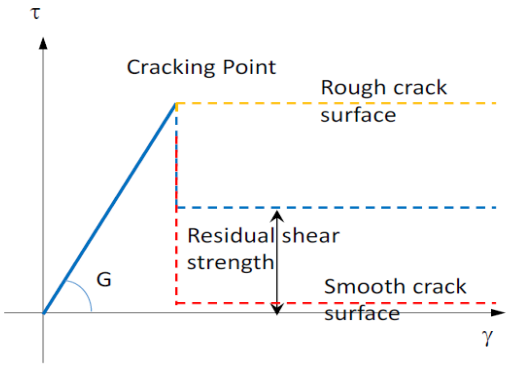

Figure (3-6): Concrete under shear stresses [47]

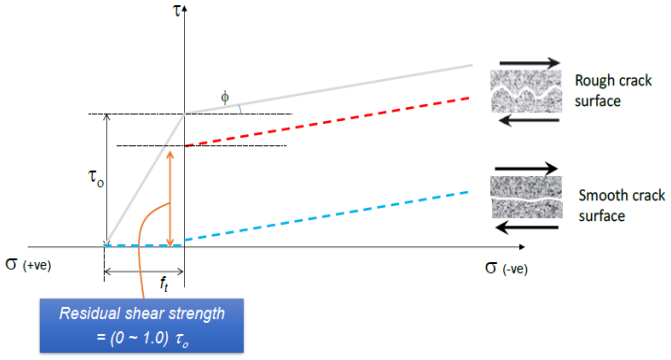

Figure (3-7): Residual shear strength [47]

The Mohr-Coulomb failure envelope as shown in Figure (3-8) is used to model the failure of the material under combined normal compressive stresses and shear stresses. When concrete is subjected to normal tensile stresses, a linear failure envelope is assumed with a maximum tensile strength of f_t where the shear stress is zero, where,

$$\tau = \tau_o + \mu\sigma \qquad \text{Eq. (3-1)}$$

τ : Shear strength under coupled normal and shear stresses
τ_o: Shear strength under pure shear
μ : Coefficient of friction = tan (ϕ)
ϕ: Angle of internal friction
σ: Normal compressive stresses

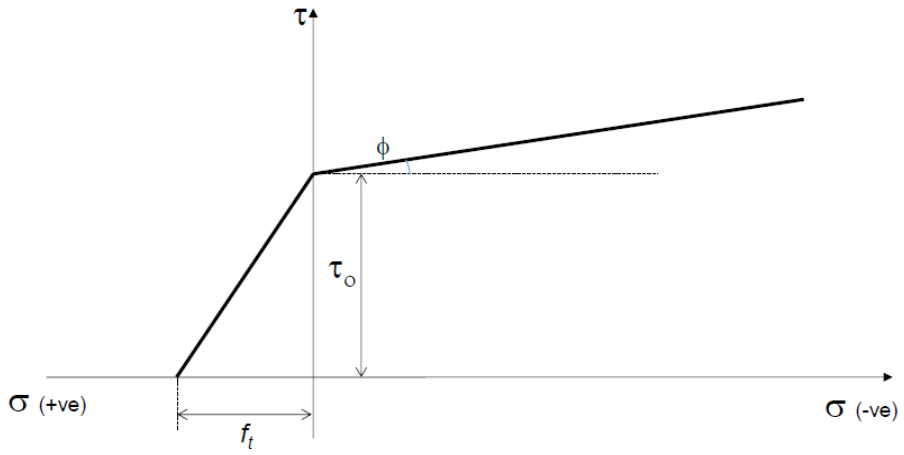

Figure (3-8): The Mohr-Coulomb failure envelope [47]

3.5.2 Reinforcing Steel Model

Reinforcement springs is exposed to three stages; elastic, yield plateau and strain hardening as shown in Figure (3-9-a).The reinforcement steel model, shown in Figure (3-9-b), presented by Menegotto and Pinto [48] is used in ELS for the analytical procedures, it illustrates unloading and reloading stress-strain models. The tangent stiffness of reinforcing steel is a function of several parameters such as the strain from reinforcing steel spring, loading status (loading or unloading), and history of steel spring which control the Baushinger's effect. The main advantage of this model is that it doesn't any additional complications to the analysis are required in order to consider the partial unloading effect and Baushinger's effect. The rupture strain of reinforcement is defined in ELS.

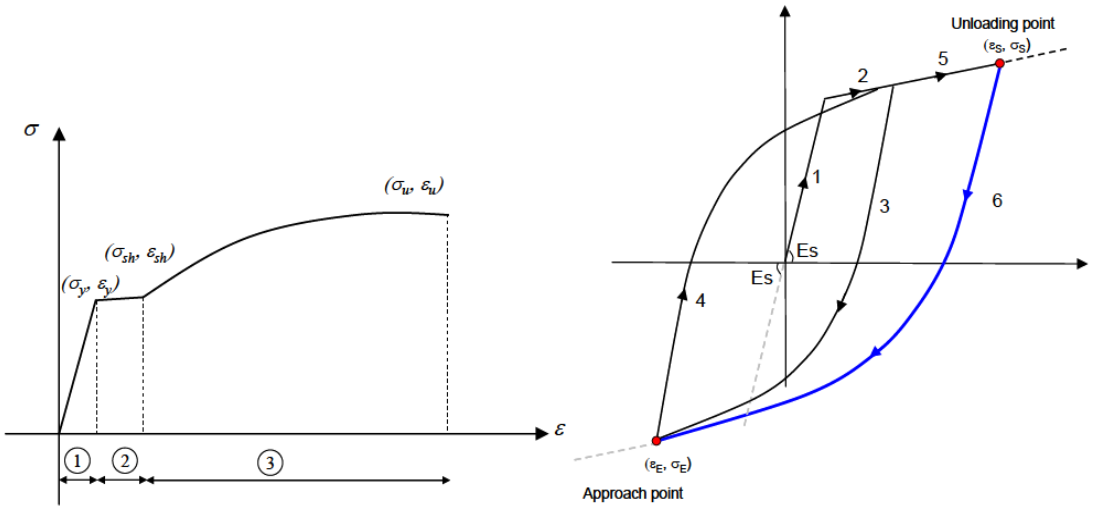

(a) (b)

Figure (3-9): Reinforcement springs under axial stresses [47]

3.6 Validation of Extreme Loading for Structures (ELS®)

The 'ELS' software was clearly validated and had shown good agreement with several cases. Several validation cases including static, dynamic, and collapse cases were covered [49][50][51][52][53][54][55][56][57][58][59]. For the current study, it's crucial to validate the behavior of the HPFRC coupling beams. Therefore, experimental data of coupling beams tested by Setkit [10] was used to validate ELS. The effect of using steel fibers on the behavior of coupling beams under cyclic loading was studied by Setkit [10]. Coupling beams of Setkit are shown in Figure (3-10). The reinforcement used for coupling beam is as shown in Figure (3-11) and reinforcement for top and bottom blocks is shown in Figure (3-12). Figure (3-13) shows the applied cyclic load. A comparison between experiment results and results obtained from ELS. The results showed good agreement with the actual case.

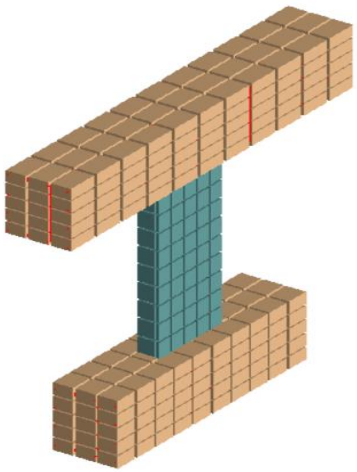

Figure (3-10) Coupling beam subjected to cyclic loading.

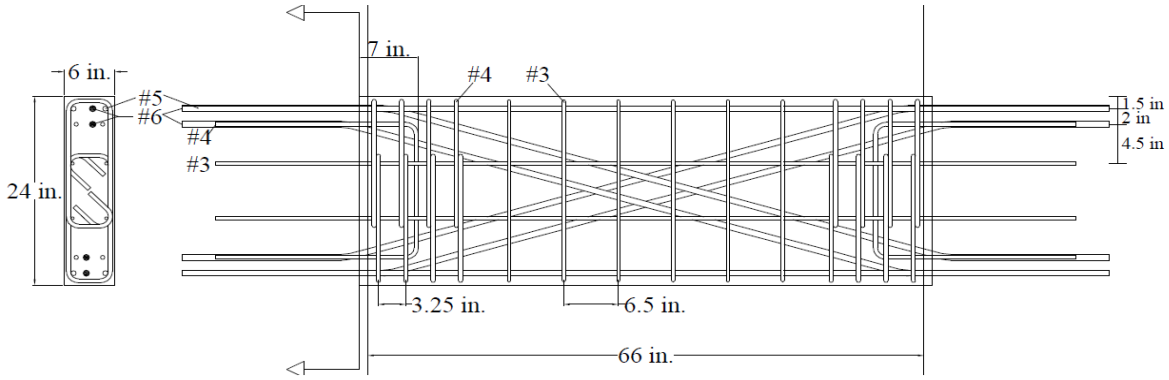

Figure (3-11): CB-4 coupling beam reinforcement [10]

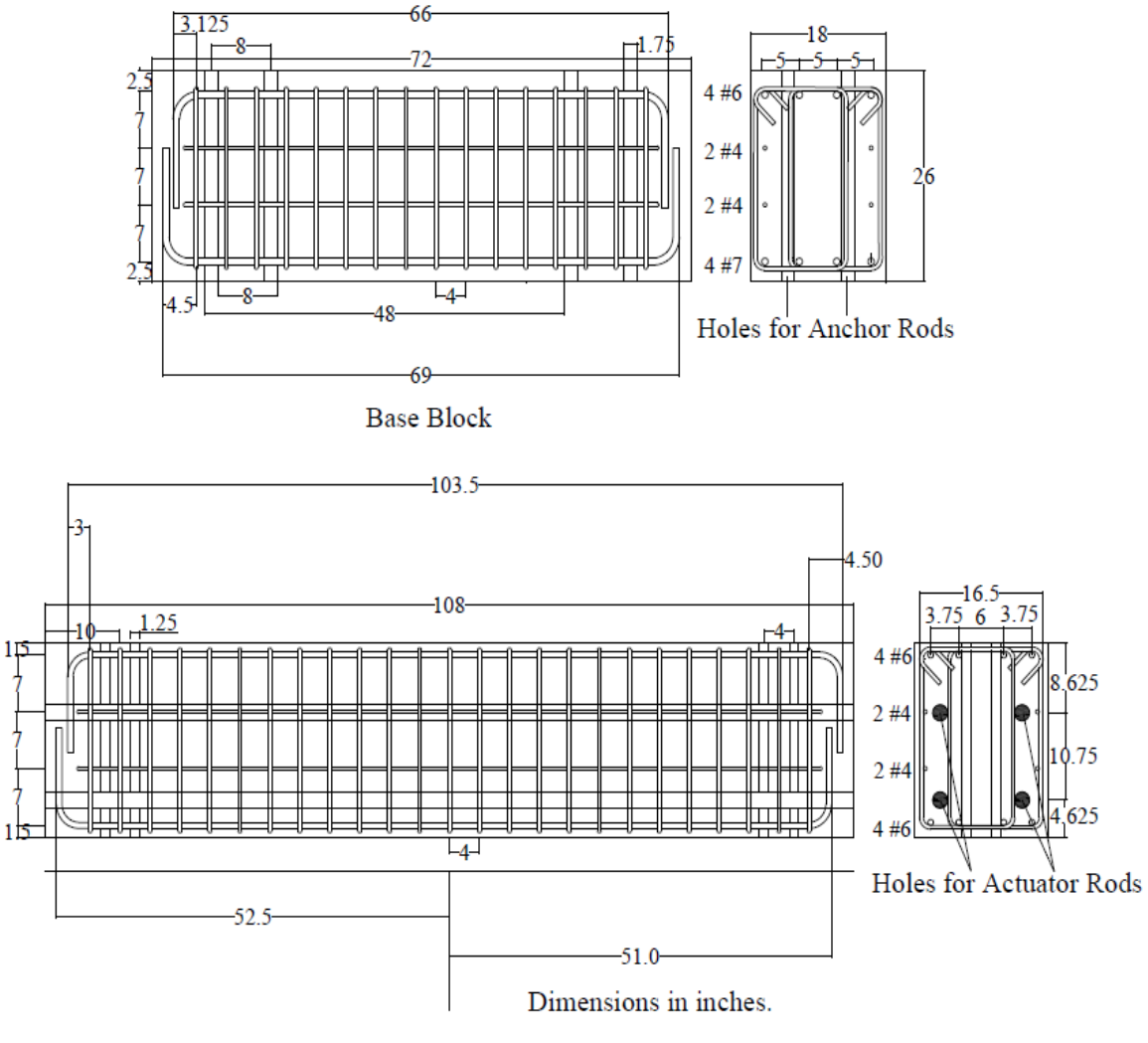

Figure (3-12): Top and bottom blocks reinforcement [10]

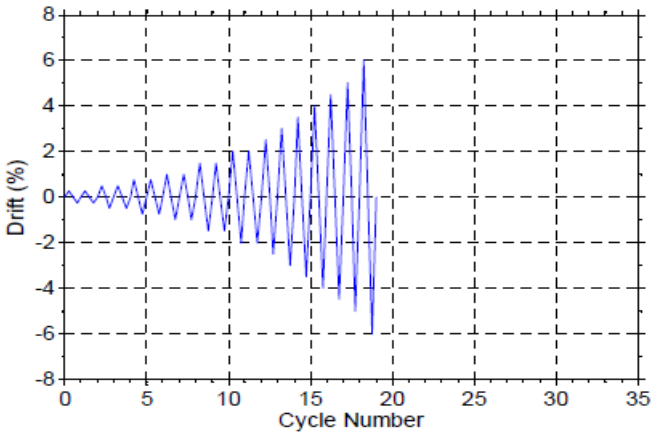

Figure (3-13): Cyclic displacement load [10]

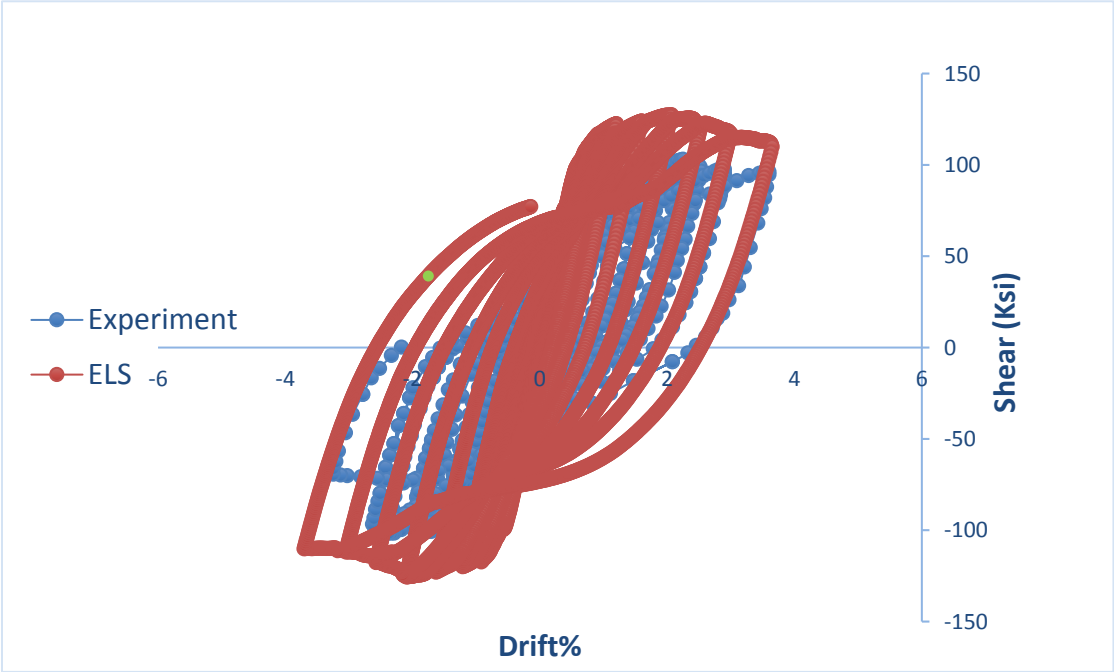

Figure (3-14): Comparison between experiment results and ELS results

User-defined material model in ELS was used to model HPFRC coupling beams. The compression model was defined according to Liao [28] as shown in Figure (3-15). The ascending part was defined as parabolic function as shown in Eq. (3-2), up to f'c of 6 and 9 ksi corresponding to compressive strain of 0.2% and 0.4% respectively. Kent and Park [60] defined the descending part as linear relation as defined by Eq. (3-3).

$$f_c = f'_c[\frac{2\varepsilon_c}{\varepsilon_o} + (\frac{\varepsilon_c}{\varepsilon_o})^2] \qquad \text{Eq. (3-2)}$$

$$f_c = f'_c[1 - Z(\varepsilon_c - \varepsilon_o)] \qquad \text{Eq. (3-3)}$$

Where,
f_c: Compressive stress of concrete at certain strain
ε_c : Compressive strain.
f'_c: Cylinder compressive strength.
ε_o: Compressive strain corresponding to f'_c
Z: Slope of the descending branch for a concrete with unit compressive strength and was assumed to be 50 to take into consideration the ductile behavior of fiber reinforced concrete.

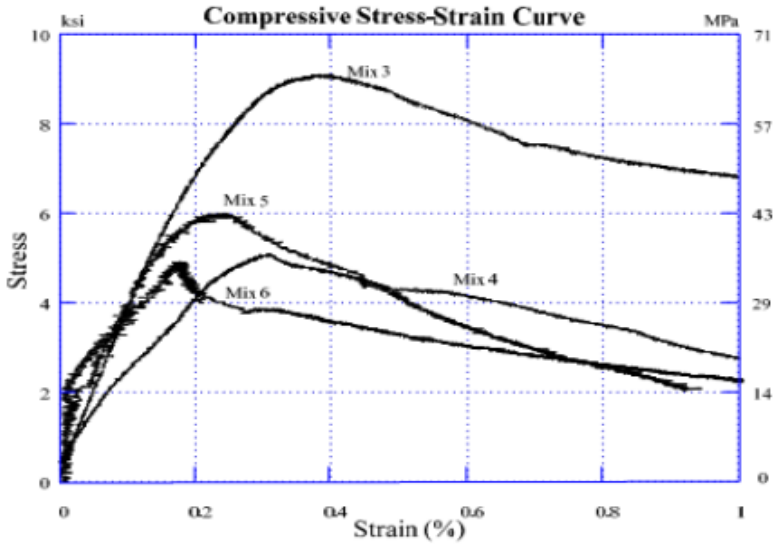

Figure (3-15): Compressive stress strain model [28]

Linear relationships were used to define the fiber reinforced concrete stress-strain behavior. Table (3-1) shows stress-strain value used to model the tensile behavior for regular concrete and HPFRC. These four points, shown in Figure (3-16), lead to best fit of stress-strain tensile model shown in Figure (3-17) [28].

Table (3-1): Stress-strain values for modeling the tensile response

Material	σ_{t1} (psi)	ε_{t1}	σ_{t2} (psi)	ε_{t2}	σ_{t3} (psi)	ε_{t3}	σ_{t4} (psi)	ε_{t4}
Regular concrete	450	0.00008	0	0.00008	-	-	-	-
HPFRC[1]	400	0.0001	500	0.005	200	0.015	100	0.02
HPFRC[2]	650	0.0001	700	0.005	200	0.015	100	0.02

HPFRC[1] for specimen CB-1
HPFRC[2] for specimens CB-2, CB-3, CB-5, and CB-6.

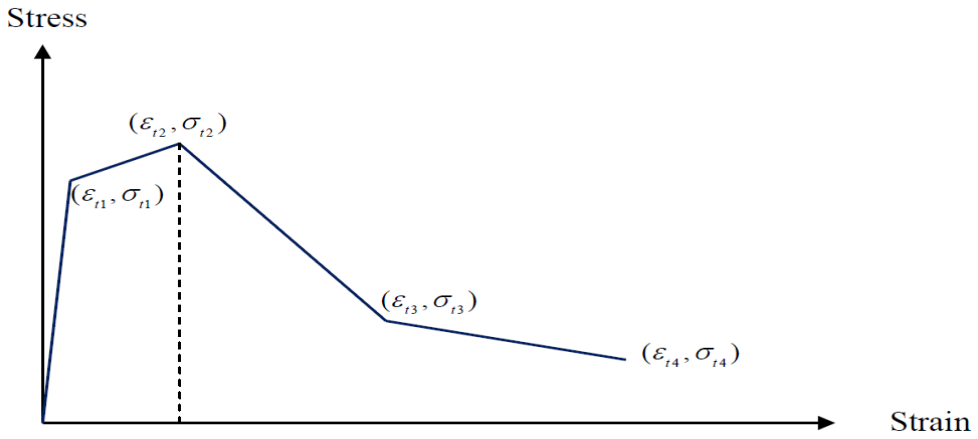

Figure (3-16): Tensile stress-strain linear relationships used in ELS [10]

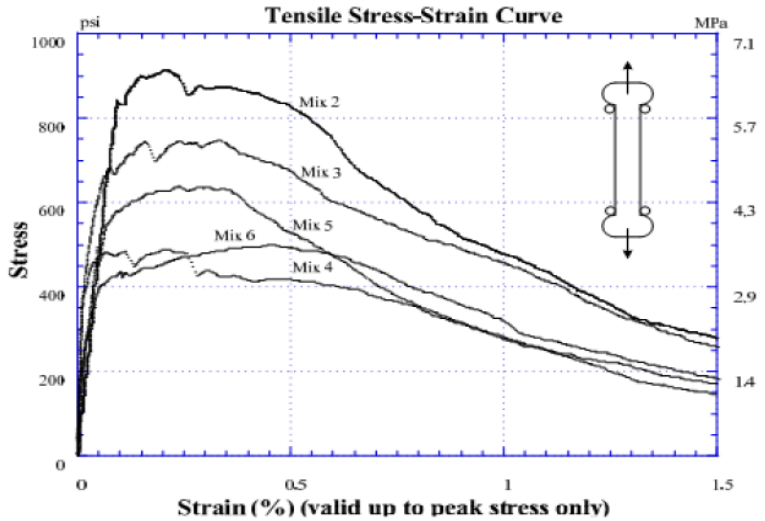

Figure (3-17): Tensile stress strain model [28]

Five specimens were modeled using ELS, namely CB1, CB2, CB-3, CB-5, and CB-6. Reinforcement detailing and concrete dimension of coupling beams for these specimens are shown in Figure (3-18). Reinforcement of top and bottom blocks is the same as specimen CB-4.

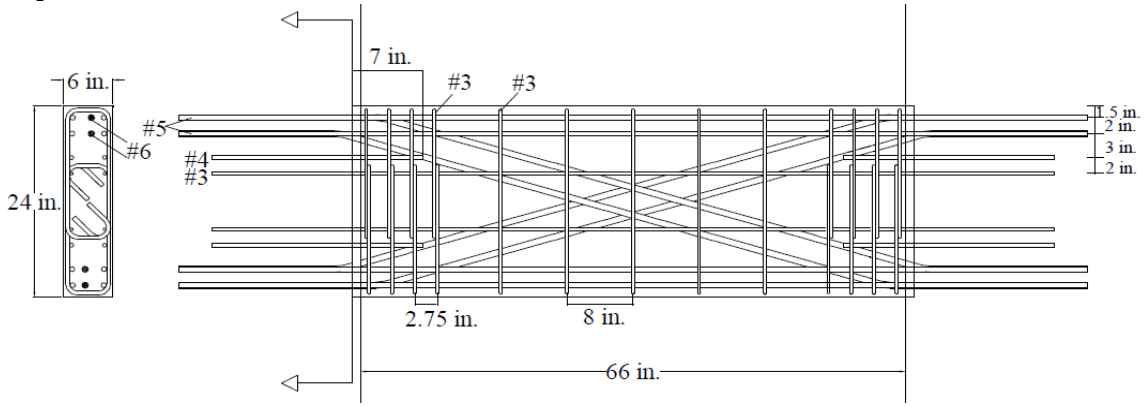

a) CB-1 coupling beam reinforcement

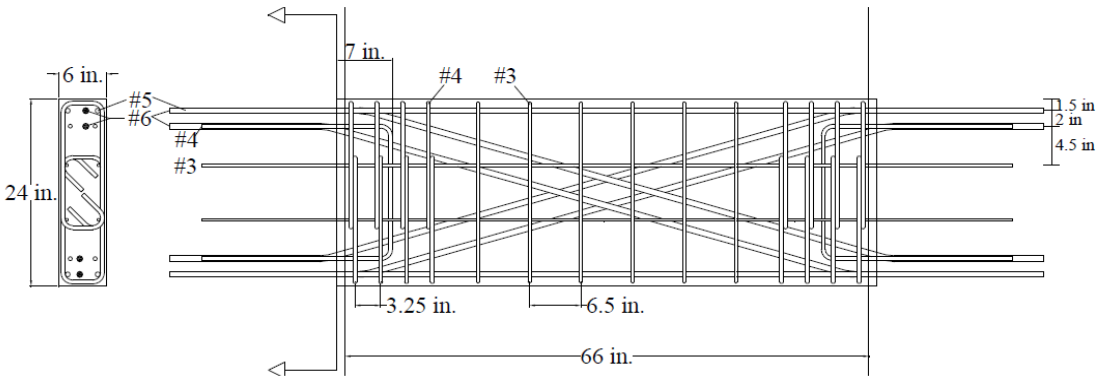

b)CB-2 coupling beam reinforcement

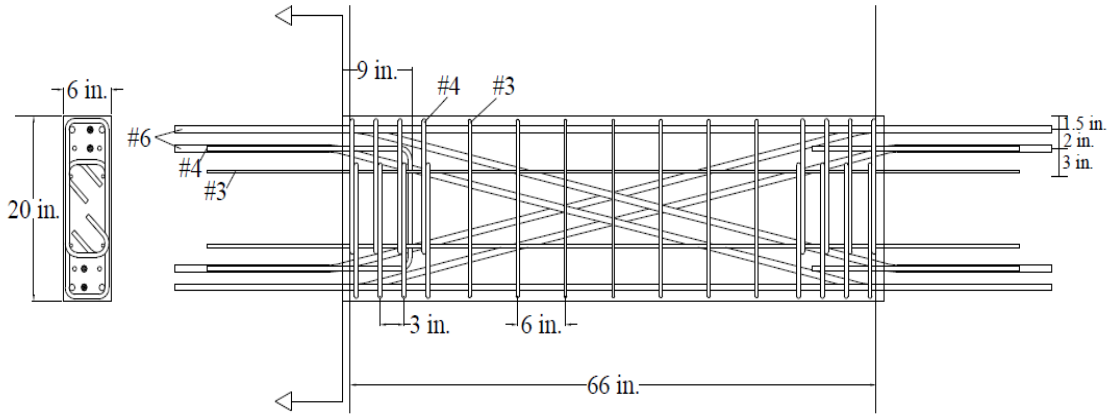

c) CB-3 coupling beam reinforcement

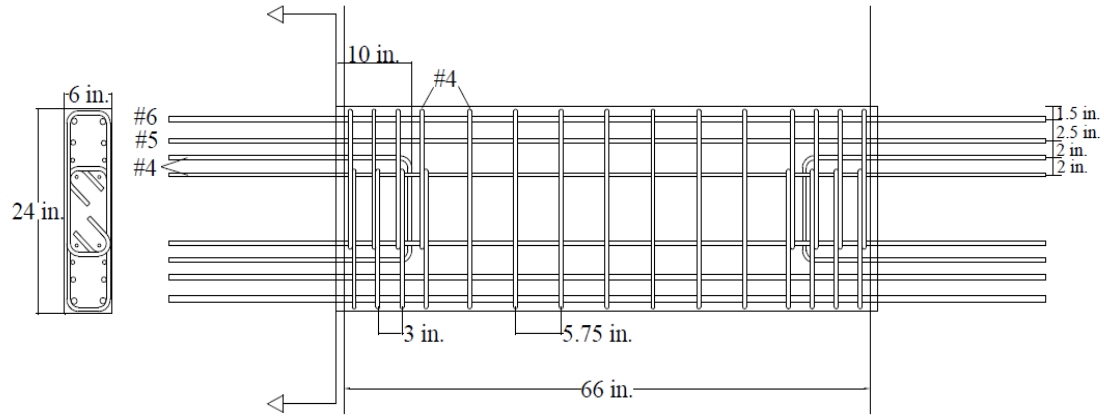

d) CB-5 coupling beam reinforcement

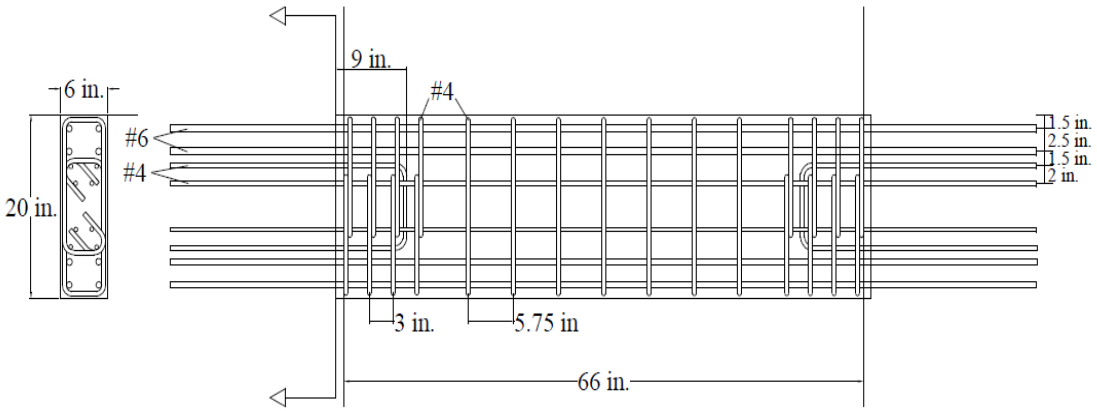

e) CB-6 coupling beam reinforcement

Figure (3-18): Coupling beams reinforcement details [10]

The specimens were subjected to cyclic displacement pattern. Displacement increases about 1 in. per minute. The whole displacement cycles are shown in Figure (3-19).

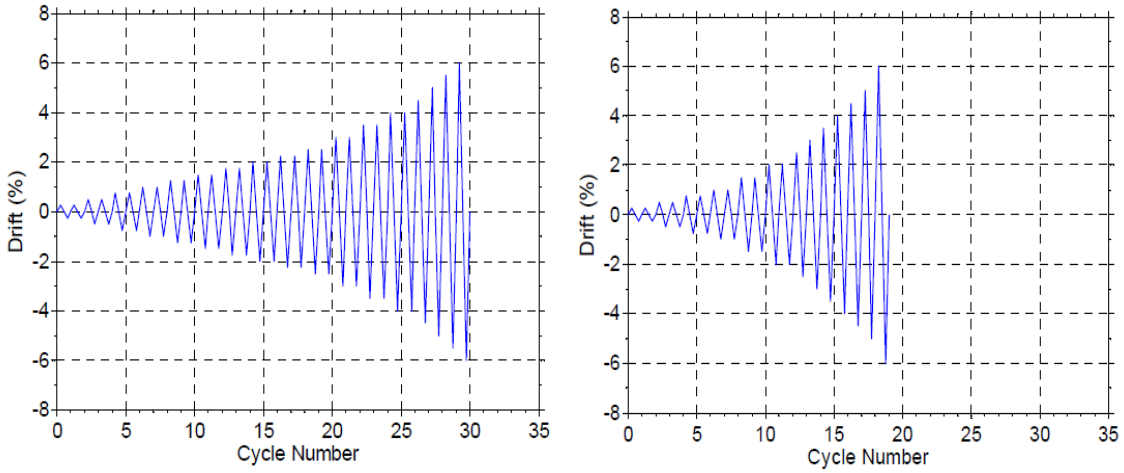

a) CB-1 **b) CB-2 to CB-6**

Figure (3-19): Cyclic displacement pattern [10]

The results obtained using ELS showed good agreement with experiment results. The comparison between ELS results and experiments results for each specimen is shown in Figure (3-20).

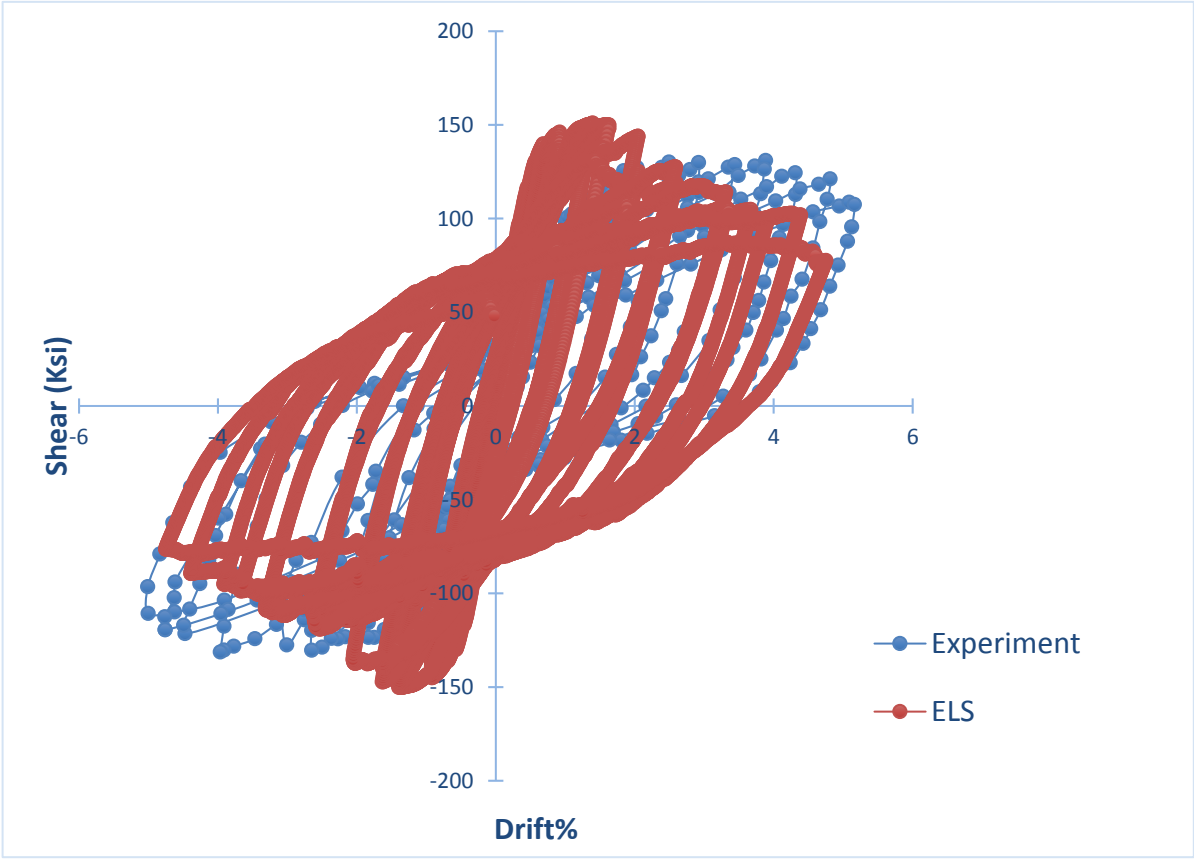

a) CB-1

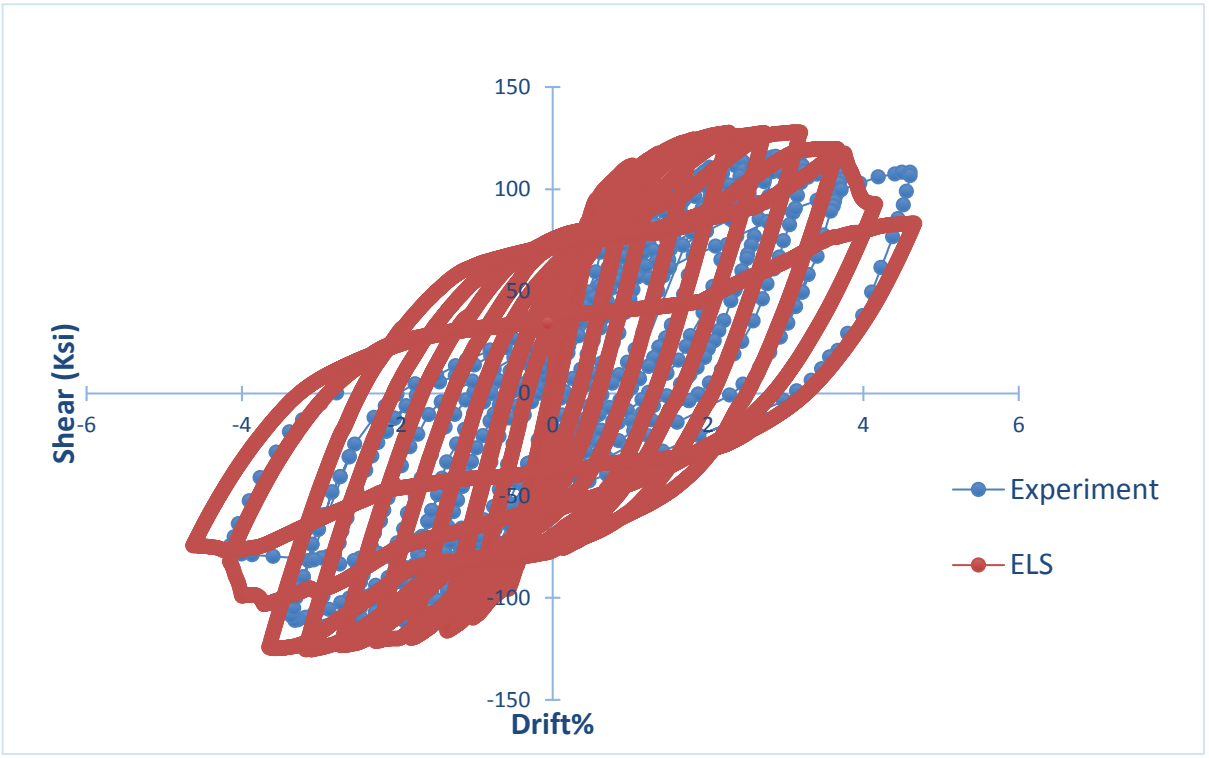
150
100
50
0
-50
-100
-150
-6
-4
-2
0
2
4
6
Shear (Ksi)
Drift%
Experiment
ELS

b) CB-2

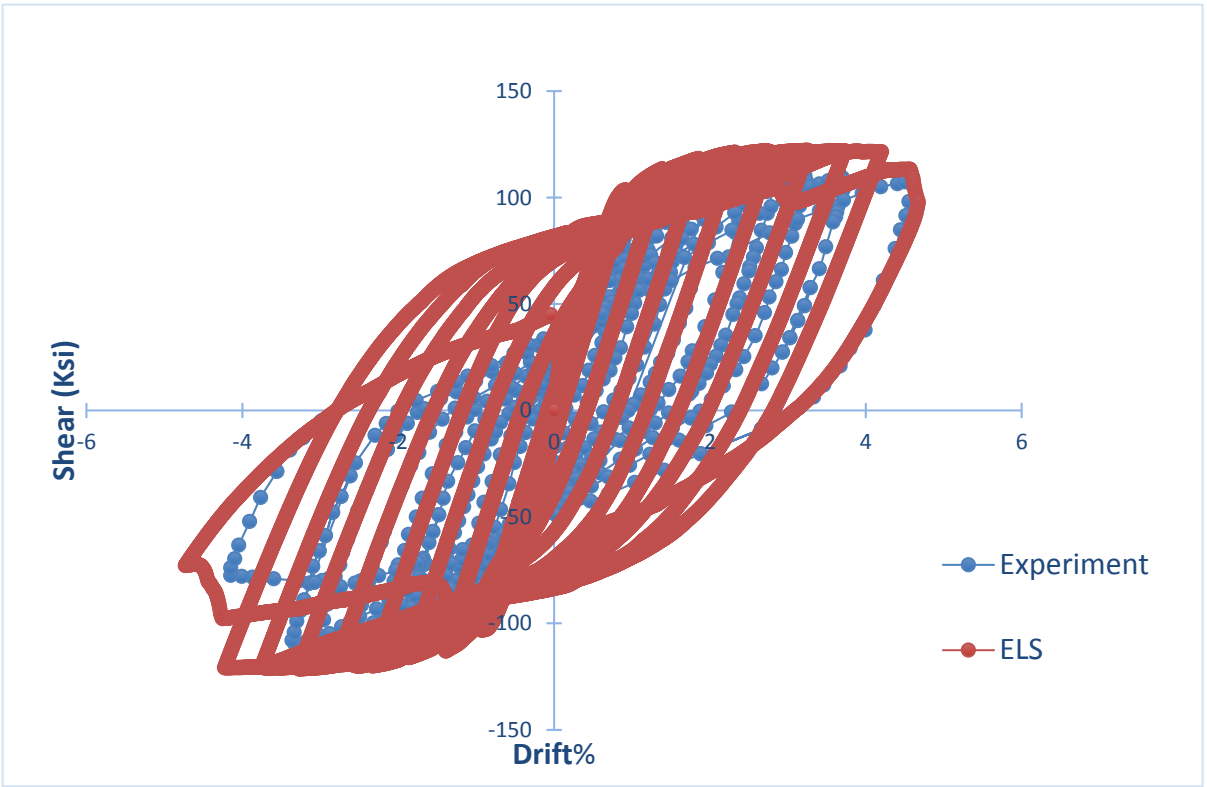
150
100
50
0
-50
-100
-150
-6
-4
-2
0
2
4
6
Shear (Ksi)
Drift%
Experiment
ELS

c) CB-3

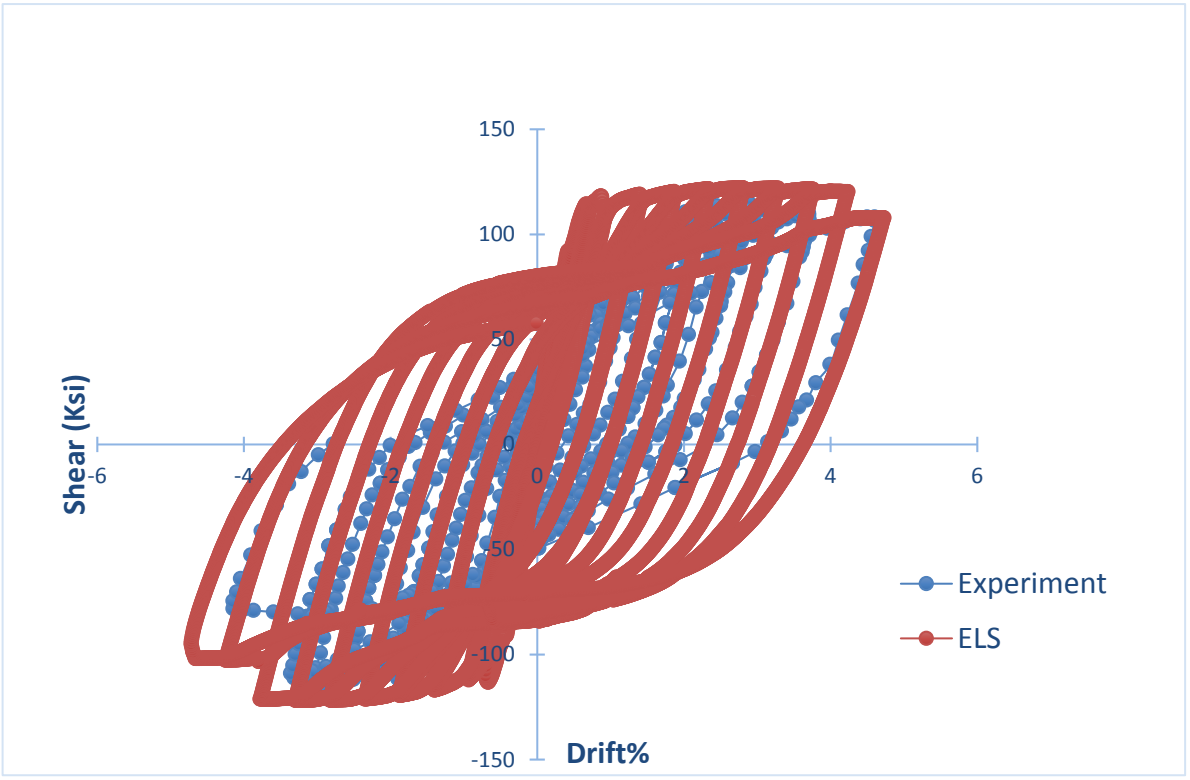

d) CB-5

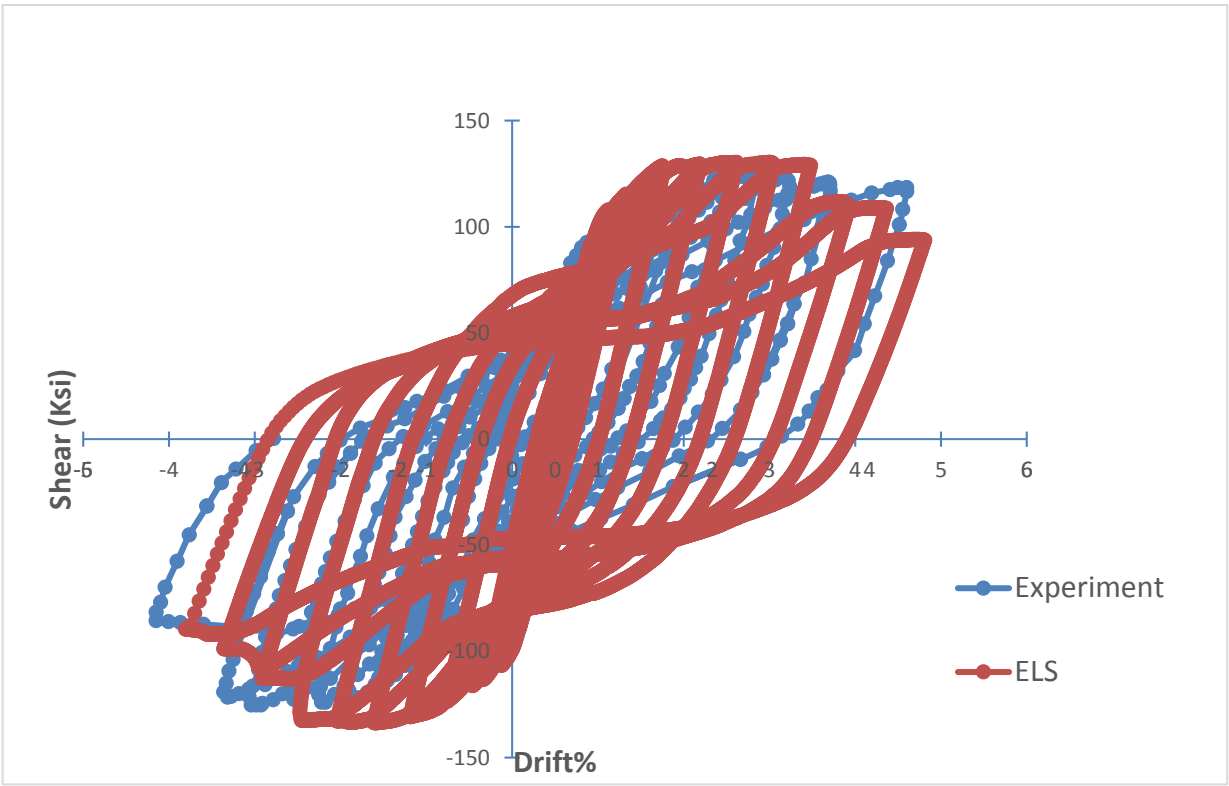

e) CB-6

Figure (3-20): Comparison between experiment results and ELS results for CB-1 to CB-6

CHAPTER 4: CASE STUDY

4.1. Introduction

This chapter presents a full illustration of the current study. The current study is carried out for a multistorey reinforced concrete structure with coupled shear wall. This chapter presents design criteria, structure details, material properties, case studied, loading conditions, and design outputs.

4.2. Reference Case Configuration

The reference case study is a twelve-storey reinforced concrete coupled shear wall extracted from residential building located in Cairo, Egypt. The building is designed to resist lateral loads by two coupled shear walls in both x-direction and y-direction. The building was analyzed in the y-direction only. Figure (4-1-a) and Figure (4-1-b) show the general configuration of the residential building. Figure (4-1-c) shows the first studied reference case that presents an individual coupling beam to focus on the behavior of beam itself, while Figure (4-1-d) shows the second studied reference case that presents the coupled walls system. The building height is 36 m and its dimensions in plan are 38 m x 38 m. The structure is designed according to the Egyptian code for design and construction of reinforced concrete structures (ECP 203-2018) [4]. The Ultimate limits state design method was used for design of the structure members and for load combinations. Three dimensional models were formed using ELS software considering cross sections and reinforcement detailing.

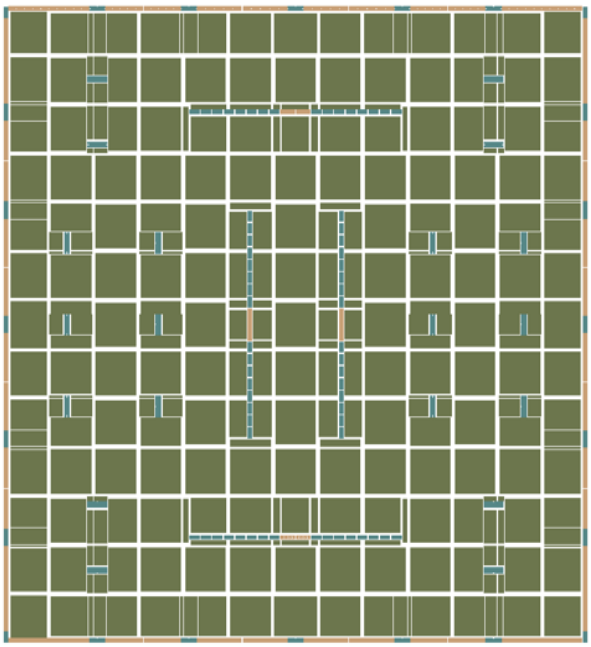

Figure (4-1-a): The building top view

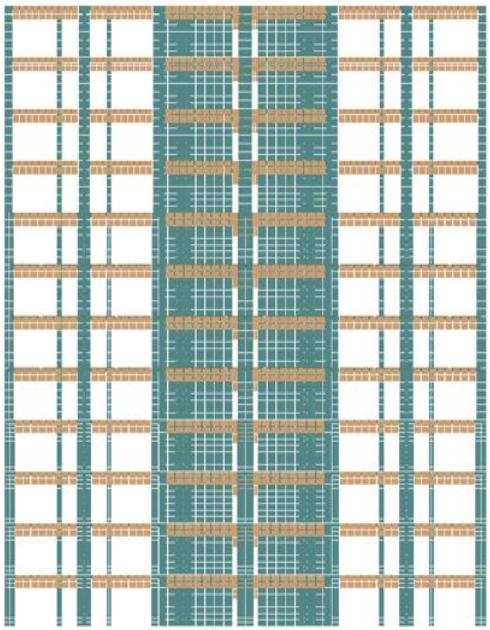

Figure (4-1-b): The building side view

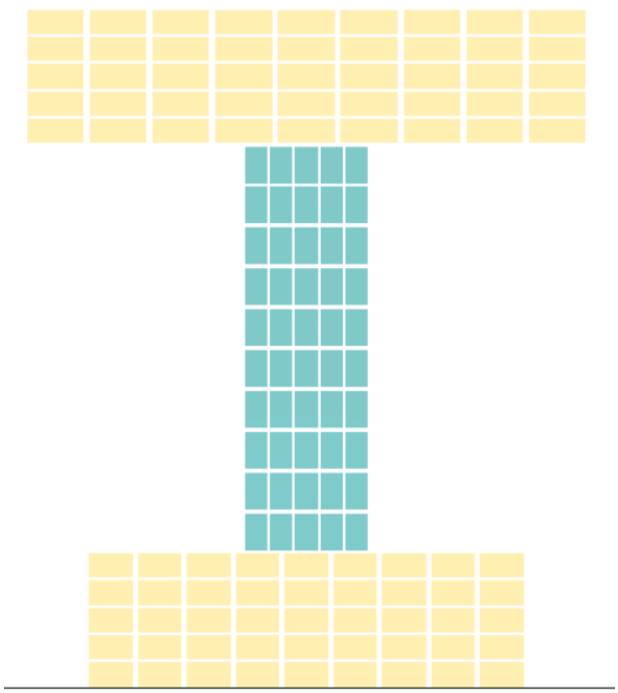

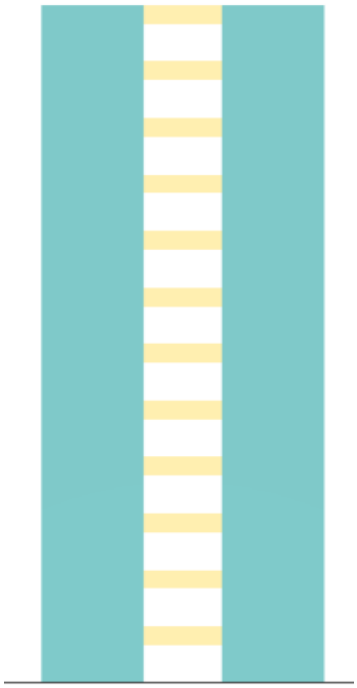

Figure (4-1-c): First reference case **Figure (4-1-d): Second reference case**

4.3. Design Codes

Design procedures followed the Egyptian Code for Practice for design of reinforced concrete structures (ECP 203-2018) [4] and Egyptian Code of Practice for loads (ECP 201-2012) [61].

4.4. Material Properties

The materials used in the models are nonlinear. The properties of regular concrete are shown in Table (4-1) and the properties of high-performance fiber reinforced concrete, used for coupling beams, are shown in Table (4-2), the properties of reinforcing steel are shown in Table (4-3), and the properties of brick walls are shown in Table (4-4).

Table (4-1): Regular concrete properties (f'c=24 N/mm^2)

Young's Modulus	24100	N/mm^2
Shear Modulus	9880	N/mm^2
Tensile strength	3	N/mm^2
Cylindrical Compressive Strength	24	N/mm^2
Friction Coefficient	0.8	---
Specific Weight	25	kN/m^3

Table (4-2): Regular concrete properties (f'c=50 N/mm^2)

Young's Modulus	43060	N/mm^2
Shear Modulus	1720	N/mm^2
Tensile strength	3.16	N/mm^2
Cylindrical Compressive Strength	50	N/mm^2
Friction Coefficient	0.8	---
Shear Strength	12	N/mm^2
Specific Weight	25	kN/m^3

Figure (4-2) shows the compression model used for high-performance fiber concrete and Figure (4-3) shows the tension model.

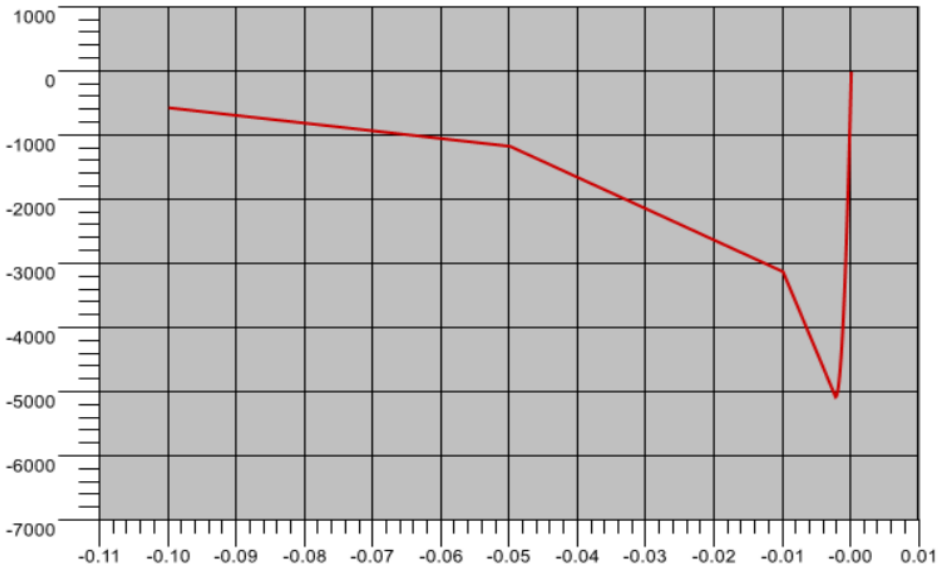

Figure (4-2): Compressive stress strain curve for steel fiber concrete

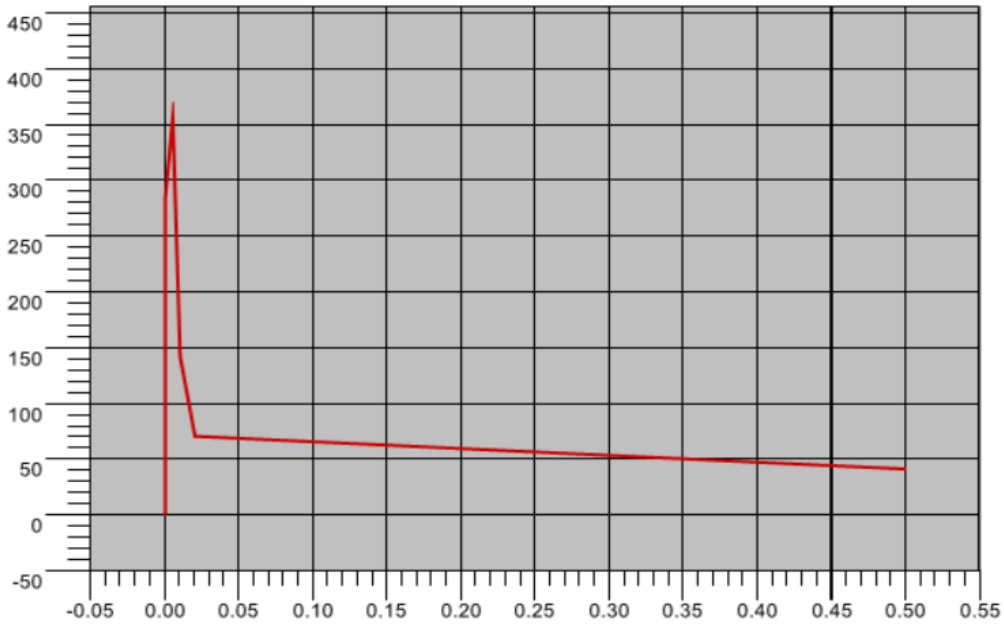

Figure (4-3): Tensile stress strain curve for steel fiber concrete

Table (4-3): Steel Properties

Young's Modulus	203890	N/mm^2
Shear Modulus	81556	N/mm^2
Tensile Yield Stress	420	N/mm^2
Ultimate Strength/ Tensile Yield Stress	1.4	---
Friction Coefficient	0.8	---
Specific Weight	78.4	kN/m^3

4.5.Design Loads

4.5.1 Gravity Loads

All gravity loads were included in design, including dead loads (own weight, flooring cover weight, wall loads) and live loads.

4.5.1.1 Dead Loads (DL)

Dead loads include:

- Own weight of structural elements.
- Floor Cover = 1.5 kN/m^2
- Equivalent wall uniform load = 1.8 kN/m^2

4.5.1.2 Live Load (LL)

According to ECP 201-2012 [61], live load is 2 kN/m^2 for residential buildings.

4.5.1.3 Seismic Load (SL)

The building was designed using the simplified response spectrum method as per (ECP 201-2012) provisions [61], the design base shear (F_b) is obtained from the following equation.

$$F_b = S_d(T_1).\lambda.\frac{W}{g} \quad \text{Eq. (4-1)}$$

Where;

$S_d(T_1)$: Design response spectrum for elastic analysis.

λ : Correction factor = 1 for $T_1 > 2T_c$

W : Design seismic load for residential building (DL+0.25LL)

g : Gravity acceleration ($g = 9.81\ m/s^2$)

T_c : Characteristics for the design response spectrum depending on soil type.

4.5.1.3.1 Design Response Spectrum $S_d(T_1)$

The design response spectrum $S_d(T_1)$ is obtained from the response spectrum curve in (ECP201-2012) [61] as shown in Figure (4-4). The reference case study is for a building in Cairo; Type (1) curve was used for seismic design. The curve is plotted using the following equations

$0 \le T \le T_B$ $S_d(T) = a_g . \gamma_1 . S \left(\frac{2}{3} + \frac{T}{T_b}\left(\frac{2.5\eta}{R} - \frac{2}{3}\right)\right)$ Eq. (4-2a)

$T_B \le T \le T_c$ $S_d(T) = a_g . \gamma_1 . S \left(\frac{2.5}{R}\eta\right)$ Eq. (4-2b)

$T_c \le T \le T_D$ $S_d(T) = a_g . \gamma_1 . S \left(\frac{2.5}{R} . \frac{T_c}{T}\eta\right) \ge 0.2\ a_g \gamma_1$ Eq. (4-2c)

$T_D \le T \le 4$ sec $S_d(T) = a_g . \gamma_1 . S \left(\frac{2.5}{R} . \frac{T_c T_D}{T^2}\eta\right) \ge 0.2\ a_g \gamma_1$ Eq. (4-2d)

Where,

a_g : Design earthquake acceleration according to seismic zone

γ_1 : Importance factor depends on building zone.

S : Soil factor depends on soil class.

η : Damping factor depends on building materials.

R : Response modification factor depends on structural system.

T_B : Lower limit of the constant spectral acceleration segment.

T_C : Upper limit of the constant spectral acceleration segment.

T_D : Start of the displacement-sensitive spectral segment.

The building is located in Cairo, so it's located in seismic zone (3). Also, it rests on medium dense sandy soil which is classified according to ECP (201-2012) [61] as soil class (C). Table (4-5) shows the values required to plot the design response spectrum.

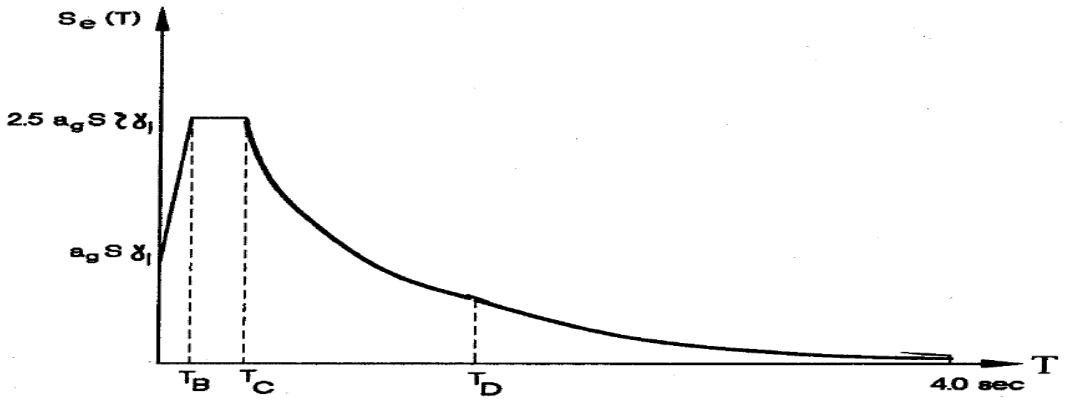

Figure (4-4): Design response spectrum (Type 1) [61]

Table (4-5): Response spectrum Parameters

a_g	0.15g
γ_1 for residential buildings	1
S	1.5
η	1
R for shear wall systems	5
T_B	0.1 sec
T_C	0.25sec
T_D	1.2 sec

4.6 Design Load Combinations

According to ECP (203-2018) [4], the design load combinations used are as follows:

- 1.4 DL+1.6LL
- 1.12 DL+0.25 LL+ SL
- 0.9 DL+ SL

Where;
DL: Dead load
LL: Live load
SL: Seismic load

4.7 Design Outputs

4.7.1 First Reference Case

4.7.1.a Top and Bottom Blocks

Top and bottom blocks are 500×1000×6000 mm and reinforced as shown in Figure (4-5).

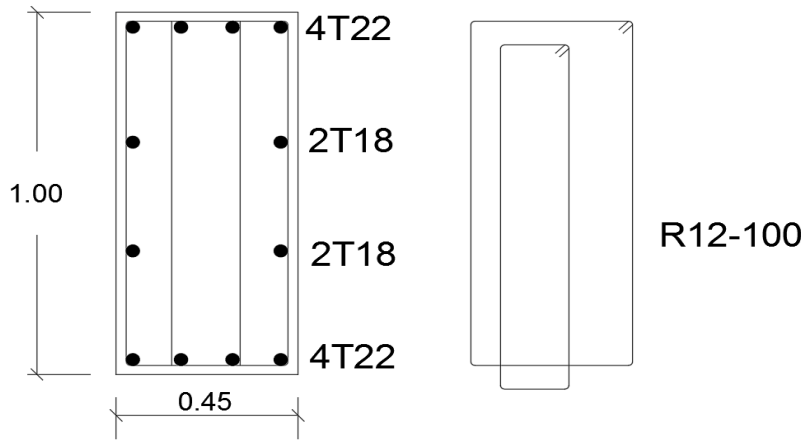

Figure (4-5): Top and Bottom Blocks cross section reinforcement

4.7.1.b Coupling Beam Design

Coupling beams is reinforced according to ACI 318-11 (2011) [5]. Figure (4-6), Figure (4-7) illustrate the reinforcement. All coupling beams are 300×1000 mm and with a height equals to 3000 mm.

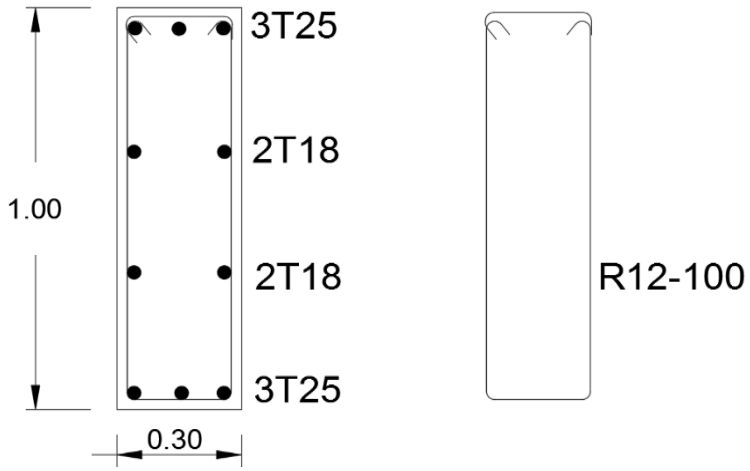

Figure (4-6): Coupling beam reinforcement (cross section)

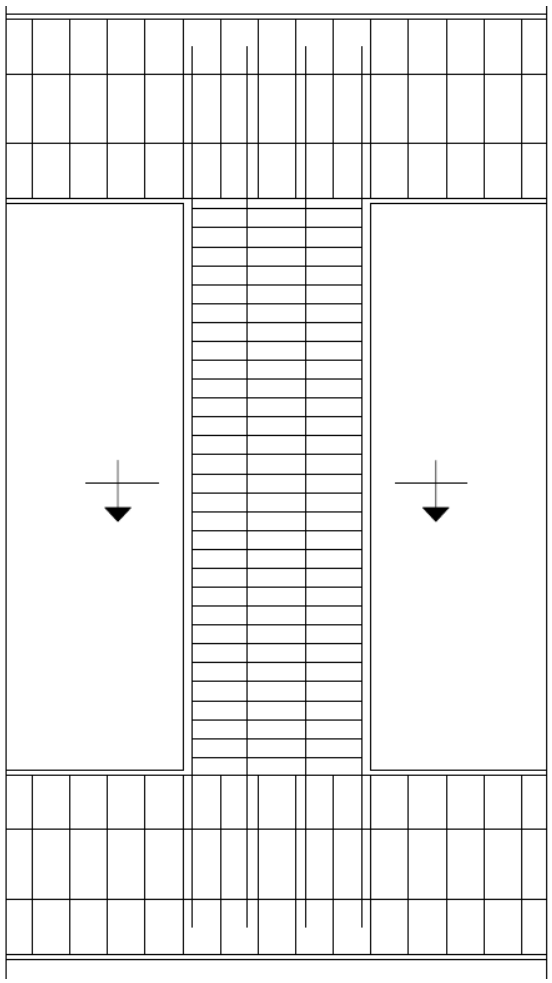

Figure (4-7): Coupling beam reinforcement (elevation)

4.7.2 Second Reference Case

4.7.2.a Shear Wall Design

All shear walls are 300×4000 mm and reinforced as shown in Figure (4-8).

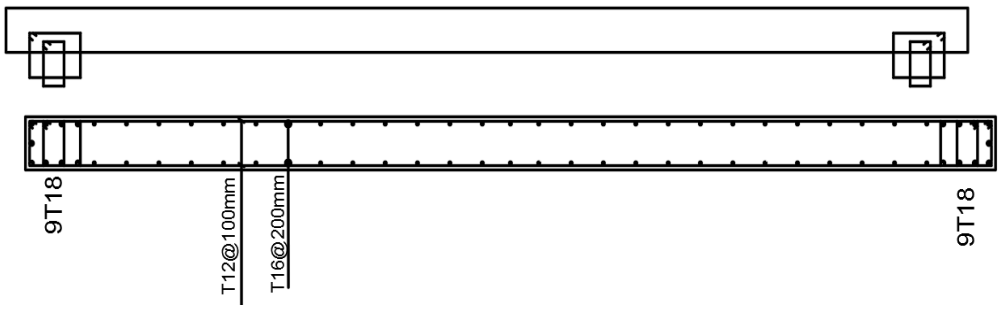

Figure (4-8): Shear wall reinforcement

4.7.2.b Coupling Beam Reinforcement

Coupling beams are reinforced according to ACI 318-11 (2011) [5]. Figure (4-9), Figure (4-10) illustrate the reinforcement. All coupling beams are 300×1000 mm and with a span equals to 3000 mm.

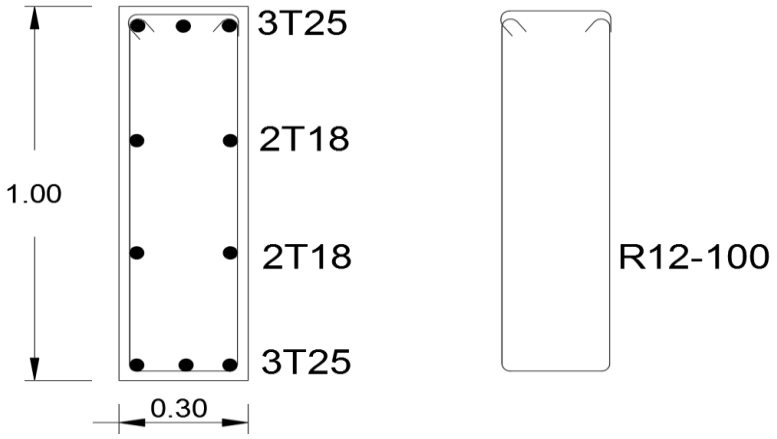

Figure (4-9): Coupling beam reinforcement (cross section)

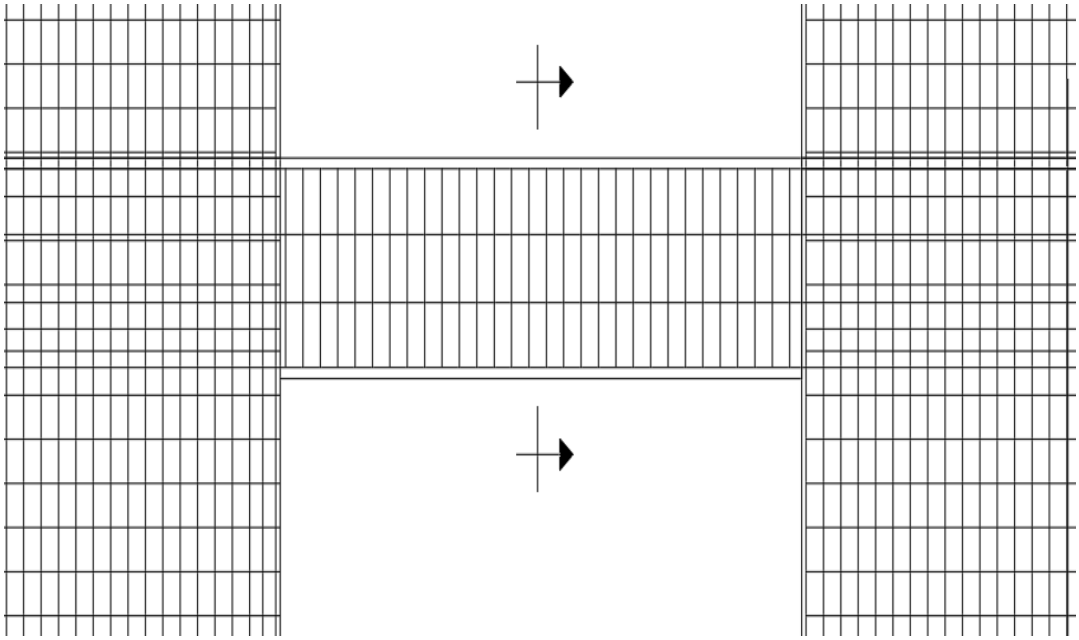

Figure (4-10): Coupling beam reinforcement (elevation)

4.8 Modeling in ELS

A 3D model was constructed in the ELS as shown in Figure (4-11-a) and Figure (4-11-b).

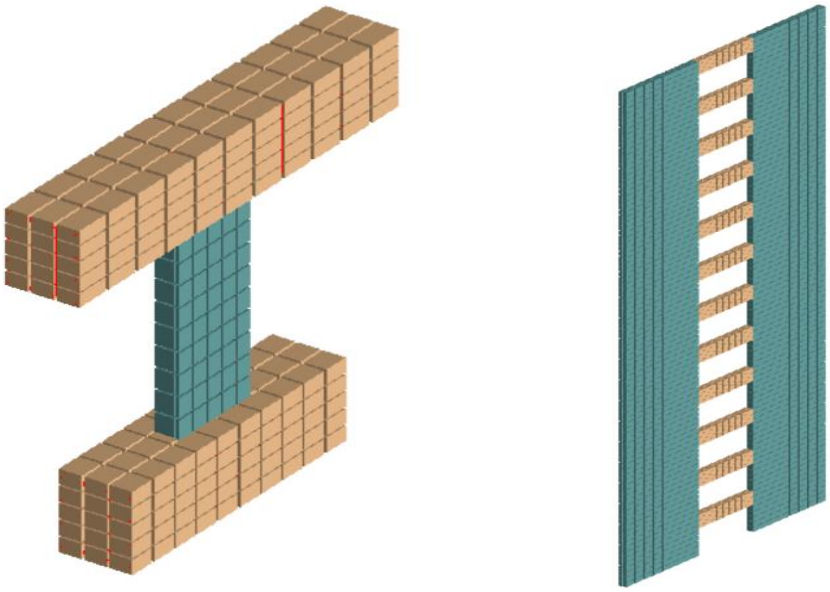

(a) (b)

Figure (4-11): ELS model (a) First reference case (b) second reference case

4.8.1 Mesh Sensitivity Analysis

Mesh sensitivity analysis was created to reach accurate results in a reasonable analysis time. The mesh size was varied for walls and beams in four mesh groups as

shown in Table (4-6) and Table (4-7). A monotonic load in Y direction equals to 350 kN was applied. Figure (4-12) and Figure (4-13) show the relation between the number of elements in each mesh group. mesh group and the lateral displacement in Y direction for the reference cases.

Table (4-6): Mesh group for first reference case

Mesh group	Number of elements	Top Block	Bottom Block	Coupling beam
Group 1	162	6×3×3	6×3×3	8×3×3
Group 2	276	7×3×4	7×3×4	9×3×4
Group 3	420	9×3×5	9×3×5	10×3×5
Group 4	768	11×4×6	11×4×6	10×4×6

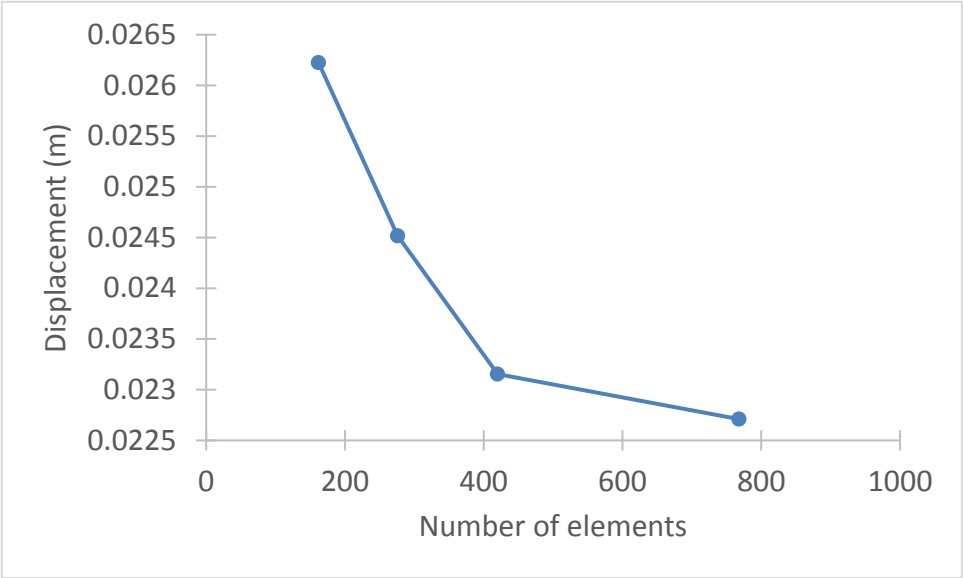

Figure (4-12): Displacement corresponding to number of elements for first reference case

Table (4-7): Mesh group for second reference case

Mesh group	Number of elements	Walls	Coupling beams
Group 1	2184	7×2×5	7×2×3
Group 2	3504	7×2×7	8×3×4
Group 3	4692	8×2×8	9×3×5
Group 4	8712	9×3×9	10×4×6

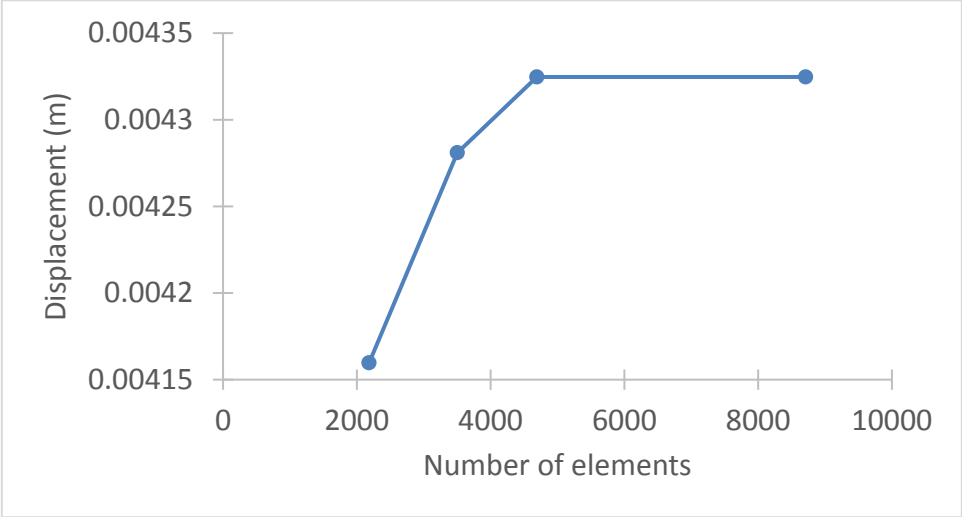

Figure (4-13): Displacement corresponding to number of elements for second reference case

As shown from Table (4-6), Table (4-7), Figure (4-12), and Figure (4-13), when the number of elements increase from first mesh group to forth mesh group, the displacement in Y direction decreased. Displacement is almost constant starting from third mesh group indicating that accuracy is not affected from this point, thus mesh arrangement in group (3) was selected for analysis. On the other hand, the displacement in Y direction increased by increasing number of elements for the second reference case until it started to be constant from third mesh group, thus third mesh group was selected for analysis.

4.8.2 Loading in ELS

4.8.2.1 First Reference Case

This case was subjected to quasi-static loading in a displacement-controlled mode. A displacement rate of 2.4 mm per cycle is used. Therefore, the lateral displacement history for this case consisted of 10 cycles and started with 2.4 mm as shown in Figure (4-14).

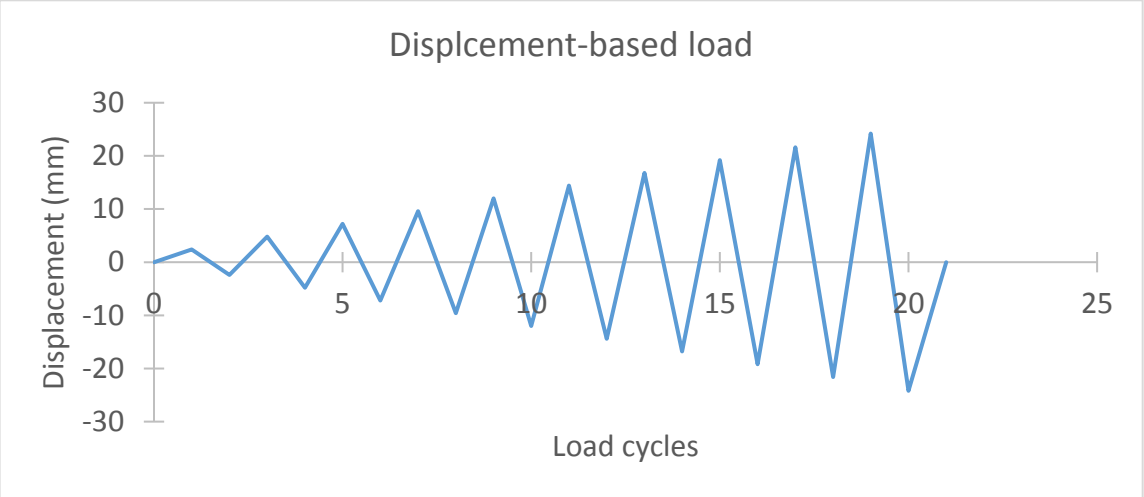

Figure (4-14): Pre-defined displacement cycles

4.8.2.2 Second Reference Case

According to the material of coupling beam, loading history was determined. For high-performance reinforced concrete coupling beams, the structure was subjected to quasi-static loading in a load-controlled mode, following a predefined reversed cyclic load pattern with a load rate of approximately $\frac{1}{10}$ F_{max} per cycle as shown in Figure (4-15). F_{max} was estimated by applying monotonic displacement on $\frac{2}{3}$ wall's height, F_{max} was divided to form 12 load-based cycles with $\frac{1}{10}$ F_{max} load increment. Loads were distributed to follow triangular distribution using Eq 4.3. On the other hand, for conventional reinforced concrete coupling beams, the cycles shown in Figure (4-16) were assigned. These cycles were calculated to have the same drift as high-performance fiber reinforced concrete case.

$$F_i = \frac{w_i\, h_i}{\sum_{j=1}^{j=n} w_j\, h_j}\, F_{max} \quad \text{Eq. 4.3}$$

Where,
F_i : the applied load on the floor level i.
w_i, w_j: weight of floor i,j respectively.
h_i, h_j: height of floor i,j from the foundation level respectively.
F_{max}: applied base shear.

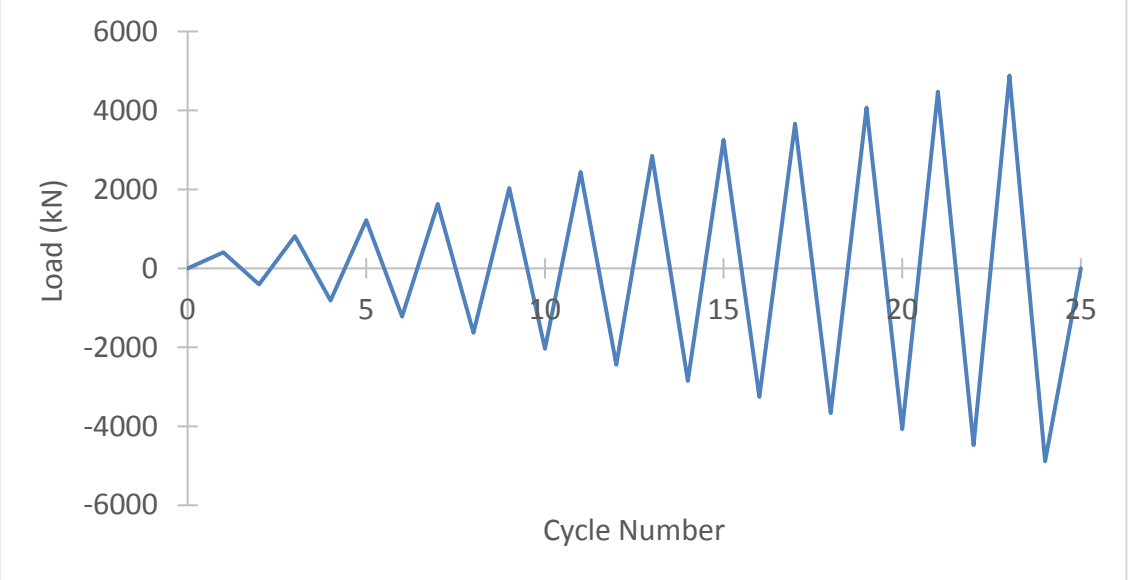

Figure (4-15): Pre-defined load cycles for HPFRC case

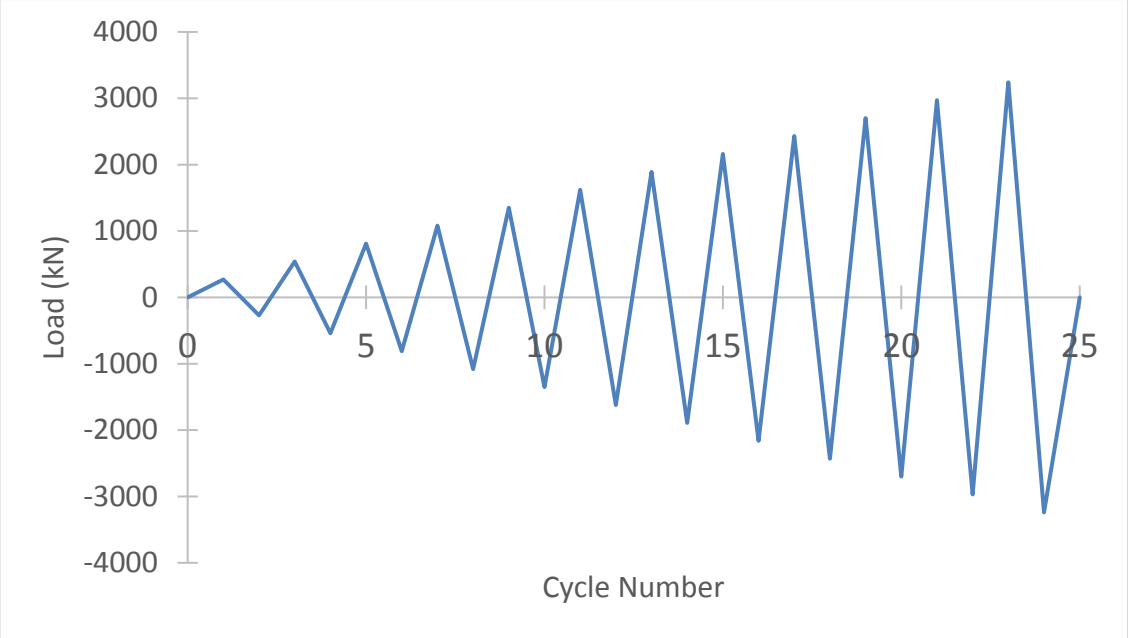

Figure (4-16): Pre-defined load cycles for RC case

4.9 Studied Parameters

4.9.1 Effect of Material Type

RC and HPFRC were investigated. Figure (4-17) and Figure (4-18) show the compression and tensile stress-strain relation for both.

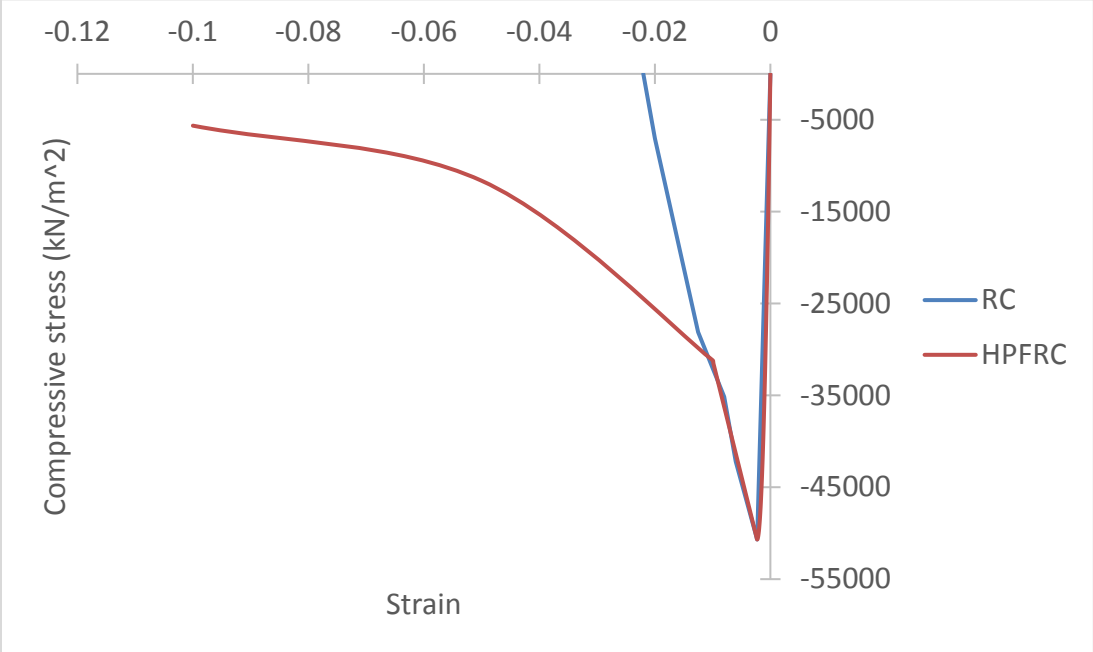

Figure (4-17): Compression stress strain for RC and HPFRC

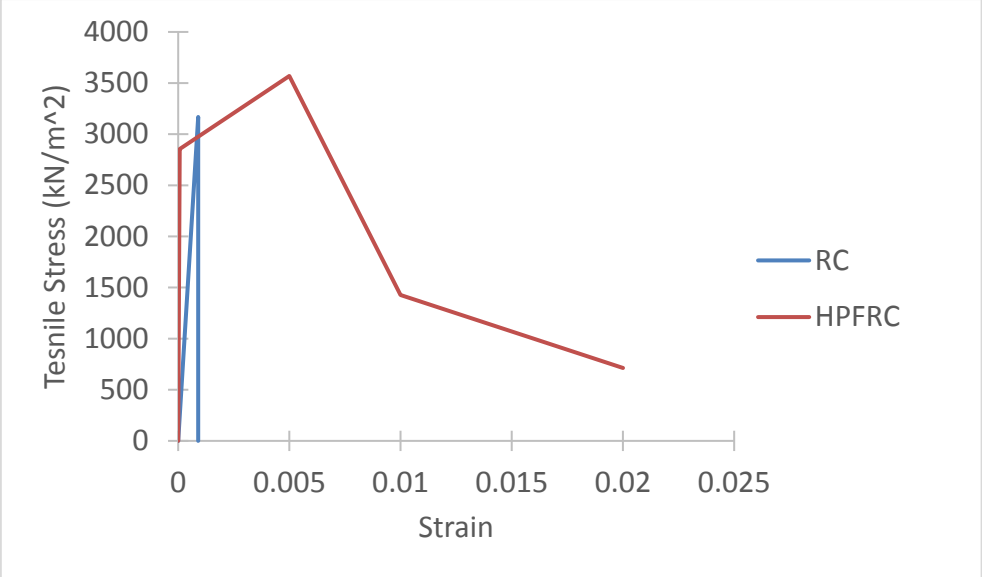

Figure (4-18): Tensile stress strain curves for RC and HPFRC

4.9.2 Longitudinal Reinforcement Ratio for Coupling Beams

Four longitudinal reinforcement ratios for coupling beams were studied, a longitudinal reinforcement ratio of 0.5% was chosen for reference case.

- Case (A) RFT ratio = 0.8%
- Case (B) RFT ratio = 0.7%
- Case (C) RFT ratio = 0.6%
- Case (D) RFT ratio = 0.5%

4.9.3 High-Performance Fiber Reinforced Concrete Embedment inside the Coupled Walls

Four cases were studied to investigate the effect of casting part of the walls using HPFRC. HPFRC was considered with a depth equals to beam's depth and a length according to each case as shown in Figure (4-19). The case which depends on using HPFRC for the total length of the wall was considered as reference case.

- Case (A) Embedment of HPFRC from beam's edge = zero
- Case (B) Embedment of HPFRC from beam's edge = 1.00x beam's depth
- Case (C) Embedment of HPFRC from beam's edge = 2.5x beam's depth
- Case (D) Embedment of HPFRC from beam's edge = 4.00x beam's depth

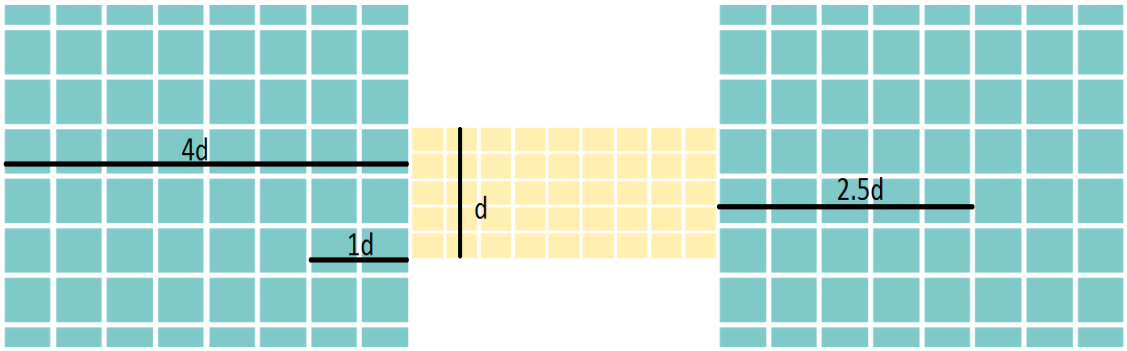

Figure (4-19): Embedment of HPFRC inside coupled walls

4.9.4 Presence of Diagonal Reinforcement with and without Confining Stirrups

Effect of using diagonal reinforcement with and without confining stirrups around each group of diagonal bars was studied here, Figure (4-20) shows beam configuration when two intersected groups of diagonal bars confined with stirrups was used, while Figure (4-21) shows the same configuration but without confining stirrups. The case with conventional longitudinal reinforcement was considered as reference case.

- Case (A) Two intersected groups of diagonal reinforcement (4T22/group) with confining stirrups.
- Case (B) Two intersected groups of diagonal reinforcement (4T22/group) without confining stirrups.
- Case (C) Two intersected groups of diagonal reinforcement (4T25/group) with confining stirrups.
- Case (D) Two intersected groups of diagonal reinforcement (4T25/group) without confining stirrups.

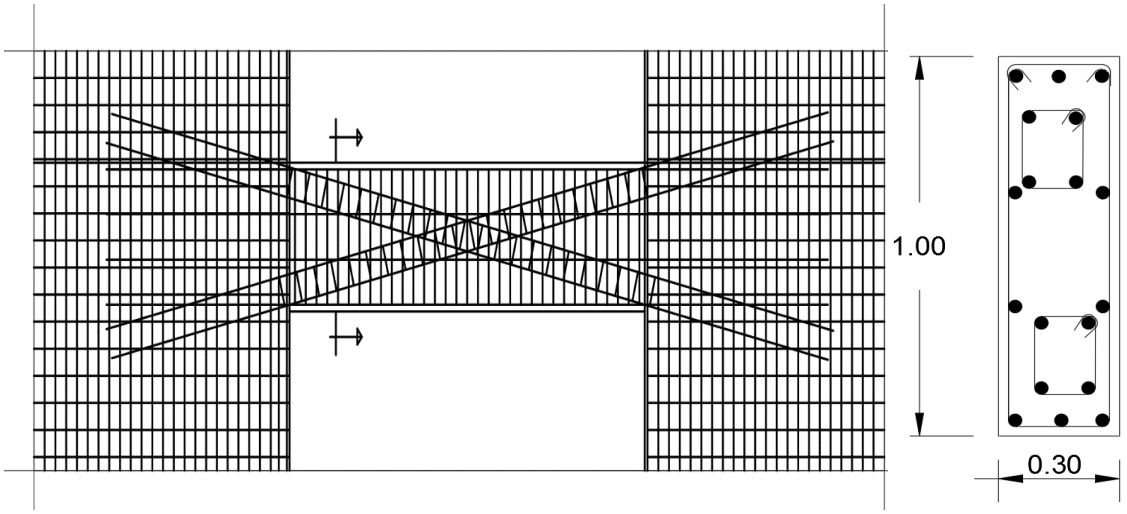

Figure (4-20): Two intersected groups of diagonal bars with confining stirrups

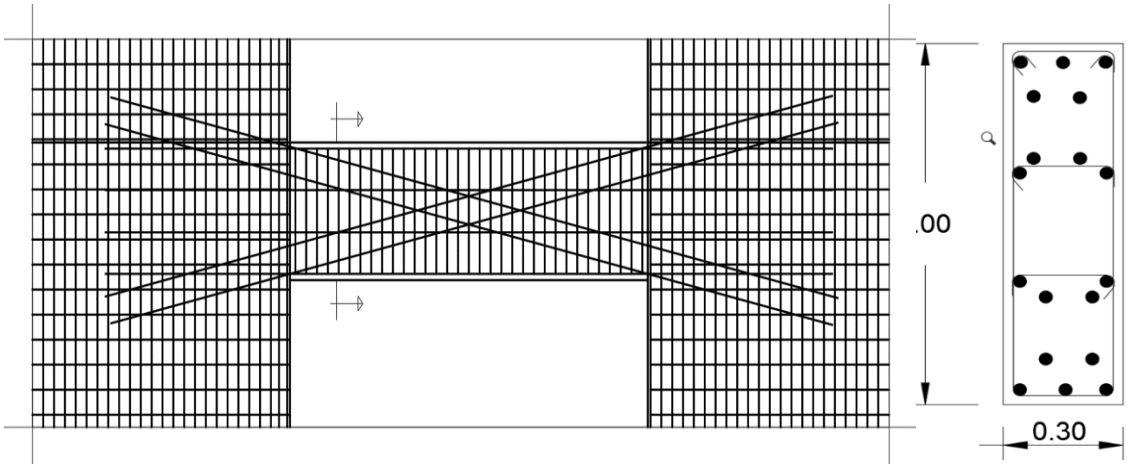

Figure (4-21): Two intersected groups of diagonal bars without confining stirrups

4.9.5 Coupling Beam's Aspect Ratio

Four aspects ratios were studied in this case. Coupling Beam with aspect ratio equals to 3.00 was considered as reference case.

- Case (A) Aspect ratio equals to 2.72
- Case (B) Aspect ratio equals to 3.00
- Case (C) Aspect ratio equals to 3.33
- Case (D) Aspect ratio equals to 3.75

4.2.2.1Different HPFRC Mixtures

Two different mixture were studied to investigate the effect of varying fiber ratio and matrix component ratios. HPFRC mixtures were based on Mix 3 and Mix 5 according to Liao [28]. Compressive and tensile constitutive models for HPFRC are shown in Figure (4-22) and (4-23). Mix 5 was considered as reference case.

- Case (A) Mix 5 f_c'=5062 ton/m^2 and ft=350 ton/m^2 with V_f=1.5%
- Case (B) Mix 3 f_c'=6045 ton/m^2 and ft=490 ton/m^2 with V_f=1.47%
- Case (C) Mix 3 f_c'=6250 ton/m^2 and ft=490 ton/m^2 with V_f=1.47%
- Case (D) Mix 3 f_c'=6960 ton/m^2 and ft=490 ton/m^2 with V_f=1.47%

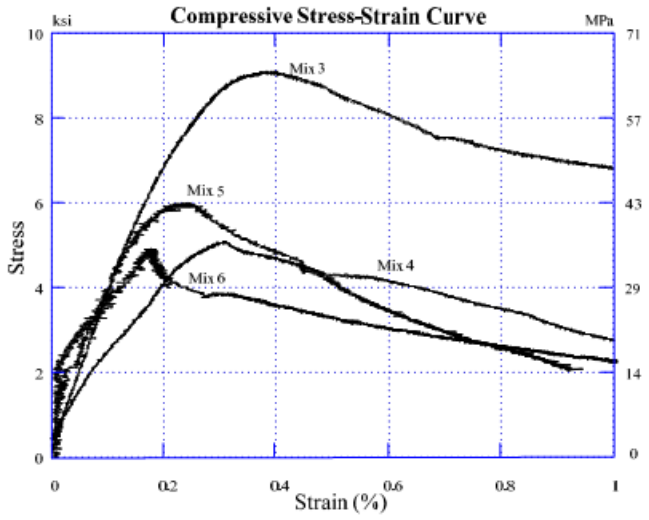

Figure (4-22): Compressive constitutive responses of HPFRC [28].

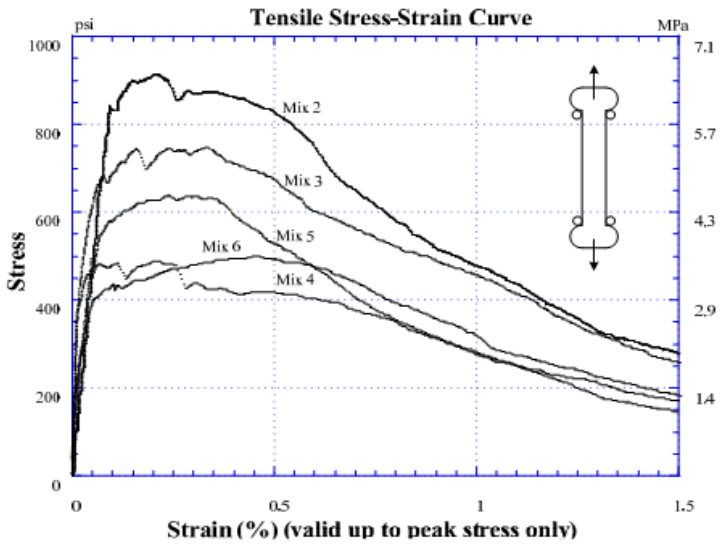

Figure (4-23): Tensile constitutive responses of HPFRC [28].

CHAPTER 5: NUMERICAL RESULTS

5.1 Introduction

In this chapter, the numerical results of the parametric study stated in chapter (4) are presented.

Outputs are divided into three groups:

1. Outputs related to the local behavior of the HPFRC coupling beam:
    - Maximum inelastic base shear (V_{max}).
    - Corresponding inelastic drift.
    - Energy dissipated up to post peak base shear, if any.

2. Outputs related to behavior of coupled walls:
    - Maximum inelastic base shear (V_{max}).
    - Corresponding inelastic drift.
    - Stresses developed at coupling beams and coupled walls at maximum load, if any.

5.2 Effect of Material Type

5.2.1 Behavior of Coupling Beam

In this section, the numerically obtained behavior of traditional reinforced concrete and high-performance reinforced concrete are investigated. Two models were created. First model uses regular reinforced concrete coupling beams while the second one uses HPFRC to construct coupling beams. Figure (5-1) shows the comparison between load-displacement response for the two models. Table (5-1) shows maximum base shear and corresponding displacement.

Table (5-1): Base shear vs. corresponding displacement for RC and HPFRC coupling beams under displacement-based load

	Maximum base shear (kN)	Corresponding displacement (mm)
RC	288	23.99
HPFRC-Mix 1	331	20.00

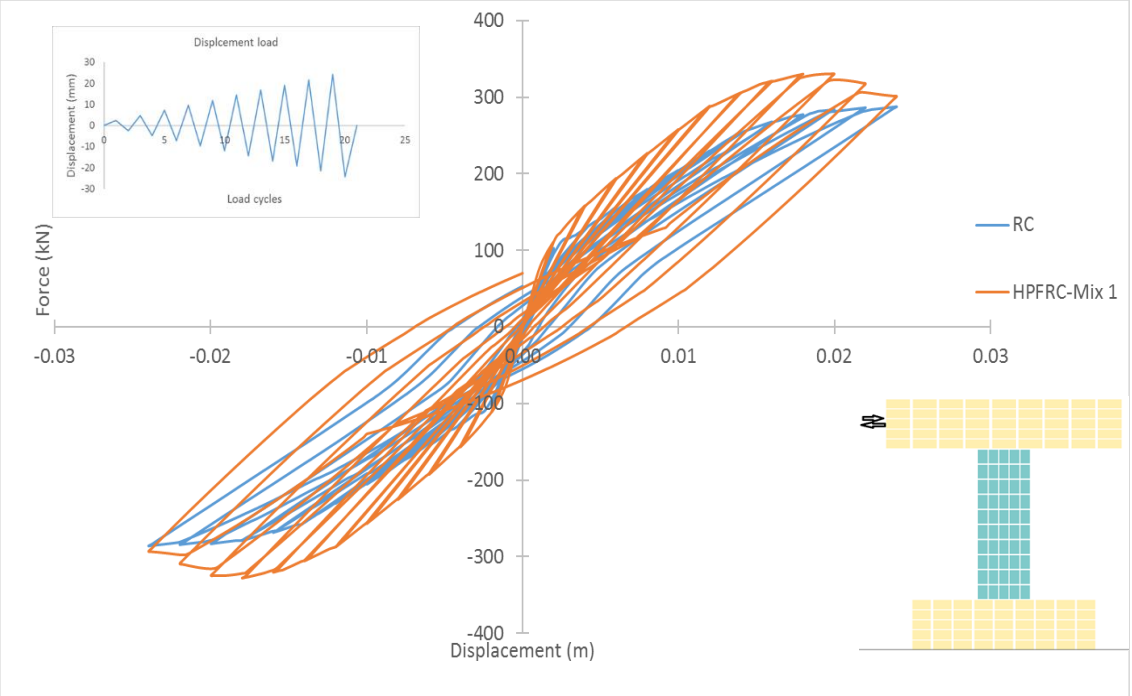

Figure (5-1): Displacement vs. Base shear for RC and HPFRC coupling beams under displacement-based load

5.2.2 Behavior of Coupled Walls

5.2.2.1 Monotonic Loading

Figure (5-2) shows comparison between the behavior of coupled walls when they were subjected to monotonic loading at 2/3 height. Energy dissipated by each coupled wall, maximum base shear, and corresponding displacement are calculated as shown in Table (5-2).

Table (5-2): Base shear vs. corresponding displacement for coupled walls with RC or HPFRC coupling beams under monotonic loading

	Maximum base shear (kN)	Corresponding displacement (mm)	Energy dissipated (kN.m)
RC	3310	229	623
HPFRC-Mix 1	4120	139	802

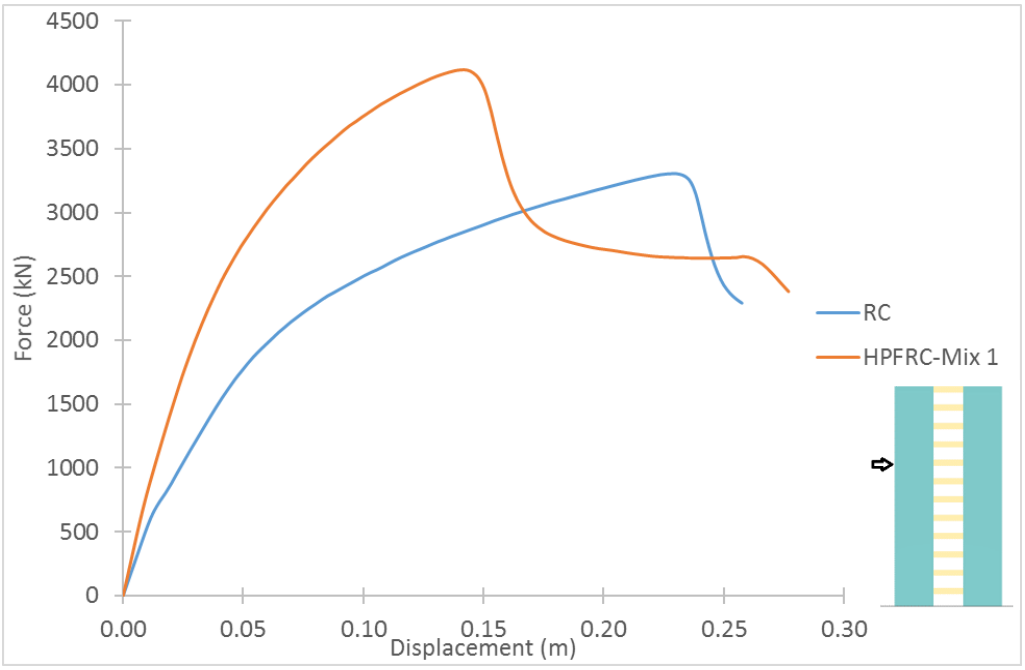

Figure (5-2): Displacement vs. Base shear for coupled walls with RC or HPFRC coupling beams under monotonic loading

5.2.2.2 Cyclic Loading

Figure (5-3) shows the maximum stresses developed in RC and HPFRC coupled walls. Figure (5-4) shows the maximum normal stresses developed in coupling beams when the coupled walls are subjected to cyclic loading. Figure (5-5) shows comparison between the behavior of RC and HPFRC coupled walls. Maximum base shears, and corresponding displacements are shown in Table (5-3).

Table (5-3): Base shear vs. corresponding displacement for coupled walls with RC or HPFRC coupling beams under cyclic loading

	Maximum base shear (kN)	Corresponding displacement (mm)
RC	3090	137
HPFRC-Mix 1	4120	137

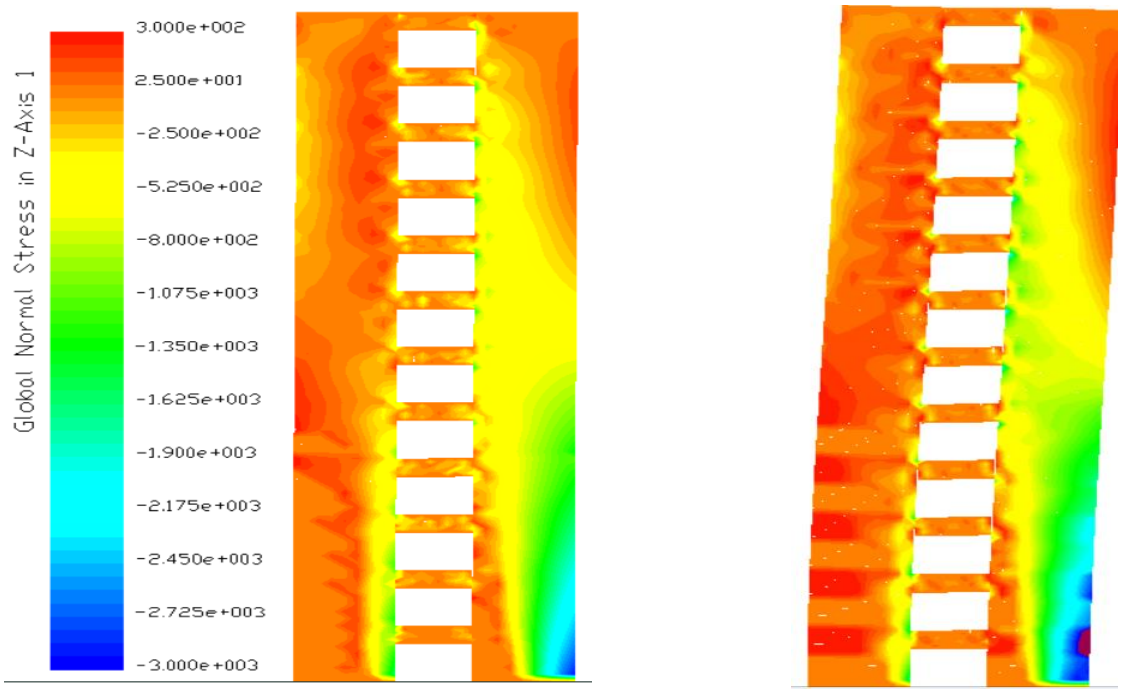

Figure (5-3): Normal stresses developed in coupled walls at maximum load

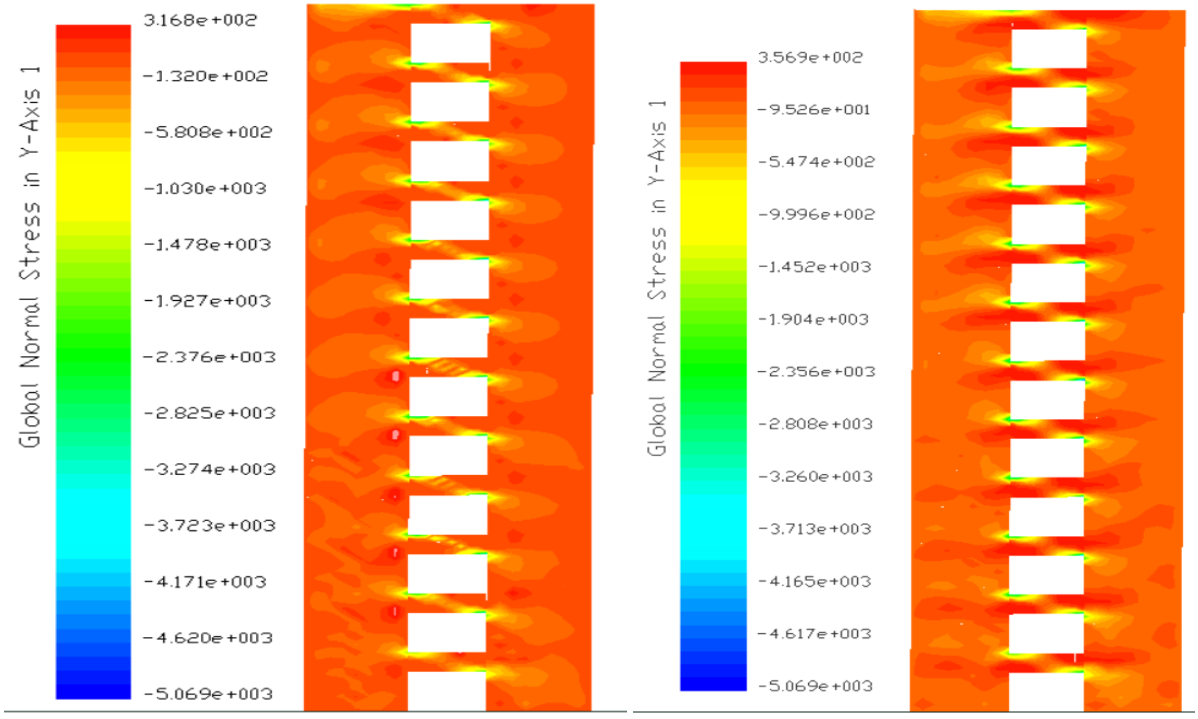

Figure (5-4): Normal stresses developed in coupling beams at maximum load

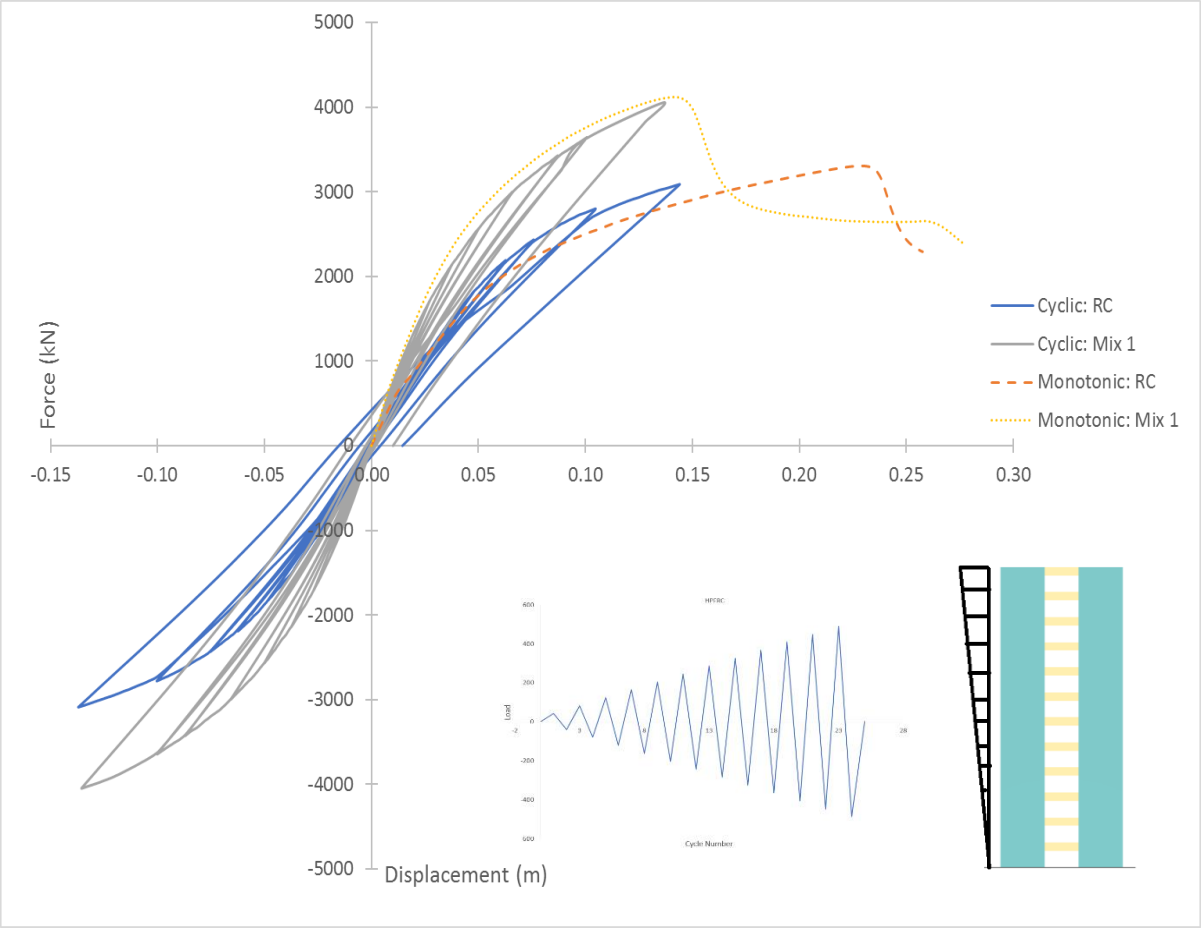

Figure (5-5): Displacement vs. Base shear for coupled walls with RC or HPFRC coupling beams under cyclic loading

5.3 Effect of Longitudinal Reinforcement Ratio of Coupling Beams

5.3.1 Behavior of Coupling Beam

In this section, the numerically obtained behavior of high-performance fiber reinforced concrete coupling beams with various longitudinal reinforcement ratios are investigated. Four models were created. Figure (5-6) shows the comparison between load-displacement response for the four models. Table (5-4) shows maximum base shear and corresponding displacement.

Table (5-4): Base shear vs. corresponding displacement for coupling beams with various longitudinal reinforcement ratios under displacement-based load

	Maximum base shear (kN)	Corresponding displacement (mm)
Model 1: 0.5%	331	19.79
Model 2: 0.6%	368	19.80
Model 3: 0.7%	402	20.00
Model 4: 0.8%	427	20.20

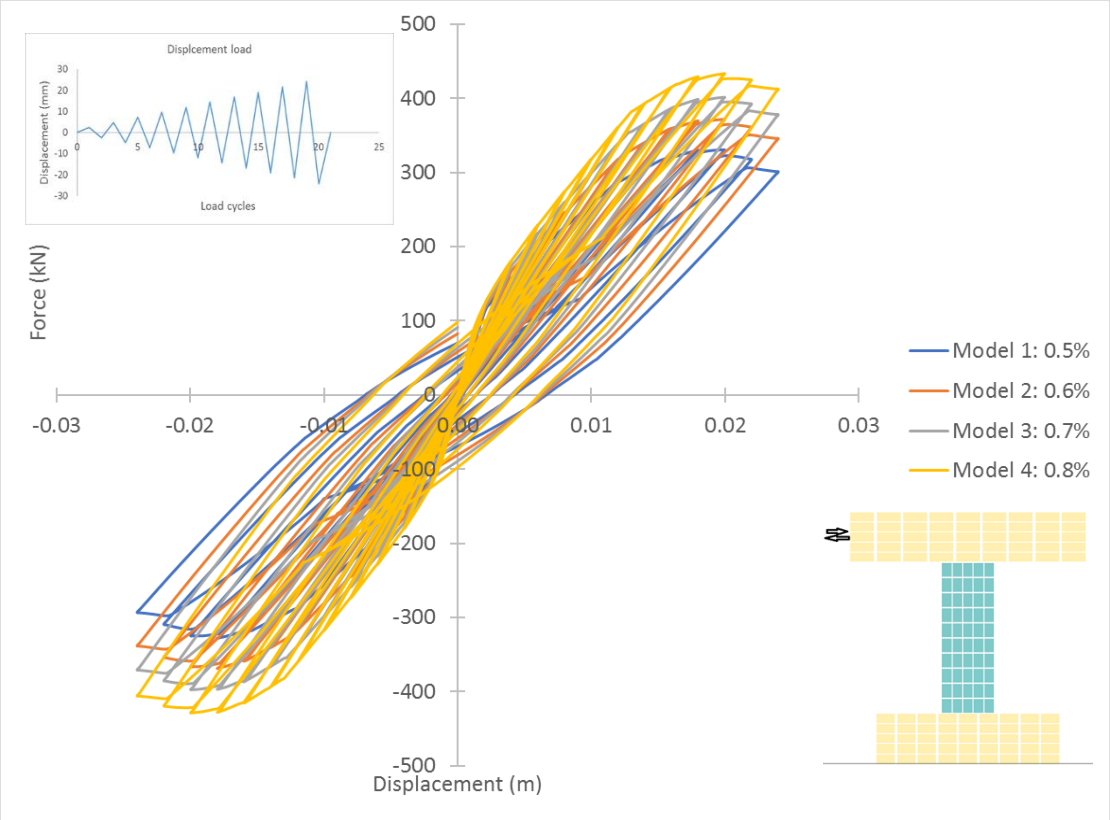

Figure (5-6): Displacement vs. Base shear for coupling beams with various longitudinal reinforcement ratios under displacement-based load

5.3.2 Behavior of Coupled Walls

5.3.2.1 Monotonic Loading

Figure (5-7) shows comparison between the behavior of coupled walls when they were subjected to monotonic loading at 2/3 height to test the effect of varying longitudinal reinforcement ratios of coupling beams. Maximum base shears, and corresponding displacements are calculated as shown in Table (5-5).

Table (5-5): Base shear vs. corresponding displacement for coupled walls with different longitudinal reinforcement ratios coupling beams

	Maximum base shear (kN)	Corresponding displacement (mm)
Model 1: 0.5%	4120	137
Model 2: 0.6%	4287	138
Model 3: 0.7%	4400	135
Model 4: 0.8%	4520	133

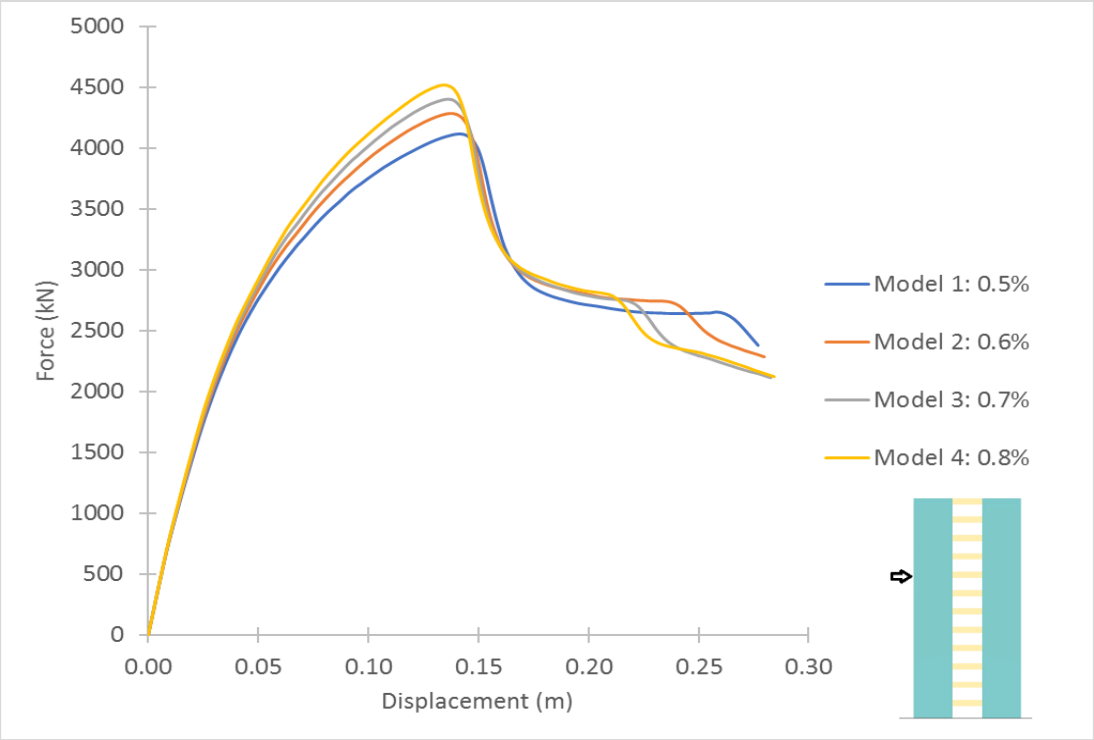

Figure (5-7): Displacement vs. Base shear for coupled walls with different longitudinal reinforcement ratios coupling beams under monotonic loading

5.3.2.2 Cyclic Loading

Figure (5-8) shows comparison between the behavior of coupled walls when they are subjected to cyclic loading for various longitudinal reinforcement ratio coupling beams. Maximum base shears, corresponding displacements are shown in Table (5-6).

Table (5-6): Base shear vs. corresponding displacement for coupled walls with different longitudinal reinforcement ratios coupling beams

	Maximum base shear (kN)	Corresponding displacement (mm)
Model 1: 0.5%	4120	137
Model 2: 0.6%	4280	141
Model 3: 0.7%	4380	137
Model 4: 0.8%	4400	129

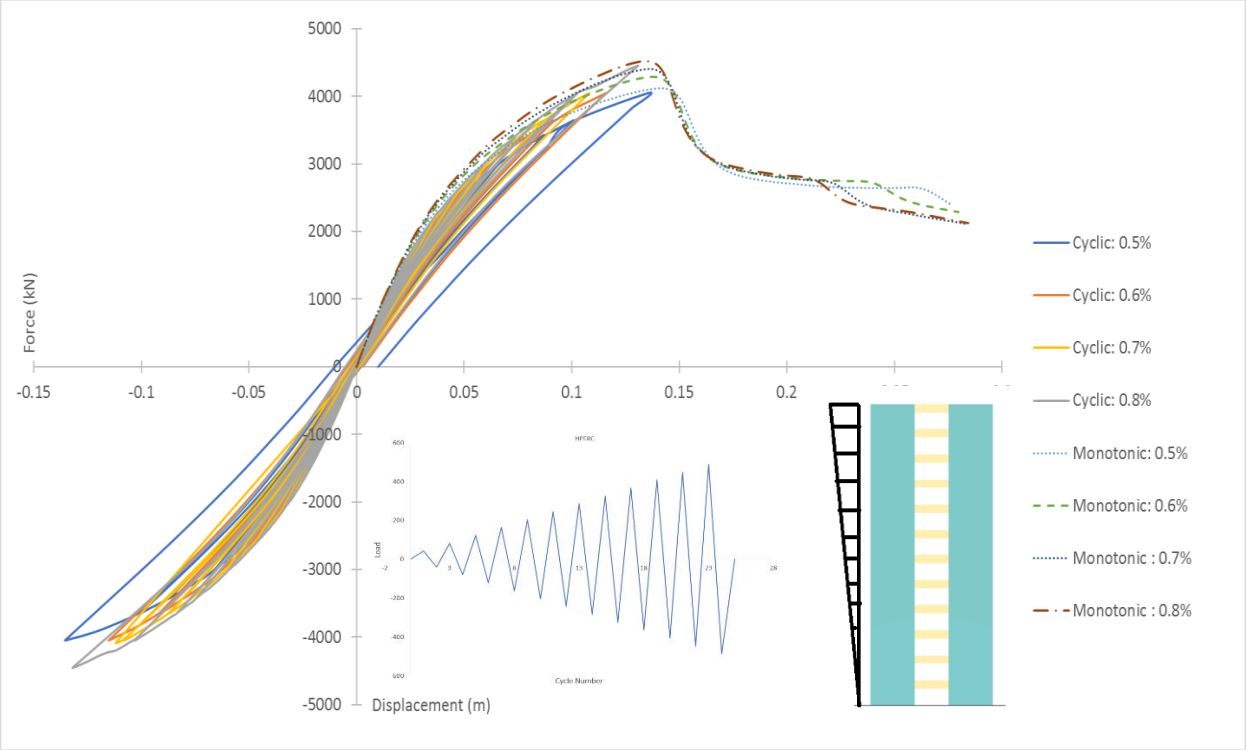

Figure (5-8): Displacement vs. Base shear for coupled walls with different longitudinal reinforcement ratios coupling beams under cyclic loading

5.4 Effect of High-Performance Fiber Reinforced Concrete Embedment inside the Coupled Walls

5.4.1 Behavior of Coupled Walls

5.4.1.1 Monotonic Loading

In this section, the effect of using HPFRC to construct part of coupled walls is investigated. Four models were created. First model uses regular reinforced concrete coupled walls while the remaining models use HPFRC coupled walls as a function of beam's depth. Figure (5-9) shows the comparison between load-displacement response for the four models. Table (5-7) shows maximum base shear and corresponding displacement.

Table (5-7): Base shear vs. corresponding displacement for coupled walls with different HPFRC embedment inside the coupled walls under monotonic loading

	Maximum base shear (kN)	Corresponding displacement (mm)
Case A: 0.00d	3991	171.82
Case B: 1.00d	4014	169.13
Case C: 2.50d	4048	168.88
Case D: 4.00d	4120	137.00

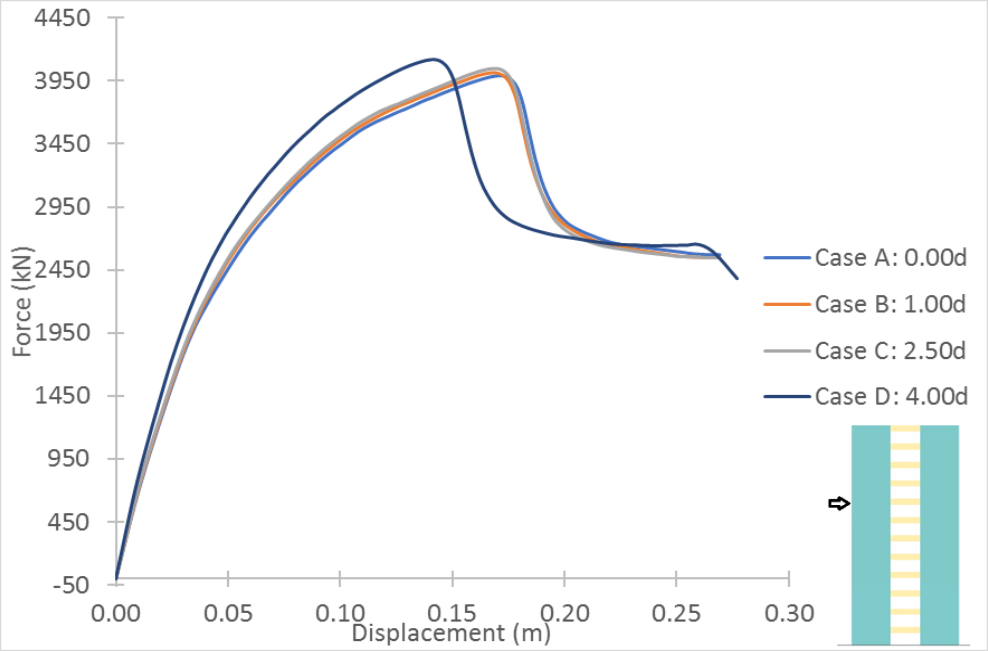

Figure (5-9): Displacement vs. Base shear for coupled walls with different HPFRC embedment inside the coupled walls under monotonic loading

5.4.1.2 Cyclic Loading

Figure (5-10) shows comparison between the behavior of coupled walls when they are subjected to cyclic loading in order to reach the preferable condition of HPFRC embedment inside the coupled walls. Maximum base shears, and corresponding displacements are shown in Table (5-8). Figure (5-11) and (5-12) show the maximum normal stresses developed in the coupled walls at failure for case A and B and the corresponding normal stresses developed in the coupled walls at the same loading point for case C and D.

Table (5-8): Displacement vs. Base shear for coupled walls with different HPFRC embedment inside the coupled walls under cyclic loading

	Maximum base shear (kN)	Corresponding displacement (mm)
Case A: 0.00d	3620	127
Case B: 1.00d	3620	118
Case C: 2.50d	3830	137
Case D: 4.00d	4120	137

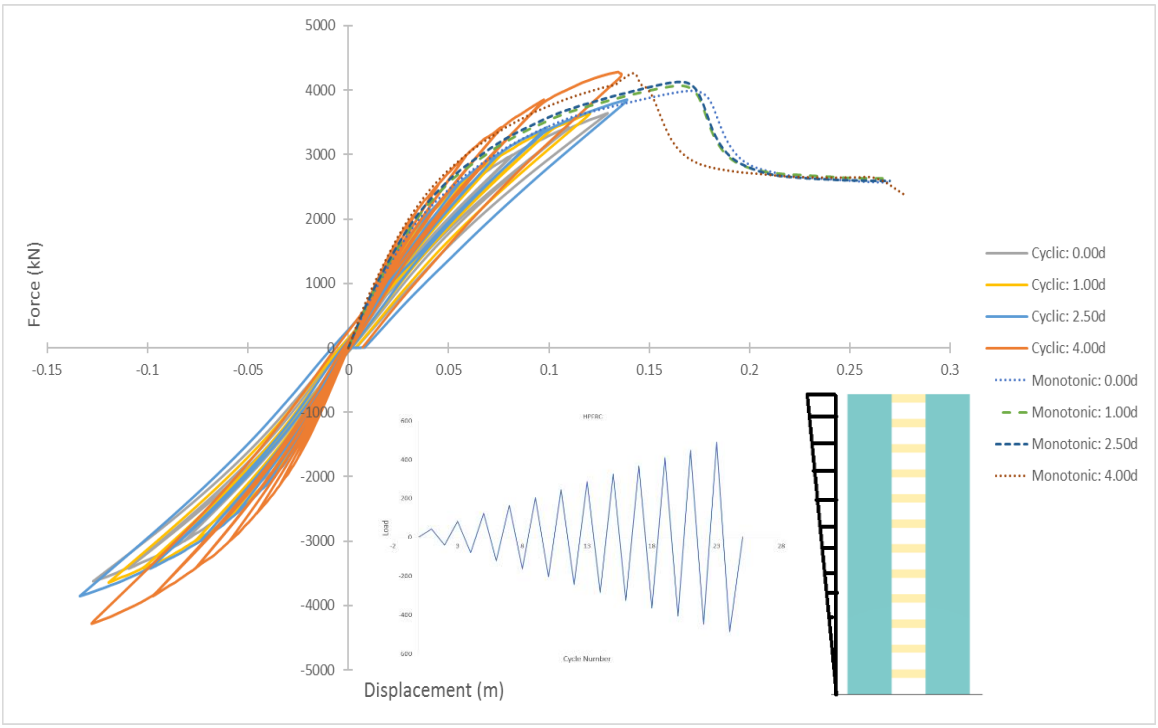

Figure (5-10): Displacement vs. Base shear for coupled walls with different HPFRC embedment inside the coupled walls under cyclic loading

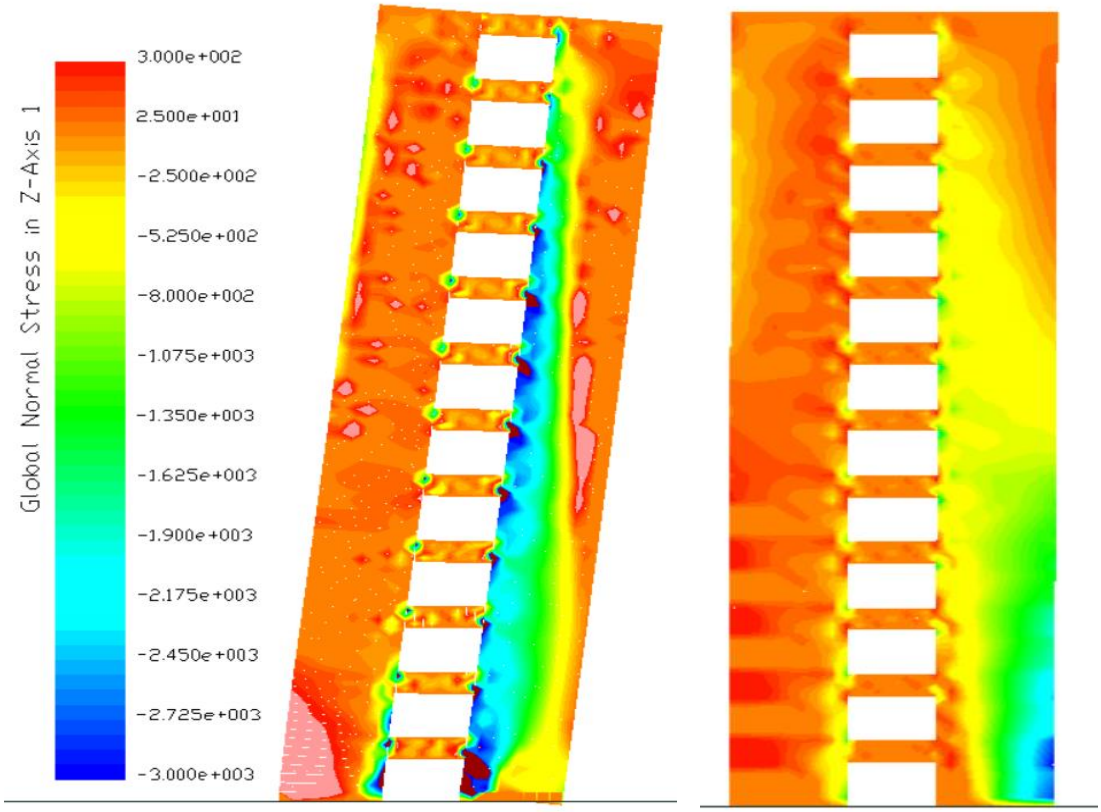

Figure (5-11): Normal stresses developed by case A (right) and case C (left)

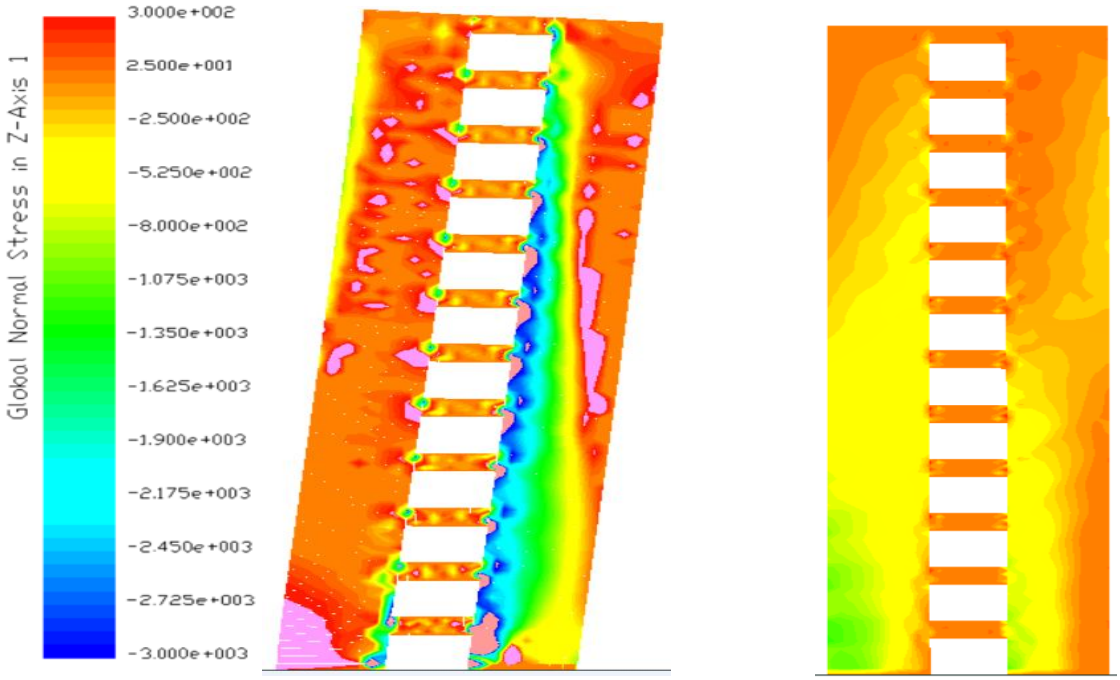

Figure (5-12): Normal stresses developed by case B (right) and case D (left)

5.5 Effect of Coupling Beam's Aspect Ratio

5.5.1 Behavior of Coupling Beam

In this section, the numerically obtained behavior of HPFRC coupling beams with different aspect ratios are investigated. Four models were created to determine the effect of varying aspect ratio on the failure criteria. Figure (5-13) shows the comparison between load-displacement response for the four models. Table (5-9) shows maximum base shear and corresponding displacement.

Table (5-9): Base shear vs. corresponding displacement for coupling beams with different aspect ratios under displacement-based load

	Maximum base shear (kN)	Corresponding displacement (mm)
Aspect ratio=2.72	371	15.80
Aspect ratio=3.00	331	19.79
Aspect ratio=3.33	286	22.00
Aspect ratio=3.75	242	24.00

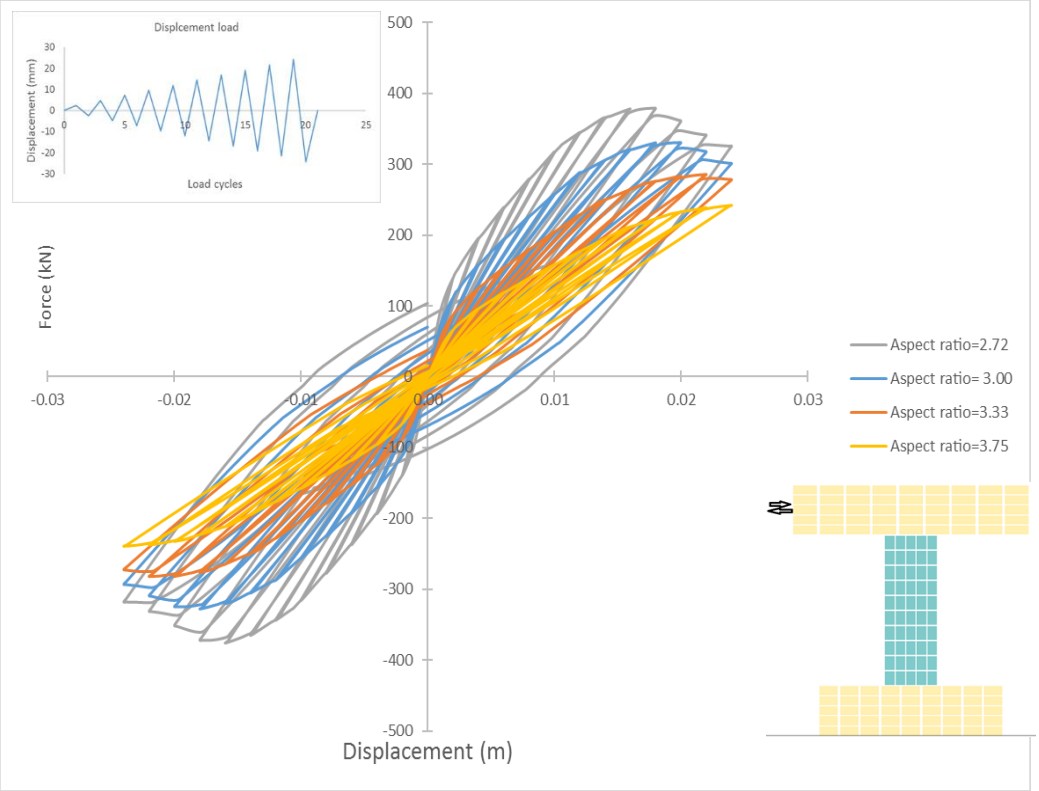

Figure (5-13): Displacement vs. Base shear for coupling beams with different aspect ratios under displacement-based load

5.5.2 Behavior of Coupled walls

5.5.2.1 Monotonic Loading

Figure (5-14) shows comparison between the behavior of coupled walls with different aspect ratios when they were subjected to monotonic loading at 2/3 height. Maximum base shears, and corresponding displacements are calculated as shown in Table (5-10).

Table (5-10): Base shear vs. corresponding displacement for coupled walls with different aspect ratios coupling beams under monotonic loading

	Maximum base shear (kN)	Corresponding displacement (mm)
Aspect ratio=2.72	4290	135
Aspect ratio=3.00	4120	141
Aspect ratio=3.33	3950	150
Aspect ratio=3.75	3760	165

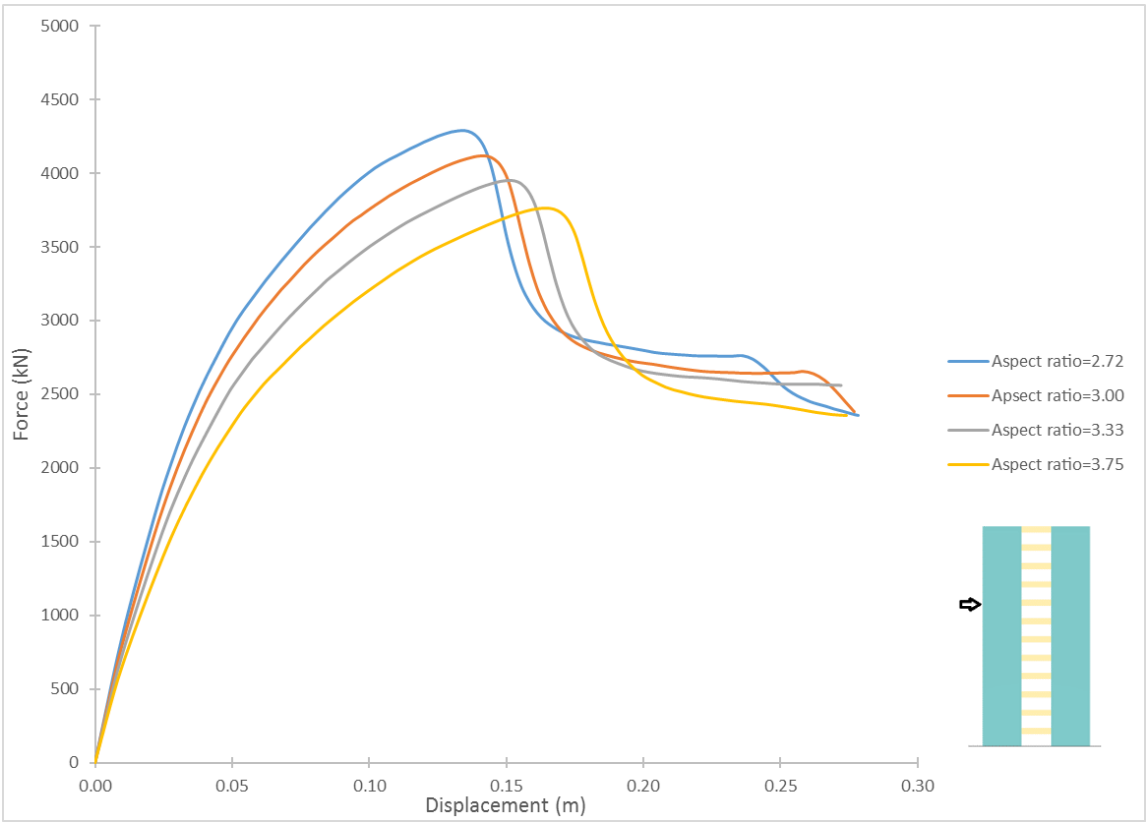

Figure (5-14): Displacement vs. Base shear for coupled walls with different aspect ratios coupling beams under monotonic loading

5.5.2.2 Cyclic Loading

Figure (5-15) shows comparison between the behavior of coupled walls when they are subjected to cyclic loading. Maximum base shears, and corresponding displacements are shown in Table (5-11). Figure (5-16) shows the maximum normal stresses developed in coupling beams for each case at maximum load.

Table (5-11): Base shear vs. corresponding displacement for coupled walls with different aspect ratios coupling beams under cyclic loading

	Maximum base shear (kN)	Corresponding displacement (mm)
Aspect ratio=2.72	4235.4	127.33
Aspect ratio=3.00	4120.0	137.00
Aspect ratio=3.33	3811.8	150.91
Aspect ratio=3.75	3388.3	142.00

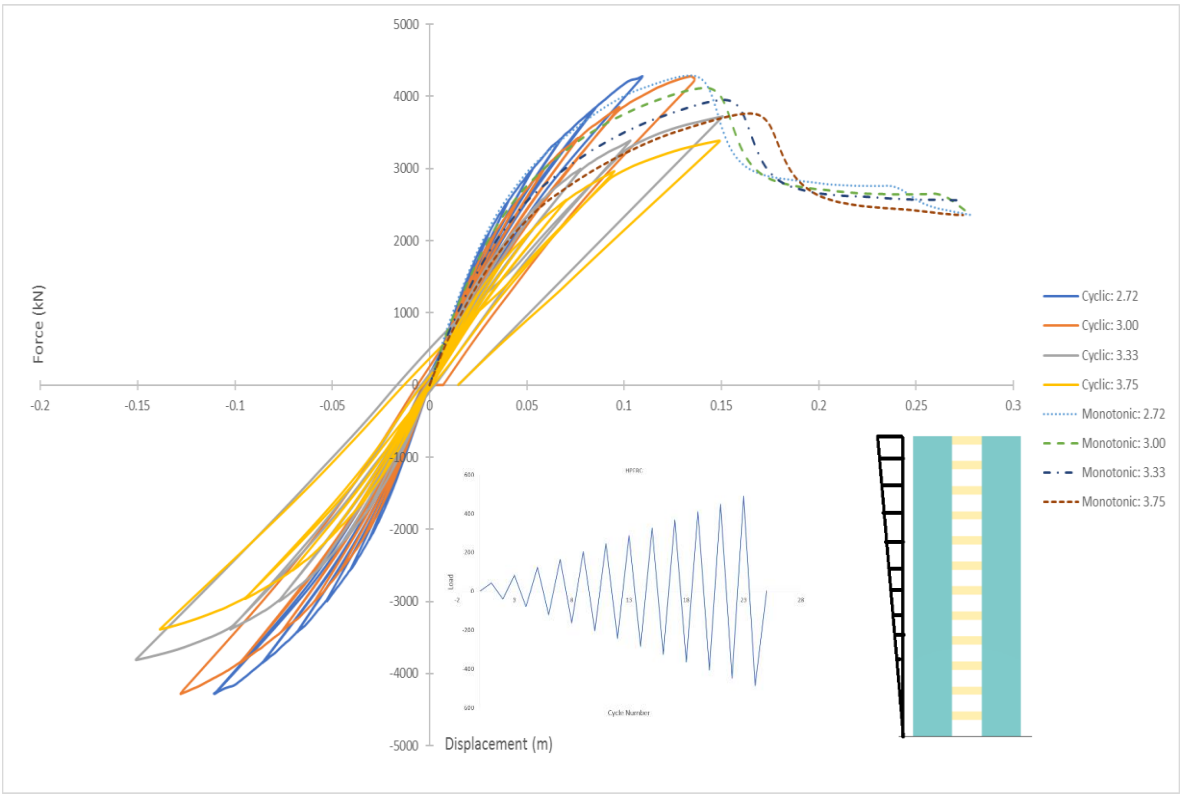

Figure (5-15): Displacement vs. Base shear for coupled walls with different aspect ratios coupling beams under cyclic loading

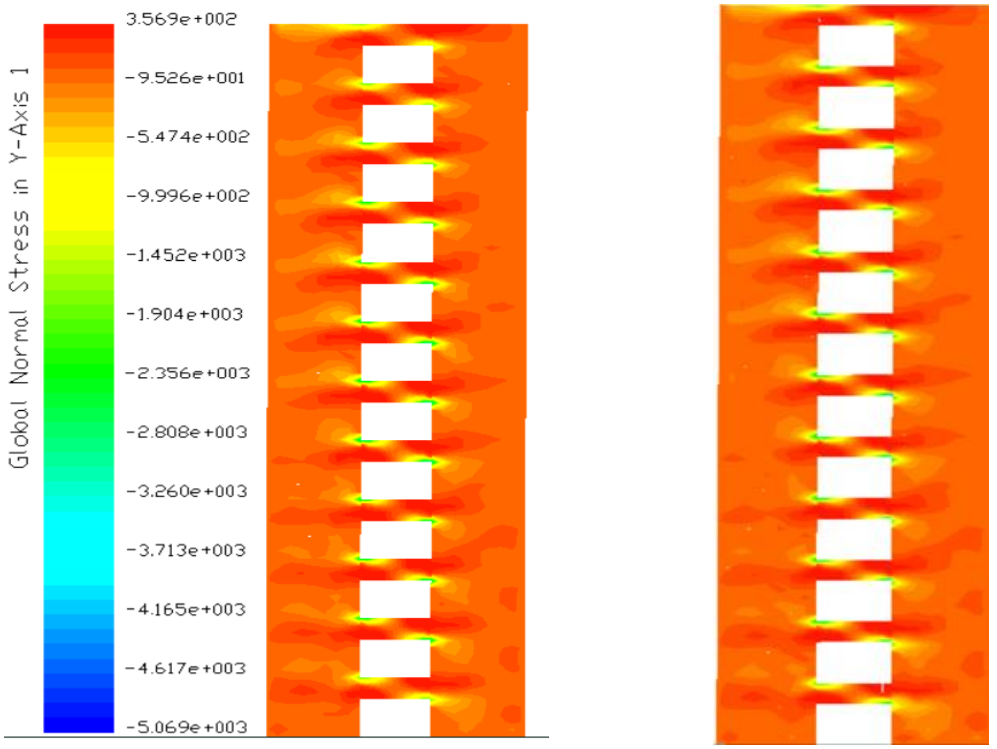

Aspect ratio=2.72 Aspect ratio=3.00

Figure (5-16-a): Normal stresses developed in coupling beams with aspect ratios 2.72 and 3.00 at maximum load

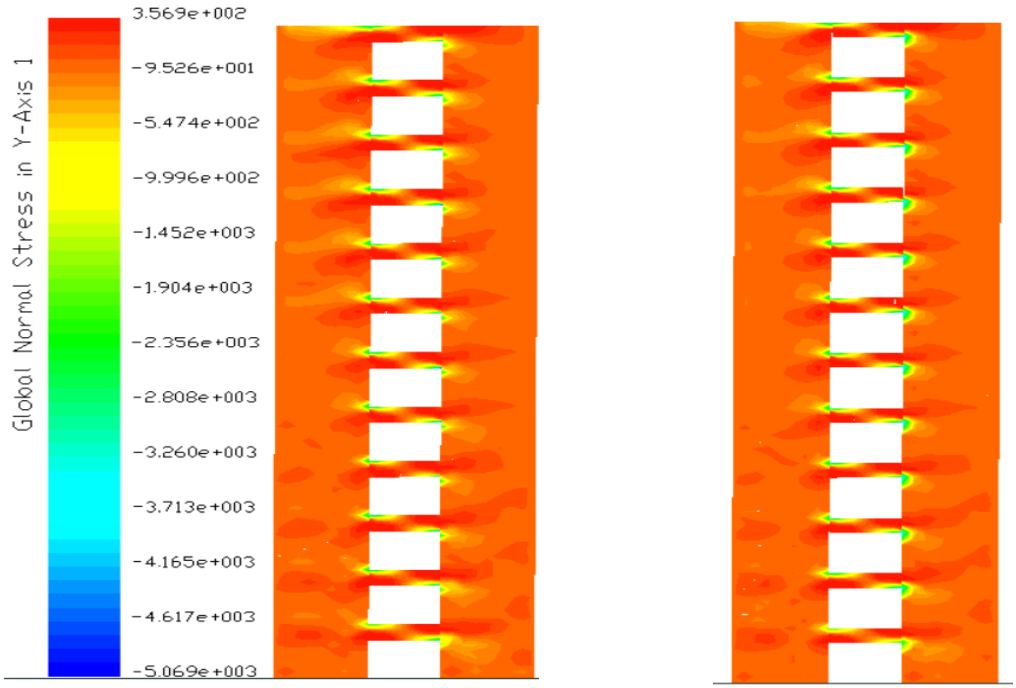

Aspect ratio=3.33 Aspect ratio=3.75

Figure (5-16-b): Normal stresses developed in coupling beams with aspect ratios 3.33 and 3.75 at maximum load

5.6 Effect of Presence of Diagonal Bars with and without Confining Stirrups

5.6.1 Behavior of Coupling Beam

In this section, the numerically obtained behavior of traditional reinforced concrete and high-performance reinforced concrete are investigated. Four models were created to investigate the effect of using diagonal bars with and without confining stirrups. Then, they compared with a model with conventional reinforcement only. Figure (5-17) shows the comparison between load-displacement response for the five models. Table (5-12) shows maximum base shear and corresponding displacement.

Table (5-12): Base shear vs. corresponding displacement for different reinforcement schemes under displacement-based load

	Maximum base shear (kN)	Corresponding displacement (mm)
Model 1	471	24
Model 2	471	24
Model 3	509	24
Model 4	509	24
Conventional RFT	331	20

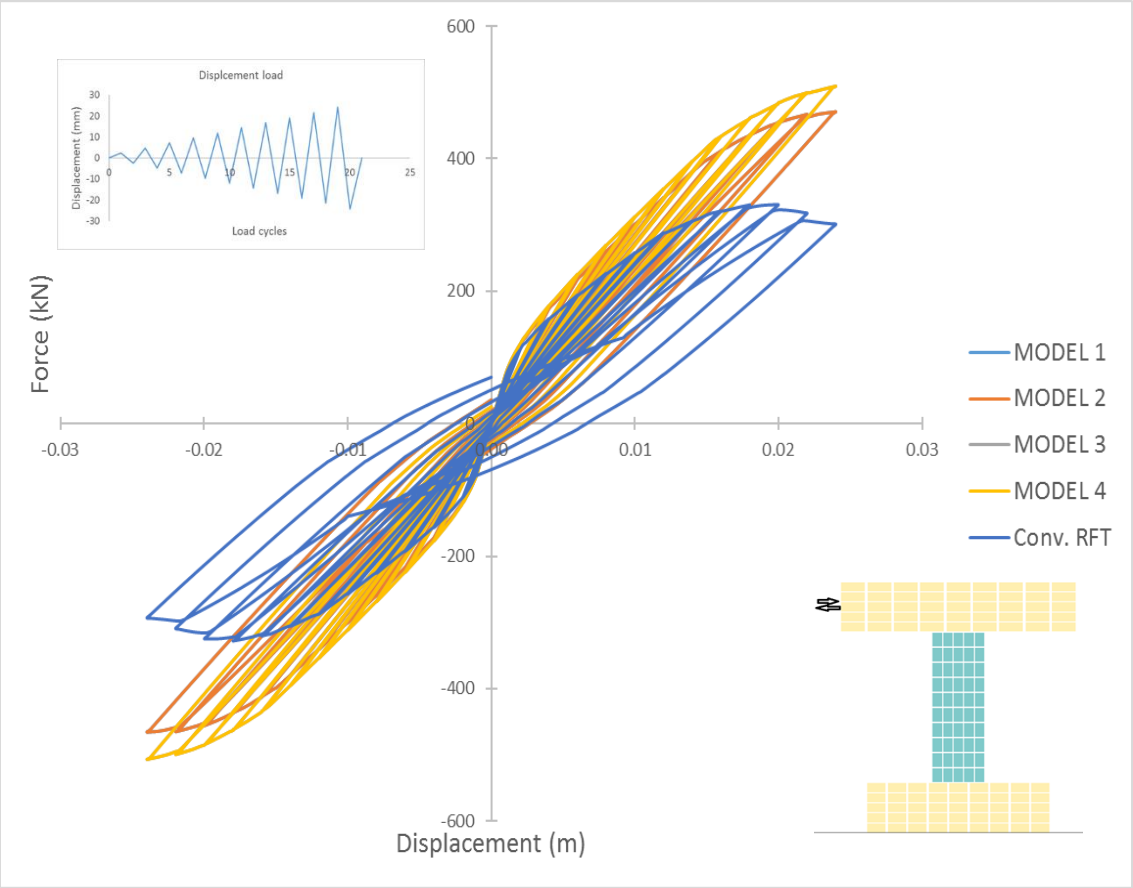

Figure (5-17): Displacement vs. Base shear for different reinforcement schemes under displacement-based load

5.6.2 Behavior of Coupled Walls

5.6.2.1 Monotonic Loading

Figure (5-18) shows comparison between the behavior of coupled walls structure when they were subjected to monotonic loading at 2/3 height. Energy dissipated by each coupled wall, maximum base shear, and corresponding displacement are as shown in Table (5-13).

Table (5-13): Base shear vs. corresponding displacement for coupled walls with different reinforcement schemes coupling beams under monotonic load

	Maximum base shear (kN)	Corresponding displacement (mm)	Energy dissipated (kN.m)
Model 1	4650	132.30	848
Model 2	4650	132.30	835
Model 3	4760	132.95	845
Model 4	4760	132.95	839
Conventional RFT	4120	139.00	802

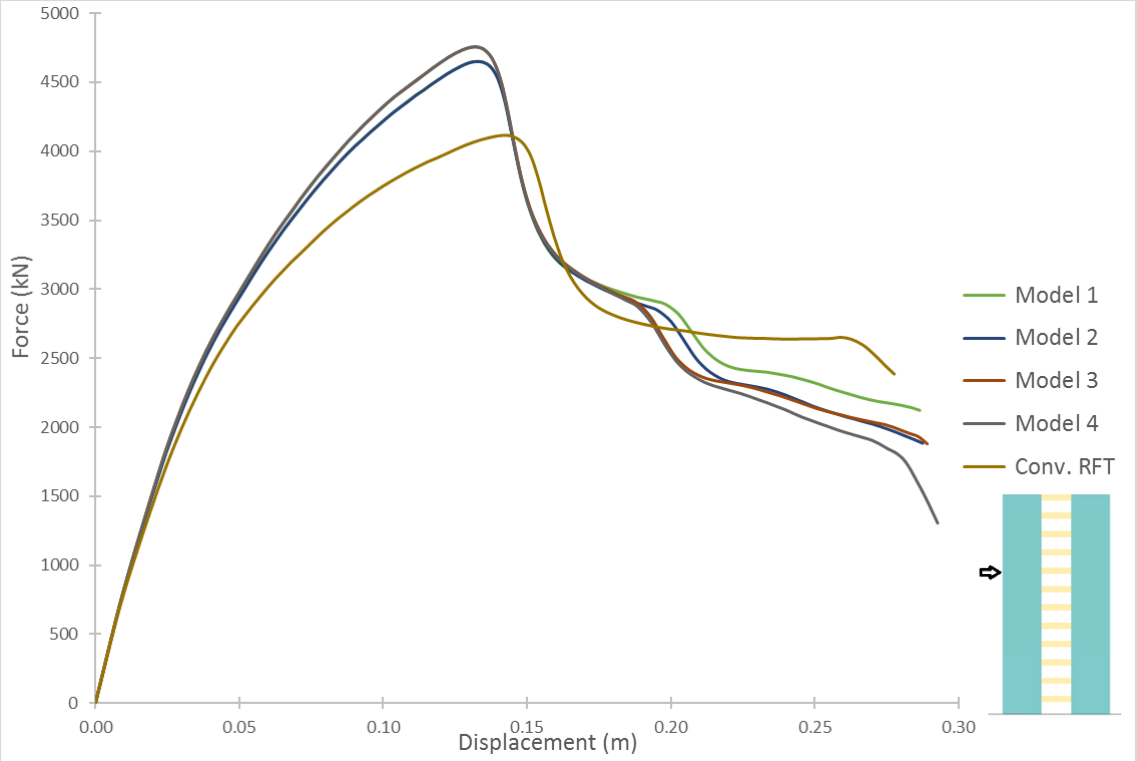

Figure (5-18): Displacement vs. Base shear for coupled walls with different reinforcement schemes coupling beams under monotonic load

5.6.2.2 Cyclic Loading

Figure (5-19) shows comparison between the behavior of coupled walls when they are subjected to cyclic loading. Figure (5-20) shows the maximum normal stresses developed in coupling beams for each case at maximum load. Maximum base shears, corresponding displacements are shown in Table (5-14).

Table (5-14): Base shear vs. corresponding displacement for coupled walls with different reinforcement schemes coupling beams under cyclic load

	Maximum base shear (kN)	Corresponding displacement (mm)
Model 1	4280	114.21
Model 2	4280	114.21
Model 3	4280	110.18
Model 4	4280	110.18
Conventional RFT	4120	137.00

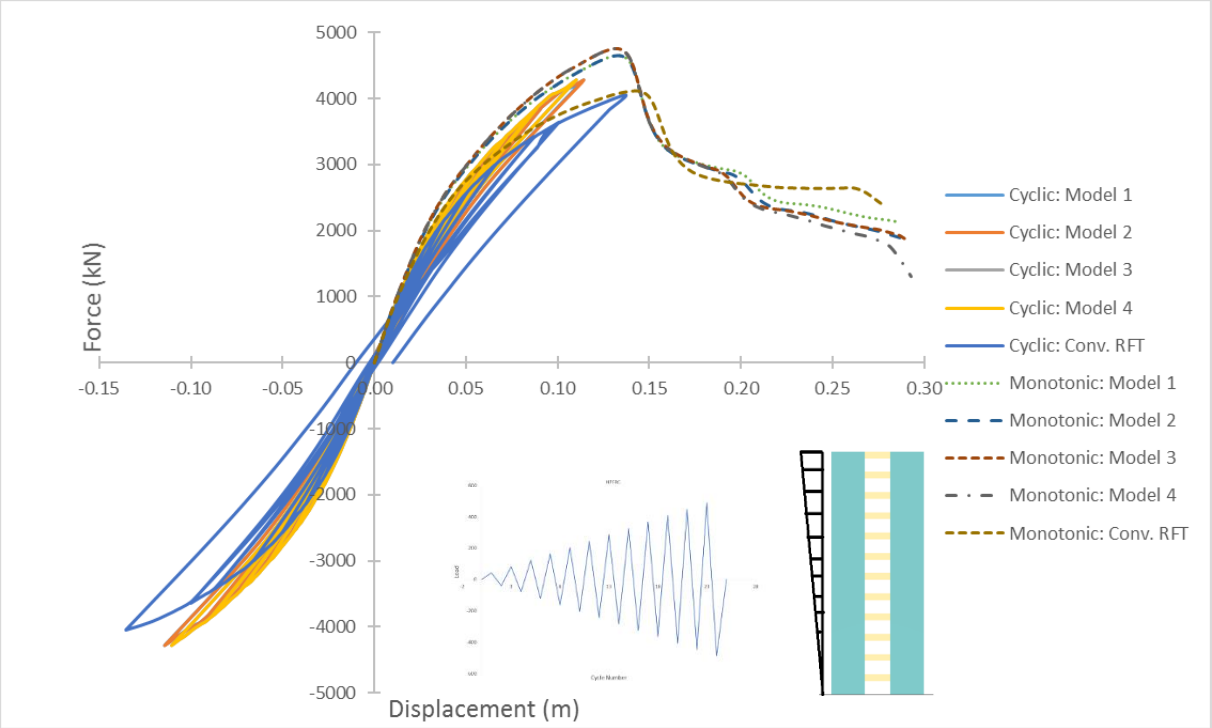

Figure (5-19): Displacement vs. Base shear for coupled walls with different reinforcement schemes coupling beams under cyclic load

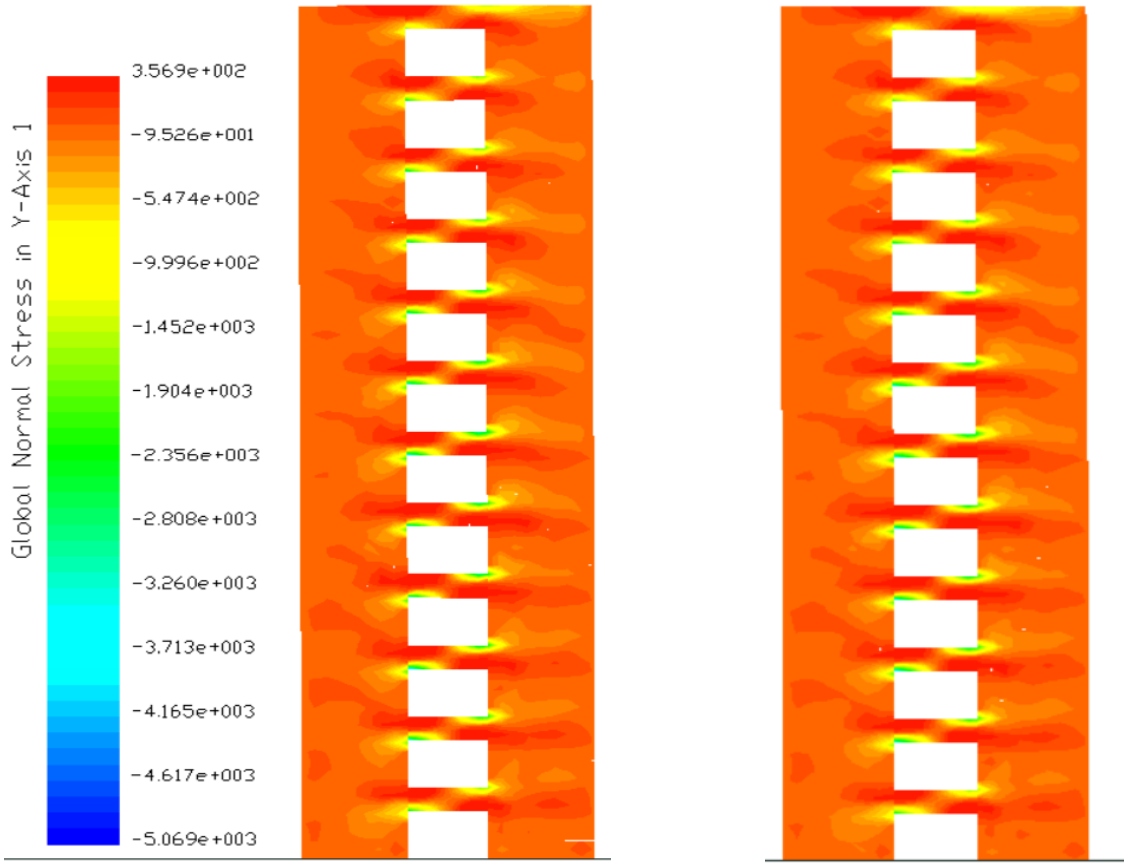

a) **Model 1,2** **b) Model 3,4**

Figure (5-20): Normal stresses developed in coupling beams for each case at maximum load

5.7 Effect of HPFRC Different Mixtures

5.7.1 Behavior of Coupling Beam

In this section, the numerically obtained behavior of HPFRC coupling beams with different high-performance steel fibers ratios are studied. Three models were created to determine the effect of using different ratio of steel fibers on the overall capacity and energy dissipation of coupling beams. Then, they were compared with traditional reinforced concrete coupling beams. Figure (5-21) shows the comparison between load-displacement response for the four models. Table (5-15) shows maximum base shear and corresponding displacements.

Table (5-15): Base shear vs. corresponding displacements for different mixtures under displacement-based load

	Maximum base shear (kN)	Corresponding displacement (mm)
RC	288	23.99
HPFRC-Case A	331	20.00
HPFRC-Case B	366	17.90
HPFRC-Case C	368	17.90
HPFRC-Mix D	375	17.90

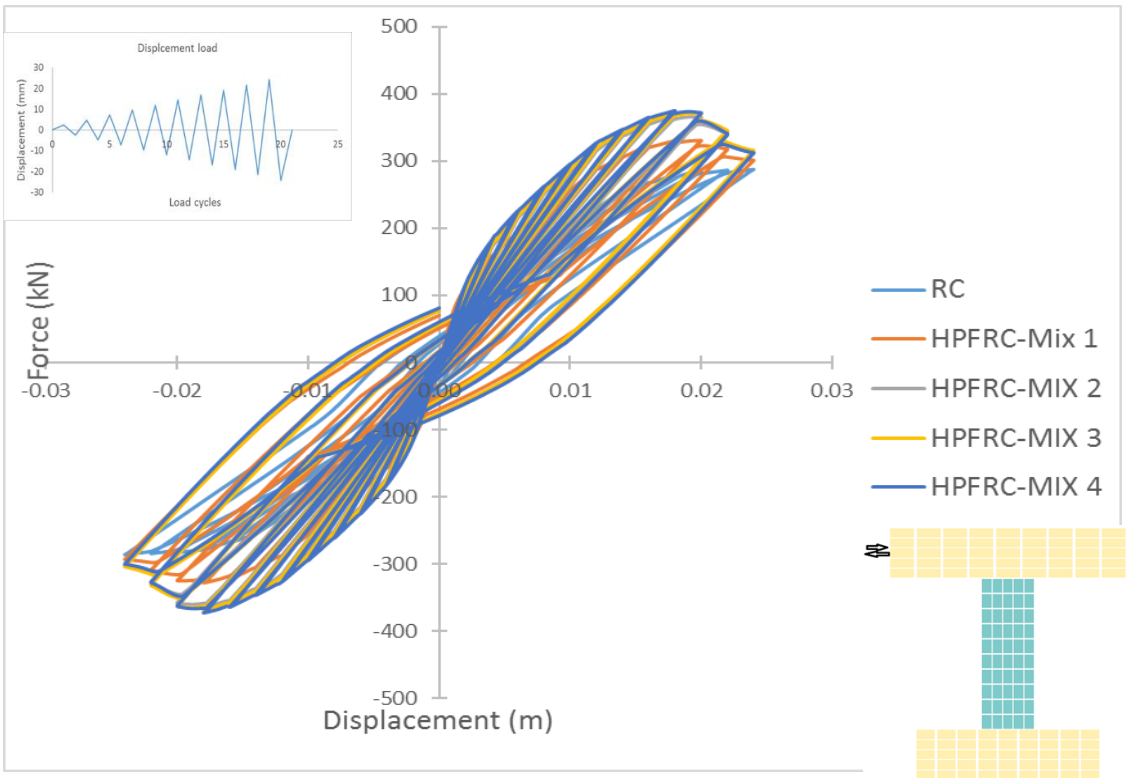

Figure (5-21): Displacement vs Base shear for different mixtures under displacement-based load

5.7.2 Behavior of Coupled Walls

5.7.2.1 Monotonic Loading

Figure (5-22) shows comparison between the behavior of coupled walls with different steel fibers ratio when they were subjected to monotonic loading at 2/3 height. Energy dissipated by each coupled wall, maximum base shear, and corresponding displacement are calculated as shown in Table (5-16).

Table (5-16): Base shear vs. corresponding displacement for different mixtures under monotonic loading

	Maximum base shear (kN)	Corresponding displacement (mm)	Dissipated Energy (kN.m)
RC	3310.00	229.00	623
HPFRC-Mix 1	4120.00	137.00	802
HPFRC-Mix 2	4260.00	148.00	808
HPFRC-Mix 3	4273.98	147.81	808
HPFRC-Mix 4	4283.38	142.60	814

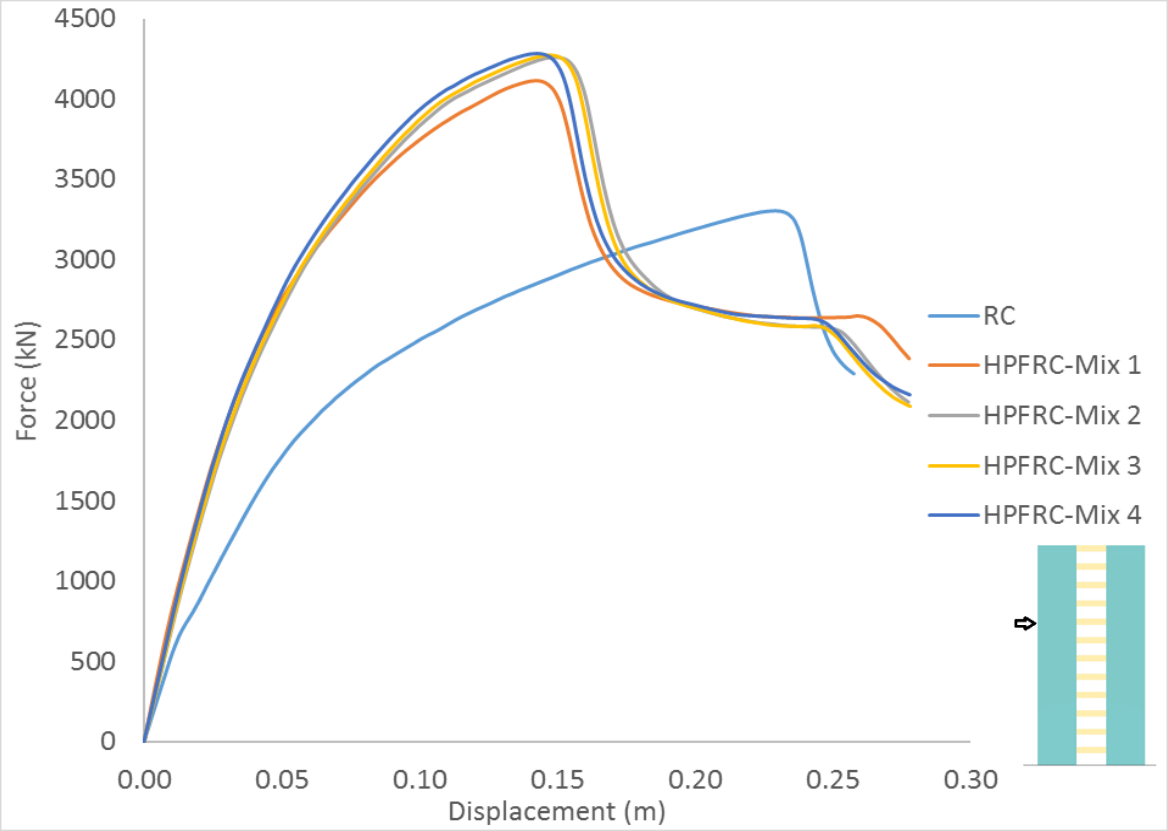

Figure (5-22): Displacement vs Base shear for different mixtures under monotonic loading

5.7.2.2 Cyclic Loading

Figure (5-23) shows comparison between the behavior of coupled walls when they are subjected to cyclic loading. Figure (5-24) shows the maximum normal stresses developed in coupling beams. Maximum base shears, corresponding displacements are shown in Table (5-17).

Table (5-17): Base shear vs. corresponding displacement for different mixtures under cyclic loading

	Maximum base shear (kN)	Corresponding displacements (mm)
RC	3090	137.00
HPFRC-Mix 1	4120	137.00
HPFRC-Mix 2	4050	120.82
HPFRC-Mix 3	4050	119.12
HPFRC-Mix 4	4050	114.31

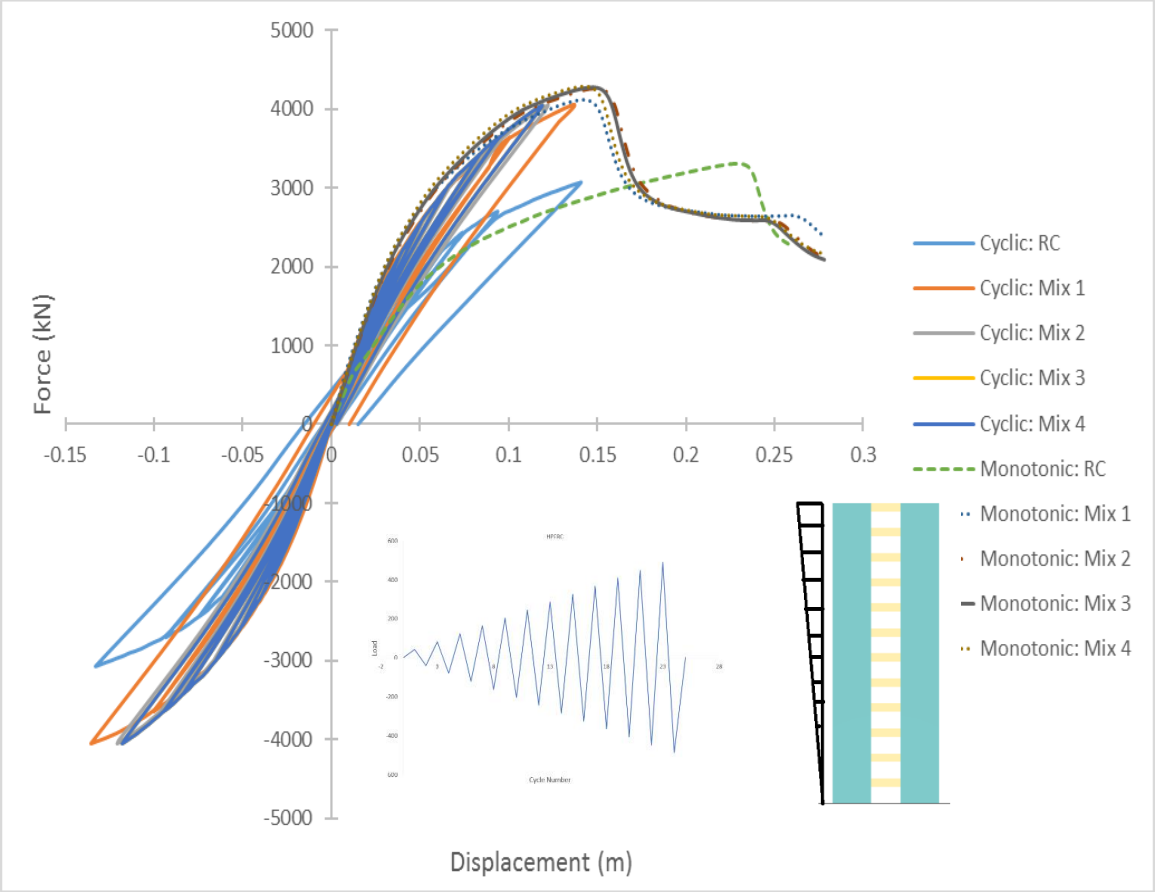

Figure (5-23): Displacement vs Base shear for different mixtures under cyclic loading

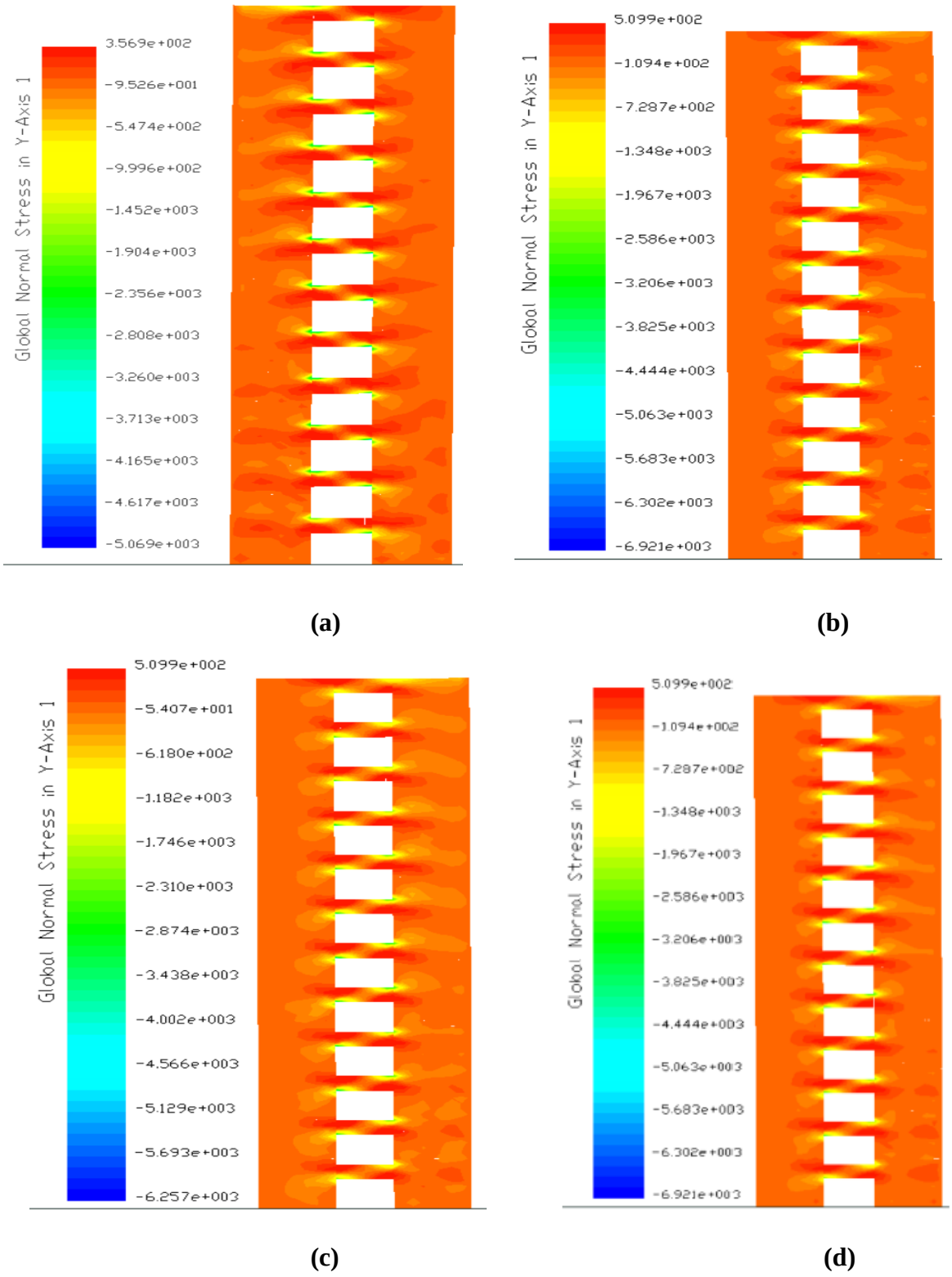

Figure (5-24): Normal stresses developed in coupling beams at maximum load for different mixtures (a) HPFRC-Mix 1, (b) HPFRC-Mix 2, (c) HPFRC-Mix 3 and (d) HPFRC-Mix 4

CHAPTER 6: DISCUSSION OF NUMERICAL RESULTS

6.1 Introduction

This chapter includes the discussion of the effect of using HPFRC in coupling beams based on the maximum capacity and energy dissipated for each case, in light of the outputs obtained in Chapter 5.

The effect of material type, longitudinal reinforcement ratio of the coupling beam, HPFRC embedment inside the coupled walls, beam's aspect ratio, presence of diagonal bars with and without the confining stirrups, and mixtures of HPFRC on the behavior of the coupled walls are then discussed.

6.2Effect of Material Type

6.2.1 Behavior of Coupling Beam

Using HPFRC in coupling beams showed an increase in the value of maximum capacity with a smaller relative drift. Coupling beam constructed with HPFRC showed an increase in capacity as much as 14.9% and a decrease of corresponding drift by 16.6% occurred.

6.2.2Behavior of Coupled Walls

6.2.2.1 Monotonic Loading

Applying a monotonic displacement loading on coupled walls at 2/3 height showed that HPFRC coupling beams resulted in showed an increase in capacity by 22.9% compared to RC coupling beams, while caused a decrease in the corresponding drift by 39.3%. Furthermore, HPFRC coupling beams enhanced the energy dissipation where an increase of 28.7% in dissipated energy was obtained.

6.2.2.2 Cyclic Loading:

Investigating the behavior of coupled walls under cyclic loading showed that HPFRC lead to an increase in capacity of 31.4% and same drift due to the assigned load which depends on forces that reach same displacement for RC and HPFRC coupling beams.

Clearly the use of HPFRC coupling beams with its ductile behavior showed a considerable enhancement in the behavior of the coupled walls.

6.3 Effect of Longitudinal Reinforcement Ratio of Coupling Beams

6.3.1 Behavior of Coupling Beam

Applying a displacement based cyclic loading on coupling beams with different longitudinal reinforcement ratios showed an increase in capacity. Increasing beam's longitudinal reinforcement ratio from 0.5% to 0.6% caused an increase in the capacity of 11.2%. However, the corresponding drift was approximately unchanged.

Increasing beam longitudinal reinforcement ratio to 0.7% and 0.8% showed an increase in capacity, compared to reference case, by 21.45% and 29%, respectively, while the corresponding drift increased by 1.06% and 2.1%, respectively.

The maximum obtained capacities are shown in Figure (6-1), while the corresponding drift are shown in Figure (6-2).

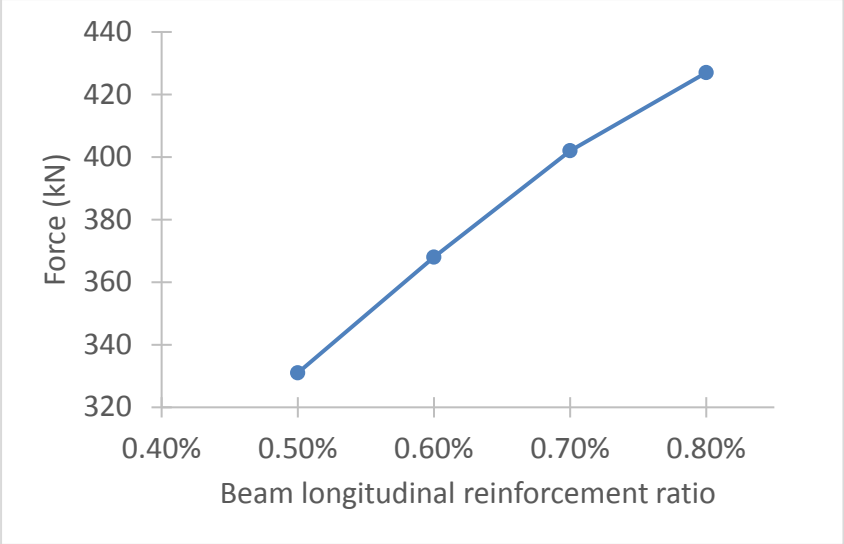

Figure (6-1): Maximum base Shear for different beam's longitudinal reinforcement ratios under displacement-based cyclic loading

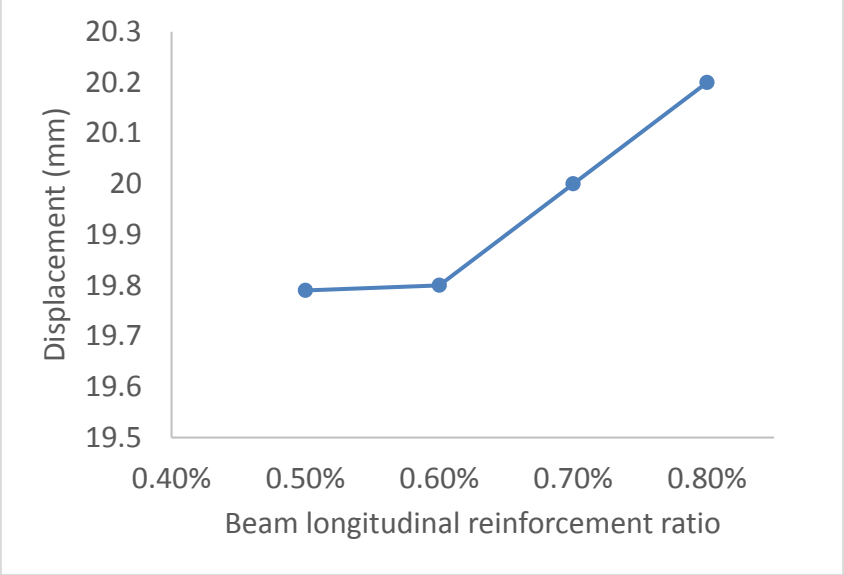

Figure (6-2): Maximum displacements for different beam's longitudinal reinforcement ratios under displacement-based cyclic loading

6.3.2 Behavior of Coupled Walls

6.3.2.1 Monotonic Loading

Increasing beam's longitudinal reinforcement ratio resulted in an increase in capacity by 4.1%, 6.9% and 9.8% for coupling beam's with longitudinal reinforcement ratio equal to 0.6%, 0.7% and 0.8% respectively, compared to reference case with longitudinal reinforcement ratio equals to 0.5%. On the other hand, a decrease in the corresponding drift by 1.74%, 3.3% and 4.8% respectively, was observed.

The maximum obtained capacities are shown in Figure (6-3), while the corresponding drift are shown in Figure (6-4).

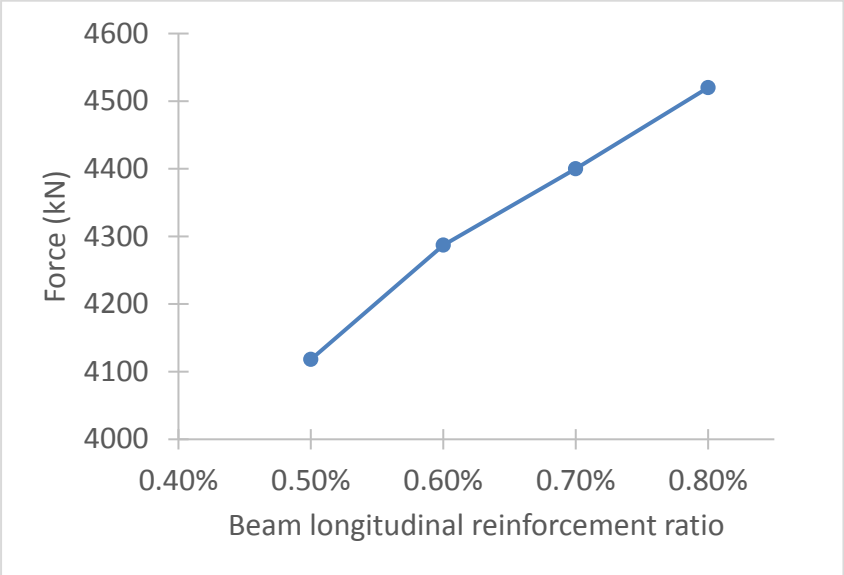

Figure (6-3): Maximum base Shear for different beam's longitudinal reinforcement ratios under monotonic loading

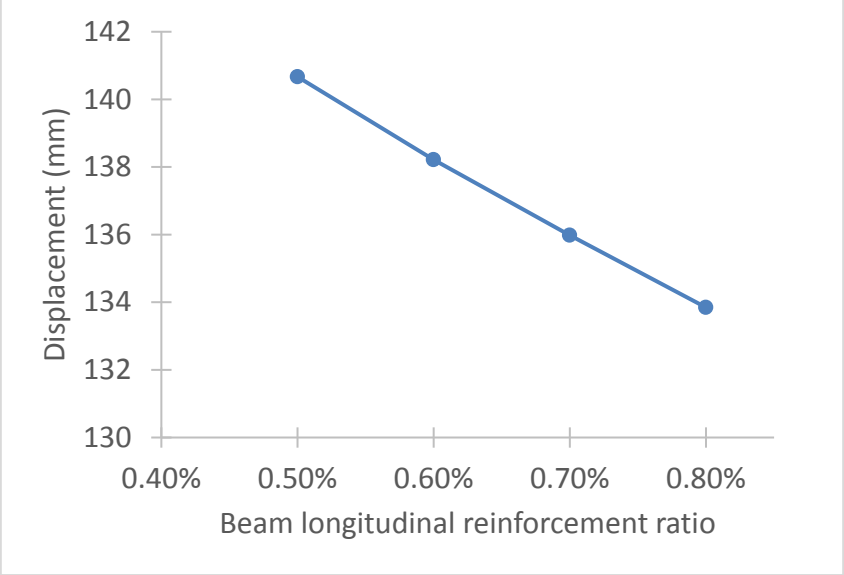

Figure (6-4): Corresponding displacements for different beam's longitudinal reinforcement ratios under monotonic loading

6.3.2.2 Cyclic Loading

Investigating the behavior of coupled walls under cyclic loading showed that increasing coupling beam's longitudinal reinforcement ratios resulted in an increase in capacity. Increasing reinforcement ratio from 0.5% to 0.6% lead to an increase of 5.7% of capacity, while increasing reinforcement ratio from 0.5% to 0.7% and 0.8% lead to an increase of 8.1% and 8.6% of capacity respectively. On the other hand, decreasing reinforcement ratio from 0.8% to 0.6% and 0.7% lead to an increase of 9.3% and 6.2% of the corresponding drift, respectively.

The maximum obtained capacities are shown in Figure (6-5), while the corresponding drifts are shown in Figure (6-6).

Clearly, increasing longitudinal reinforcement ratios for coupling beams resulted in an increase in coupled walls capacity, because of the increase in moment resisted by coupling beams. Moreover, coupling beams with 0.6% reinforcement ratio had greater displacement than 0.7% and 0.8% coupling beams due to less rigidities.

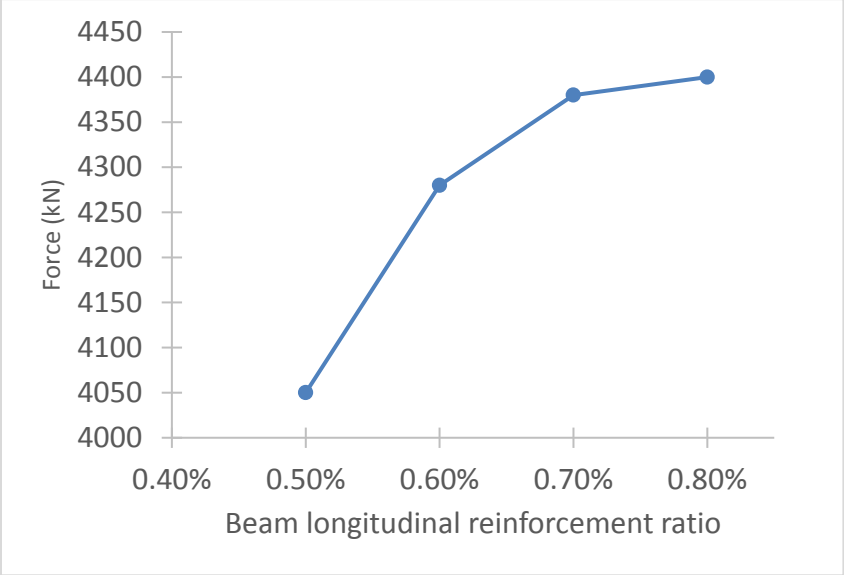

Figure (6-5): Maximum base Shear for different beam's longitudinal reinforcement ratios under cyclic loading

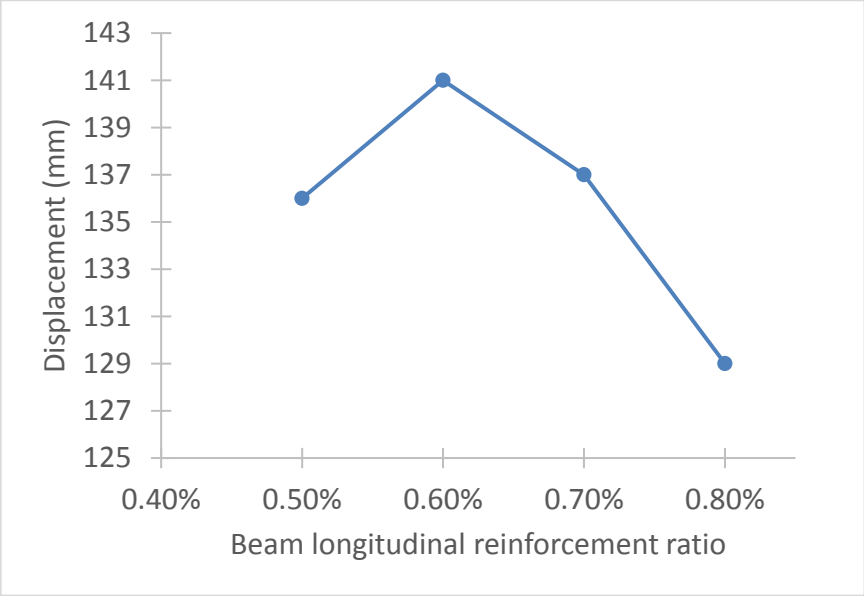

Figure (6-6): Corresponding displacements for different beam's longitudinal reinforcement ratios under cyclic loading

6.4 Effect of High-Performance Fiber Reinforced Concrete Embedment inside the Coupled walls

6.4.1 Behavior of Coupled Walls

6.4.1.1 Monotonic Loading

The maximum obtained capacities are shown in Figure (6-7), while the corresponding drift are shown in Figure (6-8). Increasing HPFRC embedment inside the coupled walls resulted in an increase in their capacity. When HPFRC was extended to a distance equals to coupling beam's depth, the coupled walls capacity increased by 0.60% while the corresponding drift decreased by 1.60%. When the HPFRC was extended to 2.5 and 4 coupling beam's depth, the capacity increased by 1.42% and 3.23% respectively, while the corresponding drift decreased by 1.71% and 20.26% respectively.

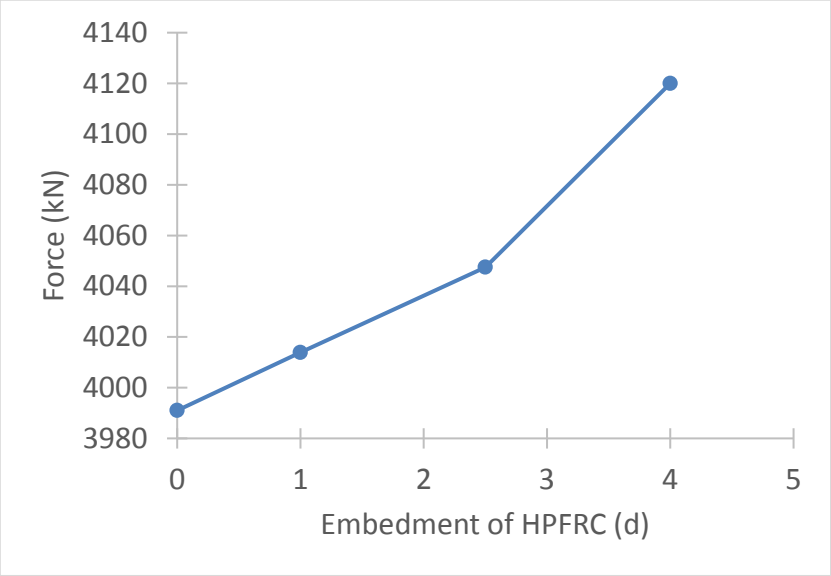

Figure (6-7): Maximum base Shear for different HPFRC embedment in terms of coupling beam's depth under monotonic loading

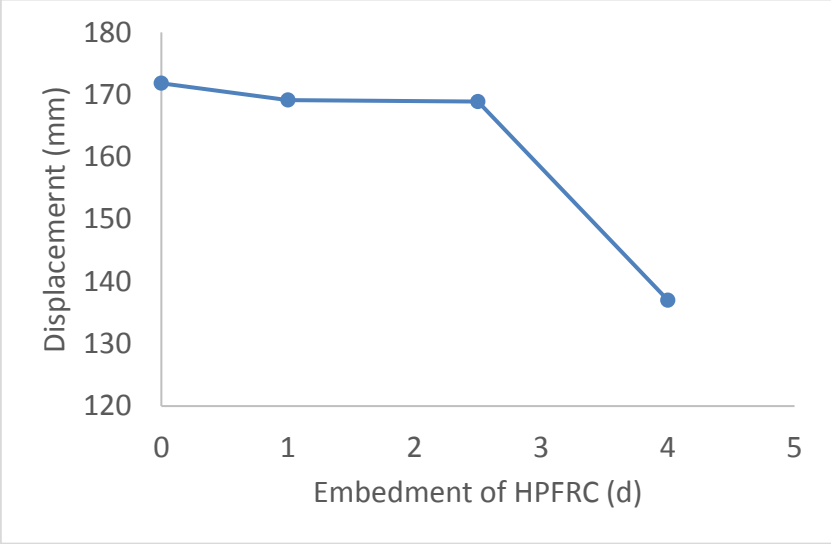

Figure (6-8): Corresponding displacements for different HPFRC embedment in terms of coupling beam's depth under monotonic loading

6.4.1.2 Cyclic Loading

Increasing HPFRC embedment inside the coupled walls resulted in an increase in their capacity. When HPFRC was extended to a distance equals to coupling beam's depth, the coupled walls capacity increased by 1.30% while the corresponding drift decreased by 4.2%. When the HPFRC was extended to 2.5 and 4 coupling beam's depth, the capacity increased by 2.20% and 4.04% respectively, while the corresponding drift decreased by 4.33% and 20.26% respectively.

Clearly the use of HPFRC to construct coupled walls showed an enhancement in the capacity of coupled walls. The maximum obtained capacities are shown in Figure (6-9), while the corresponding drift are shown in Figure (6-10).

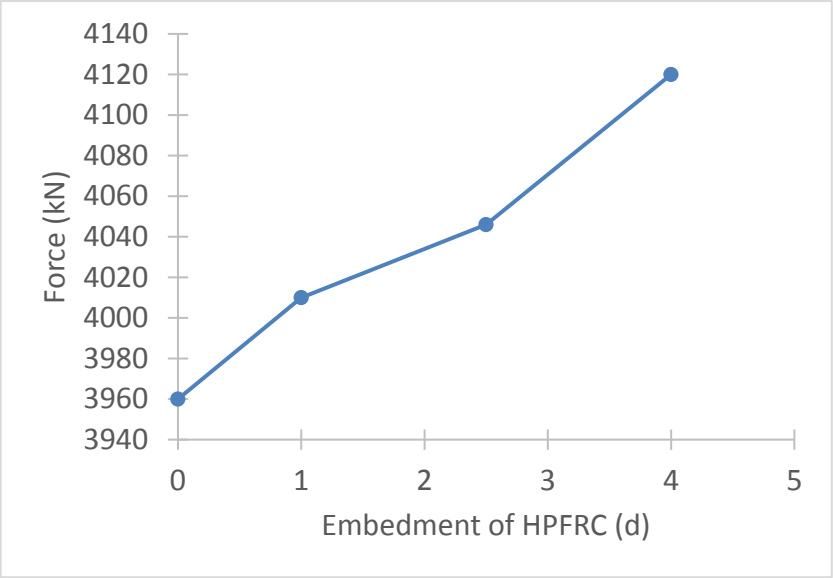

Figure (6-9): Maximum base Shear for different HPFRC embedment in terms of coupling beam's depth under cyclic loading

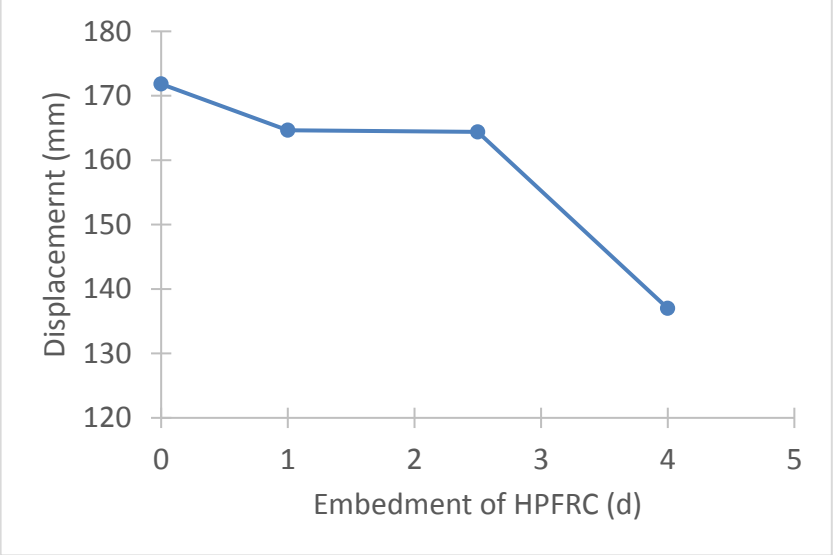

Figure (6-10): Corresponding displacements for different HPFRC embedment in terms of coupling beam's depth under monotonic loading

5.2 Effect of Coupling Beam's Aspect Ratio

6.5.1 Behavior of Coupling Beam

. The maximum obtained capacities are shown in Figure (6-11), while the corresponding drift are shown in Figure (6-12). Increasing beam aspect ratio lead to decreasing capacity and increasing drift.

Decreasing beam aspect ratio from 3.00 to 2.72 caused an increase in capacity of 14.67% and a decrease in drift of 10.11%, while increasing beam aspect ratio from 3.00 to 3.33 and 3.75 caused a decrease in capacity of 13.59% and 26.81% respectively. On the other hand, an increase in the corresponding drift by 11.17% and 21.28% respectively.

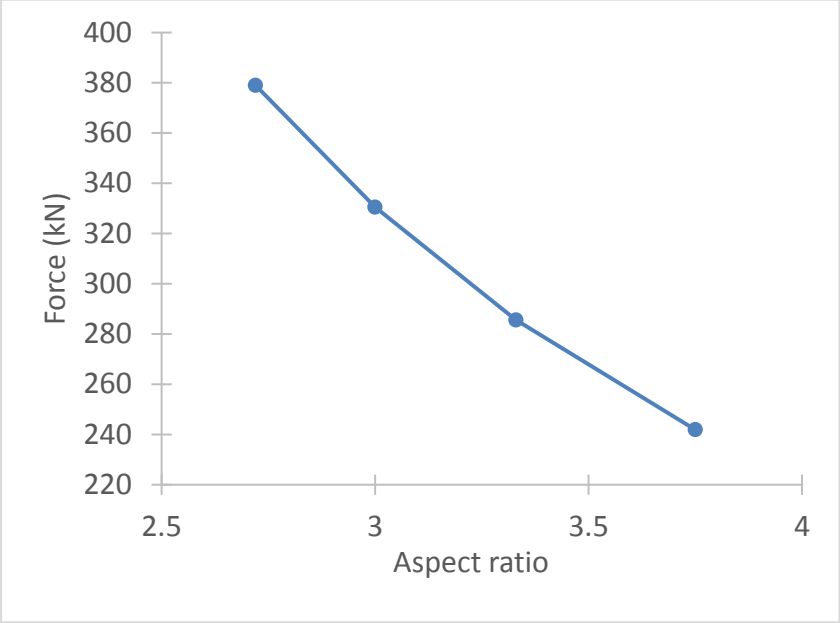

Figure (6-11): Maximum base shear for coupling beam with different aspect ratios under displacement-based cyclic loading

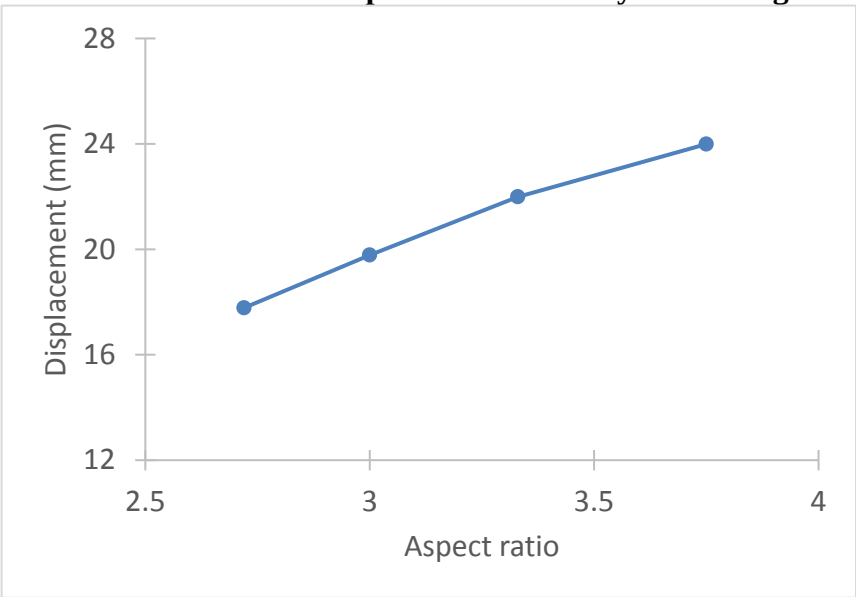

Figure (6-12): Corresponding displacement for coupling beam with different aspect ratios under displacement-based cyclic loading

6.5.2 Behavior of Coupled Wall

6.5.2.1 Monotonic Loading

The maximum obtained capacities are shown in Figure (6-13), while the corresponding drift are shown in Figure (6-14). It is obvious that increasing beam aspect ratio lead to decreasing capacity and increasing drift.

Decreasing beam aspect ratio from 3.00 to 2.72 caused an increase in capacity of 4.13% and a decrease in drift of 4.10%, while increasing beam aspect ratio from 3.00 to 3.33 and 3.75 caused a decrease in capacity of 4.12% and 8.74% respectively. On the other hand, an increase in the corresponding drift by 6.90% and 17.40% respectively.

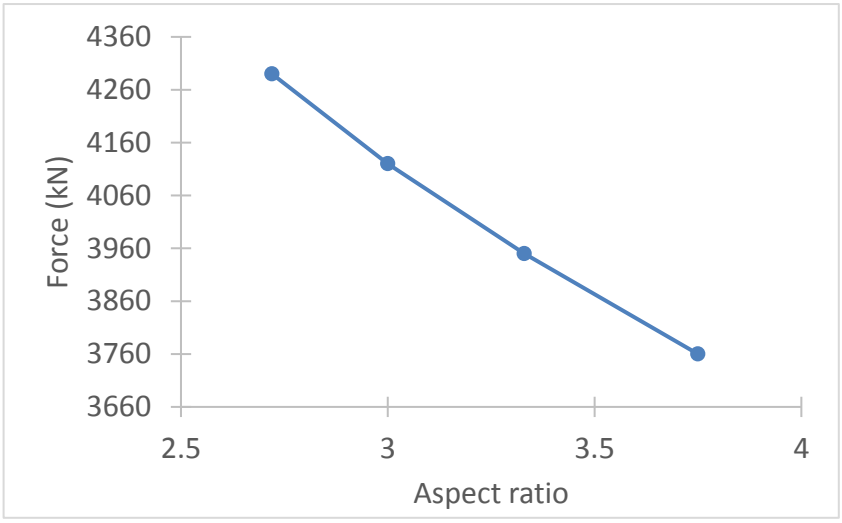

Figure (6-13): Maximum base Shear for different aspect ratios under monotonic loading

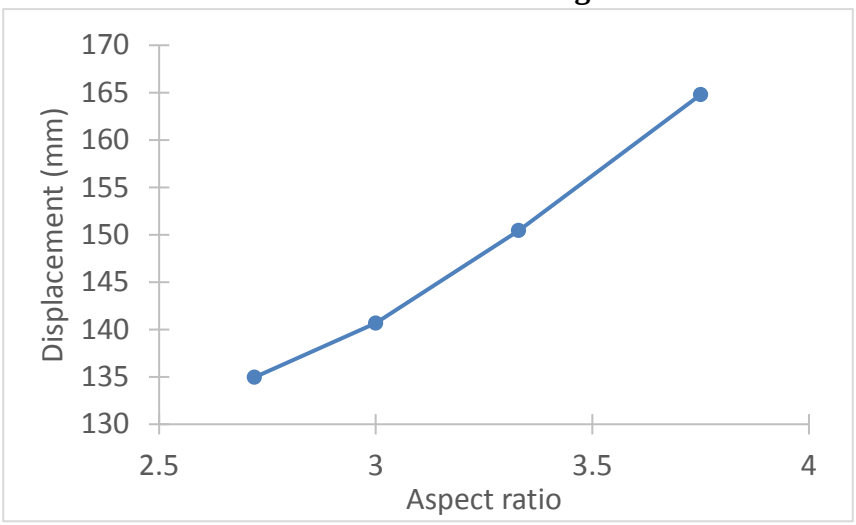

Figure (6-14): Displacements correspond to maximum base shear for different aspect ratios under monotonic loading

6.6.2.2 Cyclic Loading

Investigating the behavior of coupled walls under cyclic loading showed that increasing coupling beam's aspect ratios resulted in a decrease in capacity.

Decreasing beam aspect ratio from 3.00 to 2.72 caused an increase in capacity of 2.80% and a decrease in drift of 7.1%, while increasing beam aspect ratio from 3.00 to 3.33 and 3.75 caused a decrease in capacity of 7.48% and 15.81% respectively. On the other hand, an increase in the corresponding drift by 10.15% and 31.45% respectively

Clearly, these results showed that increasing aspect ratio by decreasing coupling beam depth, while span remains constant, resulted in decreasing capacity and increasing corresponding drift due to the decrease of rigidity. The maximum obtained capacities are shown in Figure (6-15), while the corresponding drift are shown in Figure (6-16).

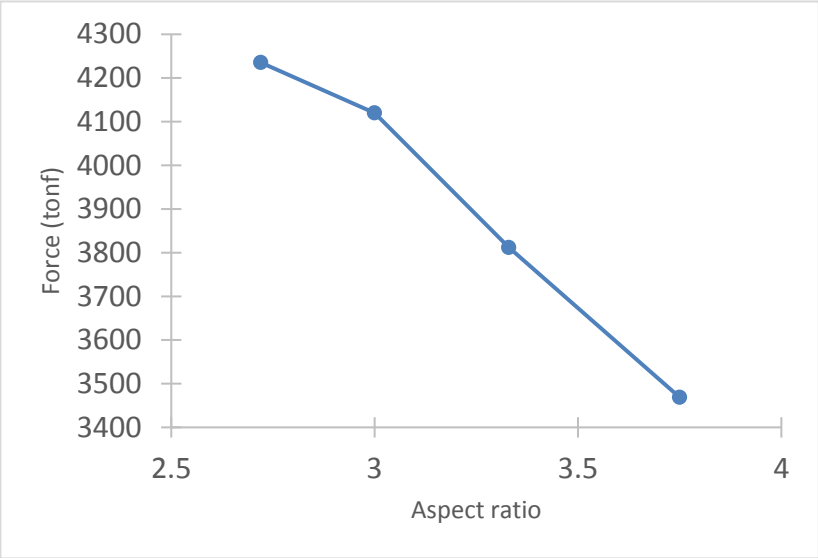

Figure (6-15): Maximum base Shear for different aspect ratios under cyclic loading

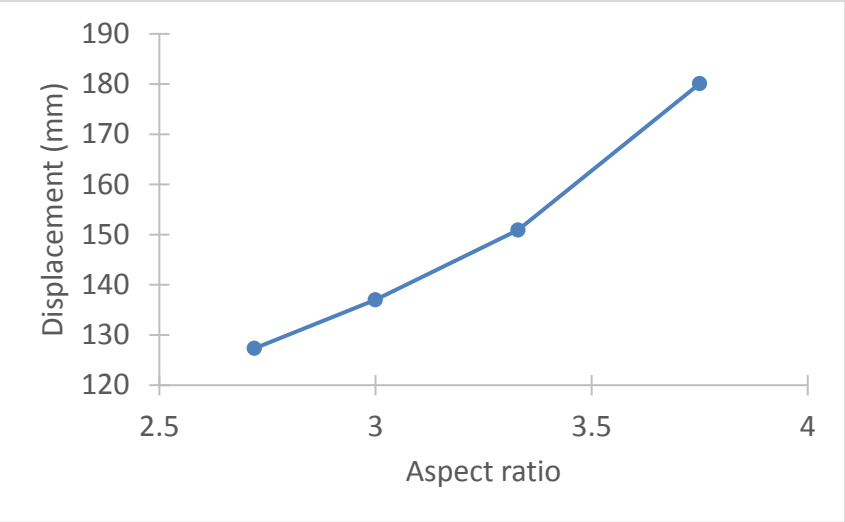

Figure (6-16): Displacements correspond to maximum base shear for different aspect ratios under cyclic loading

6.6 Effect of Presence of Diagonal Bars with and without Confining Stirrups

6.6.1 Behavior of Coupling Beam

Using diagonal bars with longitudinal reinforcement resulted in an increase in capacity and energy dissipation. When coupling beam was reinforced with two intersected groups of 4T22/ group with the longitudinal reinforcement, capacity increased by 42.3%, while the corresponding drift increased by 20%.

When coupling beam was reinforced with two intersected groups of 4T25/ group with the longitudinal reinforcement, capacity increased by 53.8%, while the corresponding drift increased by 20%.

It is obvious that confining stirrups do not affect neither maximum capacities nor corresponding drift. The maximum obtained capacities are shown in Figure (6-17), while the corresponding drift are shown in Figure (6-18).

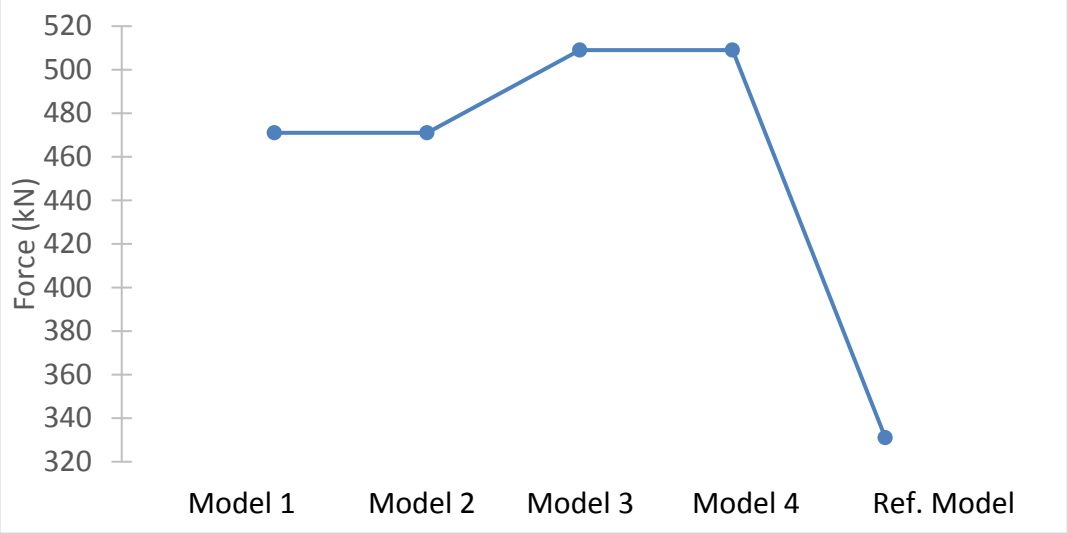

Figure (6-17): Maximum base shear for coupling beam with different RFT schemes under displacement-based cyclic loading

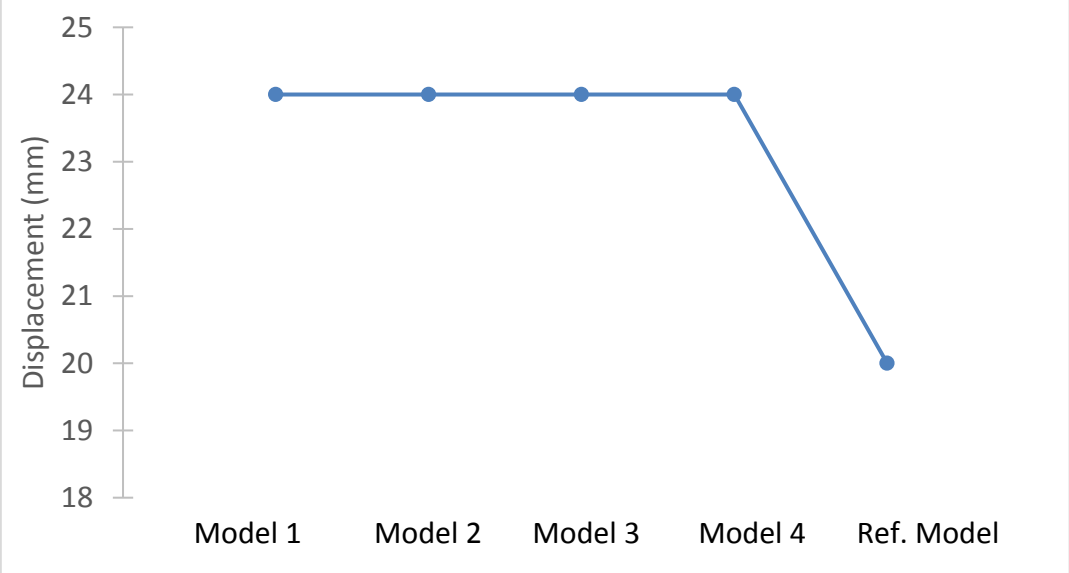

Figure (6-18): Corresponding displacement for coupling beam with different RFT schemes ratios under displacement-based cyclic loading

6.6.2 Behavior of Coupled Wall

6.6.2.1 Monotonic Loading

When coupling beams were reinforced with two intersected groups of 4T22/ group and 4T25/group with the longitudinal reinforcement, capacity increased by 12.9% and 15.5% respectively, while energy dissipated increased by 5.7% and 5.4% respectively while the corresponding drift decreased by 4.4% and 4.8% respectively, although adding the confining stirrups do not affect neither the capacity nor the corresponding displacement, it enhanced energy dissipation by 4.1% and 4.6% compared to reference case.

The maximum obtained capacities are shown in Figure (6-19), while the corresponding drift are shown in Figure (6-20), and the energy dissipated by each RFT configuration is showed in Figure (6-21).

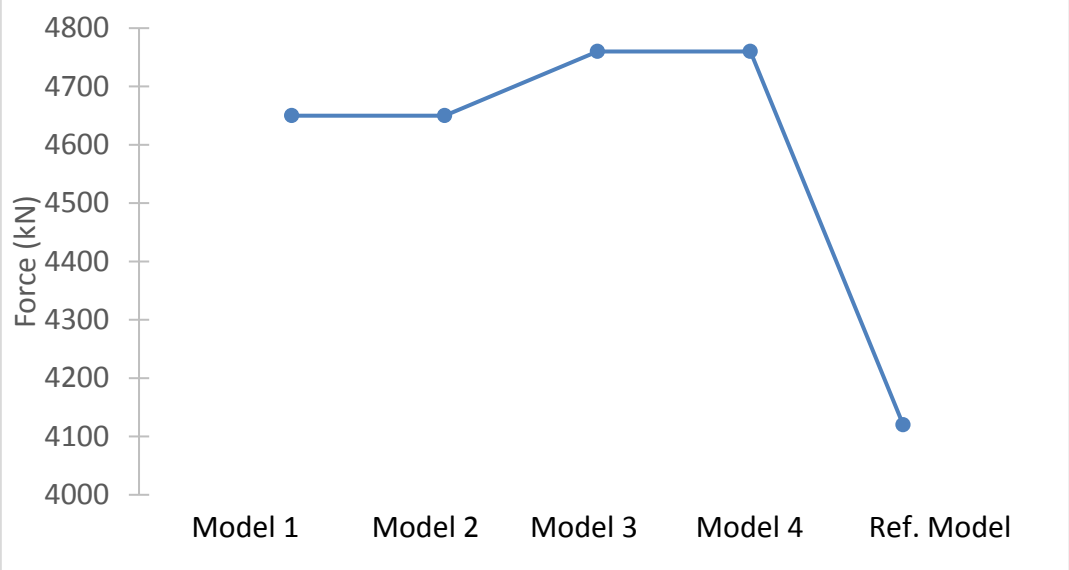

Figure (6-19): Maximum base Shear for different RFT schemes under monotonic loading

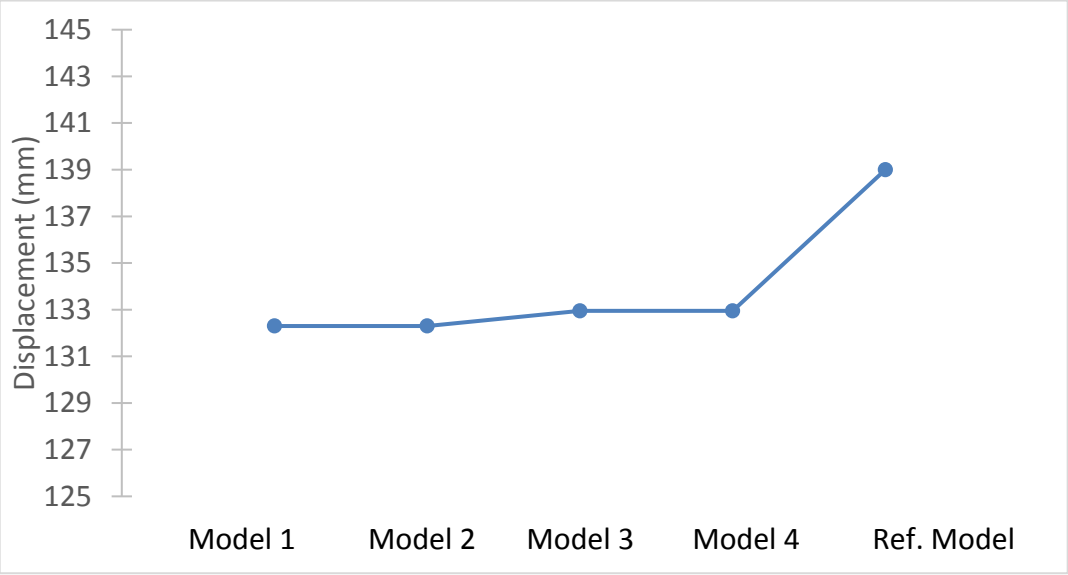

Figure (6-20): Displacements correspond to maximum base shear for different RFT schemes under monotonic loading

Figure (6-21): Energy dissipated for different RFT schemes under monotonic loading

6.6.2.2 Cyclic Loading

Investigating the behavior of using diagonal bars as a reinforcement for coupling beams under cyclic loading showed that diagonal bars enhance both capacity and energy dissipation of the coupling beams. When coupling beams were reinforced with two intersected groups of 4T22/ group and 4T25/group with the longitudinal reinforcement, capacity increased by 11.32% and 13.3% respectively. On the other hand, the corresponding drift decreased by 3.6% and 6.6%, while adding the confining stirrups do not affect neither the capacity nor the corresponding displacement.

Clearly, using diagonal bars with the longitudinal reinforcement for coupling beams increase both energy dissipation and capacities due to the effect of diagonal bars in resisting diagonal compression and improving coupling beam's ductile behavior. The maximum obtained capacities are shown in Figure (6-22), while the corresponding drift are shown in Figure (6-23).

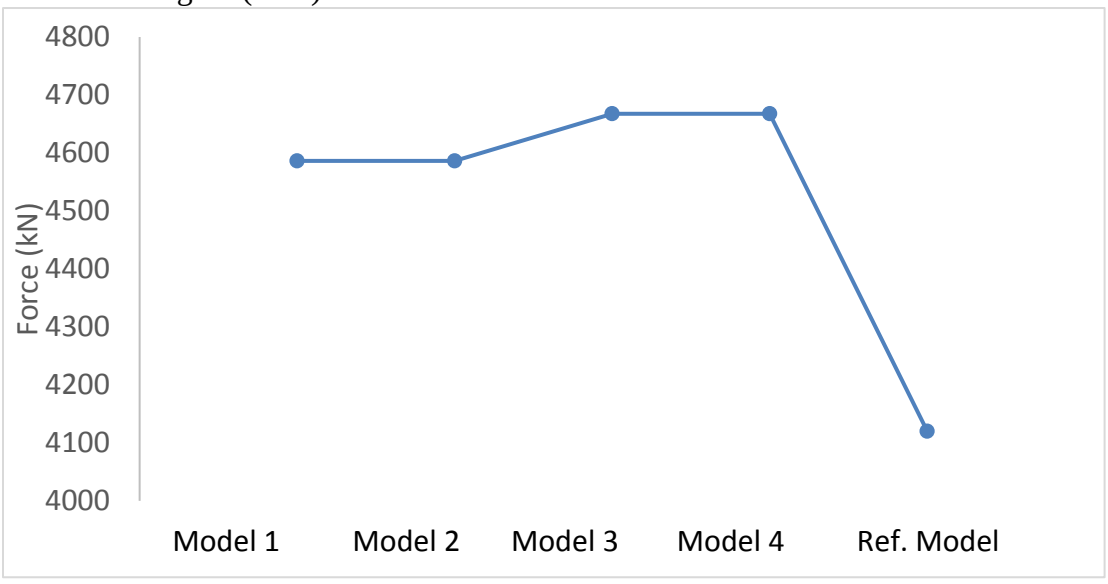

Figure (6-22): Maximum base Shear for different RFT schemes under cyclic loading

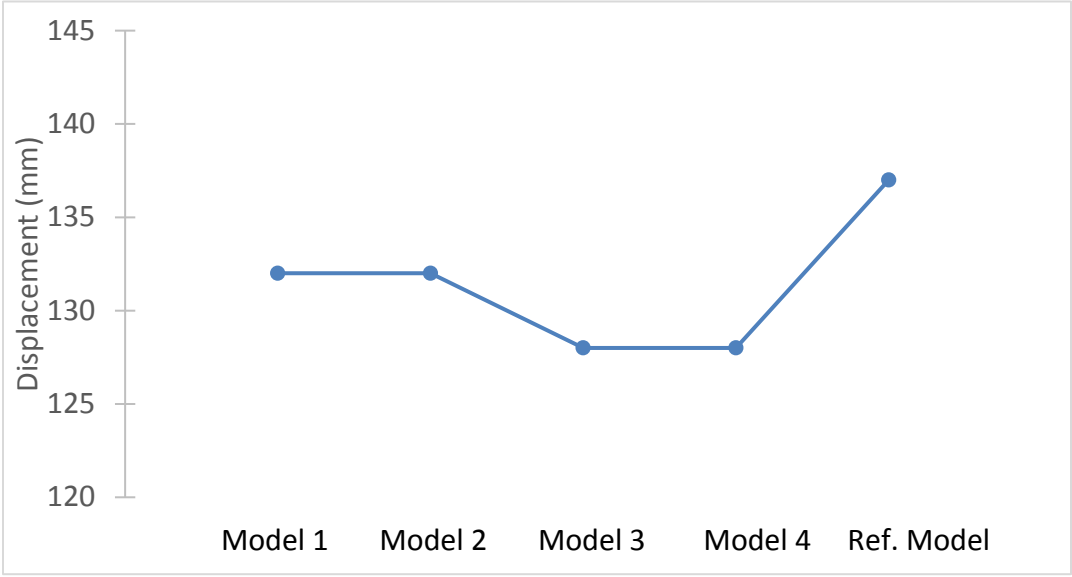

Figure (6-23): Displacements correspond to maximum base shear for different RFT schemes under cyclic loading

6.7 Effect of HPFRC Different Mixtures

6.7.1 Behavior of Coupling Beam

Different HPFRC properties affect capacities and corresponding drift. Increasing maximum tensile stress by 40%, using mix 2 rather than mix 1, resulted in an increase in capacity by 10.6%. On the other hand, the corresponding drift decreased by 10.5%. Increasing maximum compressive stress by 3.5% and 15.1% using mix 3 and mix 4 respectively, resulted in an increase in capacity by 0.5% and 2.5% respectively compared to mix 2, while the corresponding drift did not change. The maximum obtained capacities are shown in Figure (6-24), while the corresponding drift are shown in Figure (6-25).

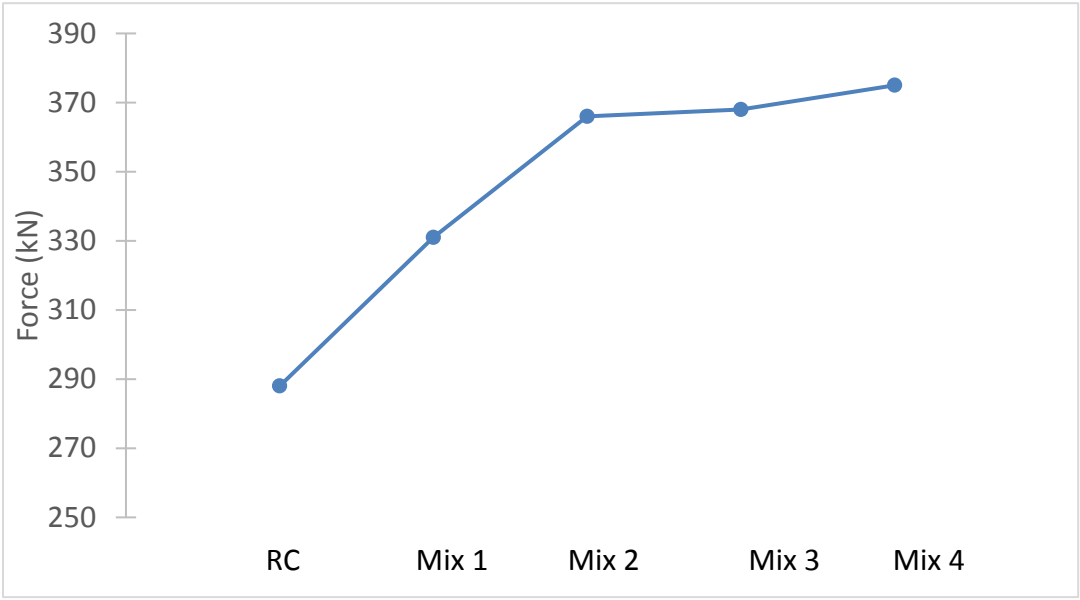

Figure (6-24): Maximum base shear for coupling beam with different HPFRC mixtures under displacement-based cyclic loading

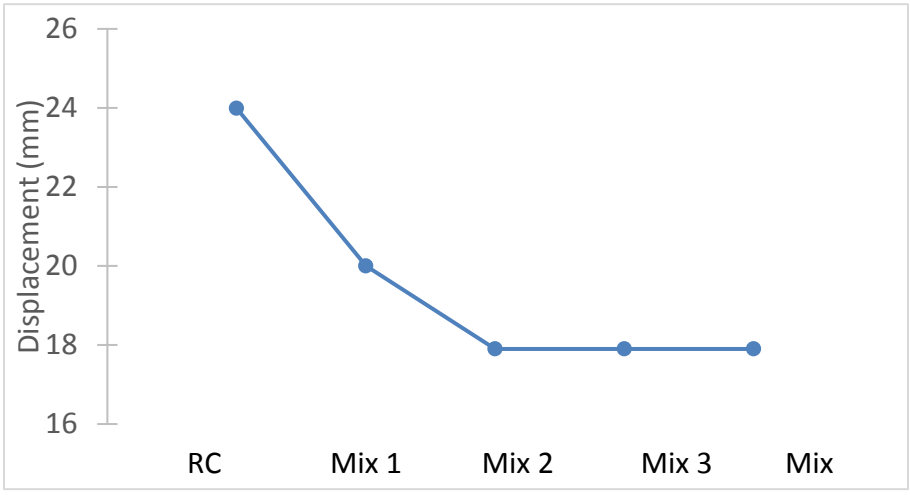

Figure (6-25): The corresponding displacements to maximum base shears for different HPFRC mixtures under displacement-based cyclic loading

6.7.2 Behavior of Coupled Wall

6.7.2.1 Monotonic Loading

Increasing maximum tensile stress by 40%, using mix 2 rather than mix 1, resulted in an increase in capacity by 4.7%. On the other hand, the corresponding drift increased by 6.5%. Increasing maximum compressive stress by 3.5% and 15.1% using mix 3 and mix 4 resulted in an increase in capacity by 0.3% and 0.5% respectively compared to mix2. On the other hand, the corresponding drift decreased by 0.1% and 3.6% respectively.

Moreover, increasing maximum tensile stress by 40% resulted in an increase in energy dissipation by 0.75%, while increasing maximum compressive stress by 15.1%. resulted in an increase in energy dissipation by 1.5%. The maximum obtained capacities are shown in Figure (6-26), while the corresponding drift are shown in Figure (6-27), and the energy dissipated by each HPFRC mixture is showed in Figure (6-28).

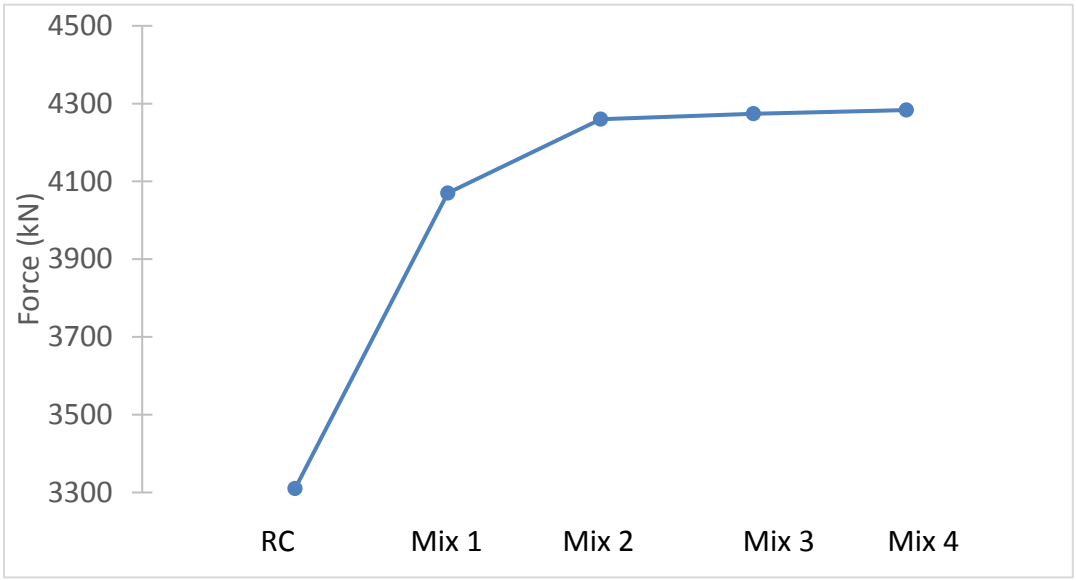

Figure (6-26): Maximum base Shear for HPFRC mixtures under monotonic loading

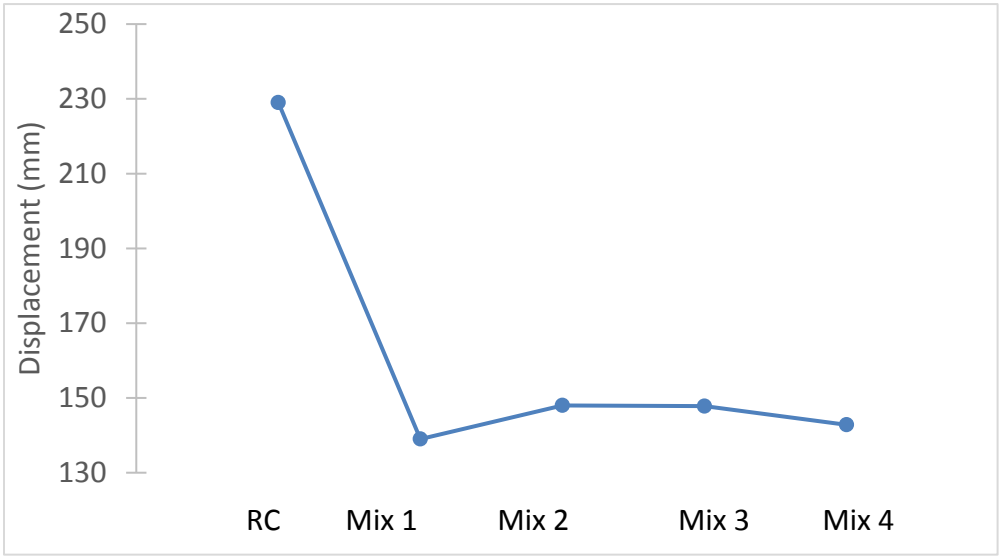

Figure (6-27): The corresponding displacement to maximum base shears for different HPFRC mixtures under monotonic loading

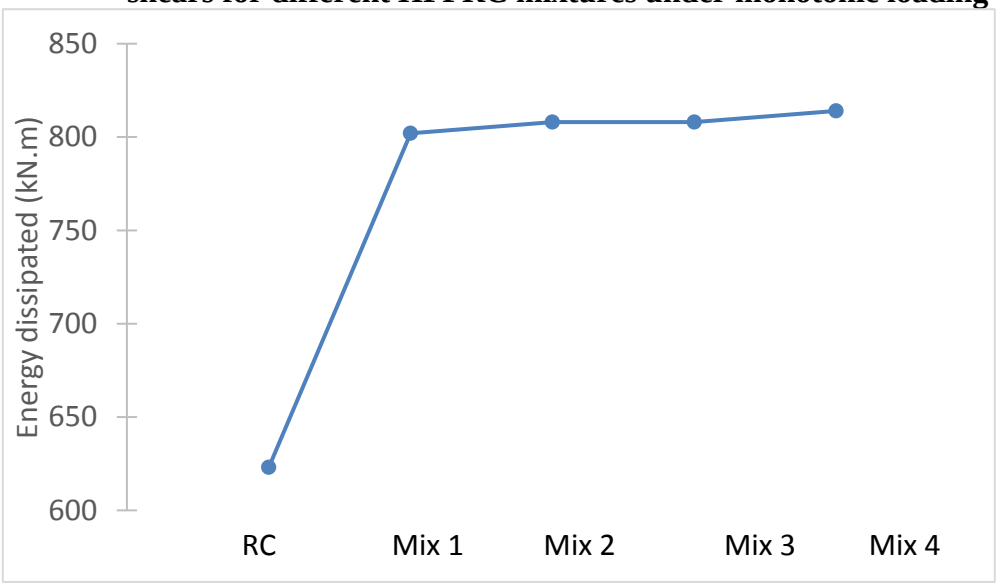

Figure (6-28): Energy dissipated for different HPFRC mixtures under monotonic loading

6.7.2.2 Cyclic Loading

Investigating the effect of using different HPFRC mixtures for coupling beams under cyclic loading showed that capacity and energy dissipation are highly affected by compressive and tensile strength of HPFRC. Increasing of HPFRC's maximum tensile stress by 40% by using mix 2 rather than mix 1, lead to an increase in capacity by 3.5%. while the corresponding drift increased by 15.1%. On the other hand, increasing HPFRC's maximum compressive stress by 3.5% and 15.1% resulted in an increase in capacity by 0.21% and 1.44% respectively, while the corresponding drift decreased by 1.7% and 6.22% respectively.

Clearly, increasing HPFRC's tensile strength resulted in an increase in capacity more than increasing HPFRC's maximum compressive strength because of strain hardening behavior.

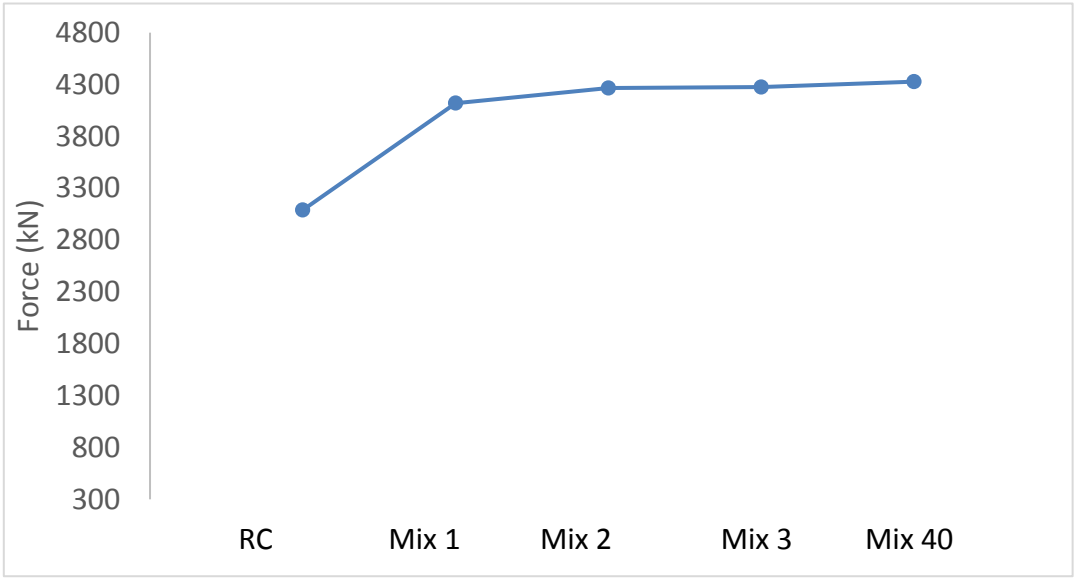

Figure (6-29): Maximum base Shear for different HPFRC mixtures under cyclic loading

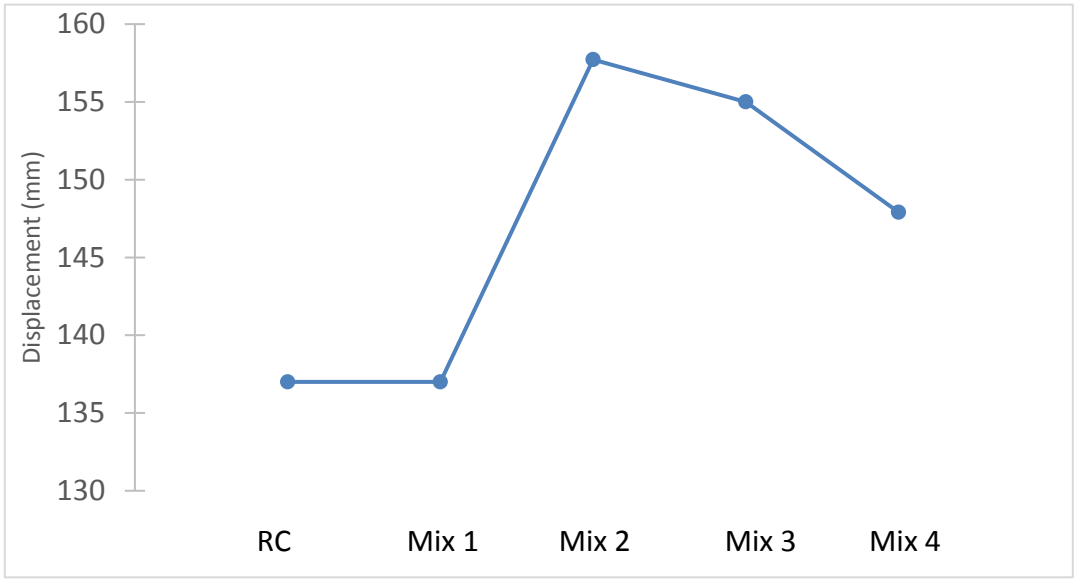

Figure (6-30): The displacement corresponding to maximum base shears for different HPFRC mixtures under cyclic loading

CHAPTER 7: CONCLUSIONS AND FUTURE RESEARCHES

7.1 Introduction

This chapter includes the conclusions of the current study and recommendations for future research.

7.2 Conclusions

The behavior of high-performance fiber reinforced concrete coupling beams is numerically investigated using the Applied Element. Based on the numerical results of the case study, the following conclusions could be obtained.

1. Effect of Material Type:

   HPFRC coupling beams lead to higher energy dissipation, capacity and lower drift. Energy dissipated by HPFRC coupling beams reaches as much as 1.3 times energy dissipated by regular reinforced concrete coupling beams. This is explained by strain hardening behavior and the capability of developing multiple cracks after maximum tensile stress.

2. Effect of Longitudinal Reinforcement Ratio of Coupling Beams:

   As longitudinal reinforcement ratio of coupling beams increases, coupled walls capacity increases up to 1.1 times as reinforcement ratio increases from 0.5% to 0.8%. This is explained by the ductility enhancement through retarding coupling beam failure.

3. Effect of High-Performance Fiber Reinforced Concrete Embedment inside the Coupled Walls:

   As HPFRC embedment inside the coupled walls increases, coupled walls capacity increases up to 1.14 times as HPFRC embedment increases from zero to four coupling beam's depth. This is explained by the capability of HPFRC to resist higher stresses than regular reinforced concrete due to strain hardening behavior.

4. Effect of Coupling Beam's Aspect Ratio:

As beam's aspect ratio decreases, coupled walls capacity increases up to 1.15 times as aspect ratio varies within range 2.72 to 3.75 m. This is explained by decreasing aspect's ratio due to increasing depth results in higher capacity.

5. Effect of Presence of Diagonal Bars with and without Confining stirrups:

a. Coupled walls capacity is affected by using diagonal reinforcement besides the longitudinal reinforcement. Using two intersected groups of reinforcing bars of 4T22/group lead to an increase in capacity of 40% compared to beams with longitudinal reinforcement only.

b. When diagonal bars are used, energy dissipated by each structure increases. This is explained by the capability of diagonal bars to resist diagonal compression generated due to cyclic loading.

6. Effect of Different HPFRC Mixtures:

a. The coupled walls capacity increases up to 1.03 when maximum tensile stress changes from 3.45 MPa to 4.83 MPa. This is explained by enhancing strain hardening behavior.

b. As maximum compressive stress increases from 59.3 MPa to 68.3 MPa, coupled walls maximum capacity increases by 1.4%.

7.3 Recommendations and Future Researches

1. Investigate behavior of coupling beams with lower aspect ratio to trace shear failure and to study the effect of using diagonal bars to avoid sudden sliding shear.

2. Investigate behavior of coupling beams with bundled diagonal bars and compare it with diagonal bars through lab experiments.

3. Investigate behavior of coupling beams with different types of fiber such as glass fibers and synthetic fibers.

REFERENCES

[1] Parra-Montesinos, G. J. (2005). High-performance fiber-reinforced cement composites: an alternative for seismic design of structures. ACI Structural Journal, 102(5), 668.

[2] Hoenderkamp, J. C. D. (2011). The influence of single shear walls on the behavior of coupled shear walls in high-rise structures. Procedia Engineering, 14, 1816-1824.

[3] Adhikari, R. K. (2015). Optimum Degree of Coupling for the Efficient Seismic Response of Reinforced Concrete Coupled Walls (Doctoral dissertation, Tokyo Institute of Technology Tokyo, Japan).

[4] ECP Committee 203-2018, "The Egyptian Code for Design and Construction of Concrete Structures", Housing and Building Research Center, Giza, Egypt, 2018.

[5] ACI Committee 318, A. C. (2011). Building Code Requirements for Structural Concrete (ACI318-11), American Concrete Institute, Farmington Hills, MI.

[6] Aktan, A. E., & Bertero, V. V. (1981). The seismic resistant design of R/C coupled structural walls. NASA STI/Recon Technical Report N, 82.

[7] Aristizabal-Ocfaoa, J. D. (1987). Seismic behavior of slender coupled wall systems. Journal of Structural Engineering, 113(10), 2221-2234.

[8] Aristizabal-Ochoa, J. D. (1982). Dynamic response of coupled wall systems. Journal of the Structural Division, 108(8), 1846-1857.

[9] Aristizabal-Ochoa, J. D. (1983). Seismic analysis of slender coupled walls. Journal of Structural Engineering, 109(7), 1538-1552.

[10] Setkit, M. (2012). Seismic Behavior of Slender Coupling Beams Constructed with High-Performance Fiber-Reinforced Concrete.

[11] Paulay, T. (1971). Coupling beams of reinforced concrete shear walls. Journal of the Structural Division, 97(3), 843-862.

[12] Paulay, T., & Binney, J. R. (1974). Diagonally reinforced coupling beams of shear walls. Special Publication, 42, 579-598.

[13] Paulay, T., & Santhakumar, A. R. (1976). Ductile behavior of coupled shear walls. Journal of the Structural Division, 102(1), 93-108.

[14] Barney, G. B., Shiu, K. N., Rabbat, B. G., Fiorato, A. E., Russell, H. G., & Corley, W. G. (1978). Earthquake Resistant Structural Walls-Tests of Coupling Beams. Portland Cement Association.

[15] Tegos, I. A., & Penelis, G. G. (1988). Seismic resistance of short columns and coupling beams reinforced with inclined bars. Structural Journal, 85(1), 82-88.

[16] Tassios, T. P., Moretti, M., & Bezas, A. (1996). On the behavior and ductility of reinforced concrete coupling beams of shear walls. Structural Journal, 93(6), 711-720.

[17] Galano, L., & Vignoli, A. (2000). Seismic behavior of short coupling beams with different reinforcement layouts. Structural Journal, 97(6), 876-885.

[18] Gonzalez, E. (2001). Seismic response of diagonally reinforced slender coupling beams (Doctoral dissertation, University of British Columbia).

[19] Naish, D., Fry, A., Klemencic, R., & Wallace, J. (2013). Reinforced Concrete Coupling Beams--Part I: Testing. ACI Structural Journal, 110(6).

[20] ACI Committee. (2005). Building code requirements for structural concrete (ACI 318-05) and commentary (ACI 318R-05). American Concrete Institute.

[21] ACI Committee, & International Organization for Standardization. (2008). Building code requirements for structural concrete (ACI 318-08) and commentary. American Concrete Institute.

[22] Han, S. W., Lee, C. S., Shin, M., & Lee, K. (2015). Cyclic performance of precast coupling beams with bundled diagonal reinforcement. Engineering Structures, 93, 142-151.

[23] ACI Committee. (2009). Report on Fiber Reinforced Concrete (ACI 544.1 R-96).

[24] Minelli, F. (2005). Plain and fiber reinforced concrete beams under shear loading: Structural behavior and design aspects. Università di Brescia.

[25] Romualdi, J. P., & Mandel, J. A. (1964, June). Tensile strength of concrete affected by uniformly distributed and closely spaced short lengths of wire reinforcement. In Journal Proceedings (Vol. 61, No. 6, pp. 657-672).

[26] Zollo, R. F. (1997). Fiber-reinforced concrete: an overview after 30 years of development. Cement and Concrete Composites, 19(2), 107-122.

[27] Naaman, A. E., & Reinhardt, H. W. (1996). Characterization of high performance fiber reinforced cement composites—HPFRCC. In High performance fiber reinforced cement composites (Vol. 2, pp. 1-24).

[28] Liao, W. C., Chao, S. H., Park, S. Y., & Naaman, A. E. (2006). Self-Consolidating High-Performance Fiber Reinforced Concrete (SCHPFRC)–Preliminary Investigation. Report No. UMCEE 06, 2.

[29] Naaman, A. E. High performance fiber reinforced cement composites. High-performance construction materials: Science and Applications, (2008).

[30] Naaman, A. E. (2007, December). High performance fiber reinforced cement composites: classification and applications. In CBM-CI international workshop, Karachi, Pakistan (pp. 389-401).

[31] Song, P. S., & Hwang, S. (2004). Mechanical properties of high-strength steel fiber-reinforced concrete. Construction and Building Materials, 18(9), 669-673.

[32] Fanella, D. A., & Naaman, A. E. (1985, July). Stress-strain properties of fiber reinforced mortar in compression. In Journal Proceedings (Vol. 82, No. 4, pp. 475-483).

[33] Kwak, Y. K., Eberhard, M. O., Kim, W. S., & Kim, J. (2002). Shear strength of steel fiber-reinforced concrete beams without stirrups. ACI Structural Journal, 99(4), 530-538.

[34] de Lima Araújo, D., Nunes, F. G. T., Toledo Filho, R. D., & de Andrade, M. A. S. (2014). Shear strength of steel fiber-reinforced concrete beams. Acta Scientiarum. Technology, 36(3), 389-397.

[35] Zhu, H., Li, C., Gao, D., Yang, L., & Cheng, S. (2019). Study on mechanical properties and strength relation between cube and cylinder specimens of steel fiber reinforced concrete. Advances in Mechanical Engineering, 11(4), 1687814019842423.

[36] Lequesne, R. D. (2011). Behavior and Design of High-Performance Fiber-Reinforced Concrete Coupling Beams and Coupled-Wall Systems.

[37] Zhao, J., & Yao, M. (2013). Experimental Study on Load Behavior of Steel Fiber Concrete Coupled Shear Wall. In Applied Mechanics and Materials (Vol. 438, pp. 682-685). Trans Tech Publications.

[38] Cai, G., Zhao, J., Degée, H., & Vandoren, B. (2016). Shear capacity of steel fibre reinforced concrete coupling beams using conventional reinforcements. Engineering Structures, 128, 428-440.

[39] Han, S. W., Kang, J. W., Jee, H. W., Shin, M., & Lee, K. (2018). Cyclic Behavior of HPFRCC Coupling Beams with Bundled Diagonal Bars. International Journal of Concrete Structures and Materials, 12(1), 42.

[40] Applied Science International, LLC (ASI) www.appliedscienceint.com.

[41] Okamura, H., & Maekawa, K. Nonlinear analysis and constitutive models of reinforced concrete. 1991. Gihodo-Shuppan, Tokyo, Japan.

[42] Chen, W. H., & Chang, C. S. (1989). Analysis of two-dimensional mixed-mode crack problems by finite element alternating method. Computers & structures, 33(6), 1451-1458.

[43] Dutta, B. K., Kakodkar, A., & MAITI, S. (1989, January). Use of two singular point finite elements in the analysis of kinked cracks. In Proceedings of The 7th International Conference On Fracture (ICF7) (pp. 2315-2322). Pergamon.

[44] Kawai, T. (1986). Recent developments of the Rigid Body and Spring Model (RBSM) in structural analysis. In Seiken Seminar Text Book (pp. 226-237). Institute of Industrial Science, The University of Tokyo.

[45] Kikuchi, A., Kawai, T., & Suzuki, N. (1992). The rigid bodies—spring models and their applications to three-dimensional crack problems. Computers & structures, 44(1-2), 469-480.

[46] Meguro, K., & Hakuno, M. (1994). Application of the extended distinct element method for collapse simulation of a doubledeck bridge. Doboku Gakkai Ronbunshu, 1994(483), 17-27.

[47] Extreme Loading for Structures Theoretical Manual, Applied Science International (2018).

[48] Menegotto, M., and Pinto, P. E. "Method of analysis for cyclically loaded reinforced concrete plane frames including changes in geometry and non-elastic behavior of elements under combined normal force and bending", Proc., IABSE Symp. of Resistance and Ultimate Deformability of Structures Acted on by Well Defined Repeated Loads, International Association of Bridge and Structural Engineering, Libson, Portugal, Vol. 13: 15-22, 1973.

[49] Kimiro Meguro and Hatem Tagel-Din: Applied Element Simulation of RC Structures

under Cyclic Loading, ASCE, Vol. 127, Issue 11, pp. 1295-1305, November 2001.

[50] Kimiro Meguro and Hatem Tagel-Din: Applied Element Method for Structural Analysis: Theory and Application for Linear Materials, Structural Eng./Earthquake Eng., International Journal of the Japan Society of Civil Engineers (JSCE), Vol. 17, No. 1, 21s-35s, April 2000.

[51] Hatem Tagel-Din and Kimiro Meguro: Applied Element Method for Simulation of Nonlinear Materials: Theory and Application for RC Structures, Structural Eng./Earthquake Eng., International Journal of the Japan Society of Civil Engineers (JSCE) Vol. 17, No. 2, 137s-148s, July 2000.

[52] Hatem Tagel-Din and Kimiro Meguro: Applied Element Method for Dynamic Large Deformation Analysis of Structures, Structural Eng./Earthquake Eng., International Journal of the Japan Society of Civil Engineers (JSCE), Vol. 17, No. 2, pp. 215s-224s, October 2000.

[53] Kimiro Meguro and Hatem Tagel-Din: AEM Used for Large Displacement Structure Analysis, Journal of Natural Disaster Science, Vol. 24, No. 2, pp. 65-82, 2002.

[54] Hatem Tagel-Din: Collision of Structures During Earthquakes, Proceedings of the12thEuropean Conference on Earthquake Engineering, London, UK, September 9th - September 13th, 2002.

[55] Hatem Tagel-Din and Kimiro Meguro: Analysis of a Small Scale RC Building Subjected to Shaking Table Tests using Applied Element Method, Proceedings of the12th World Conference on Earthquake Engineering, New Zealand, January 30th -February 4th, 2000.

[56] Wibowo H., Reshotkina S. S., Lau D. T., CSCE F., (2009), "Modelling progressive collapse of RC bridges during earthquakes", Canadian Society of Civil Engineers 2009

Annual General conference, pp. GC-176-1-11.

[57] Griffin J. W. (2008) "Experimental and analytical investigation of progressive collapse through demolition scenarios and computer modeling", M. Sc., Civil engineering, North Carolina.

[58] Sasani M., (2008), "Response of a reinforced concrete infilled-frame structure to removal of two adjacent columns, Eng. Struc., 30, pp. 2478-2491.

[59] Hoon Park, Chul-Gi Suk, Seung-Kon Kim, Collapse Modeling of model RC Structure Using Applied Element Method, Tunnel and Underground Space Journal of Korean Society for Rock Mechanics, Vol. 19, No. 1, 2009, pp. 43-51.

[60] Kent, D. C., & Park, R. (1971). Flexural members with confined concrete. Journal of the Structural Division.

[61] ECP Committee 201-2012, "The Egyptian Code for Load Calculation", Housing and Building Research Center, Giza, Egypt,2012.

[62] Abdelhafeez, M., & Salem, H. (2022). Behavior of coupled walls with high performance fiber reinforced concrete coupling beams. In Current Perspectives and New Directions in Mechanics, Modelling and Design of Structural Systems (pp. 1364-1370). CRC Press.